EVALUATION OF BAR RACK DESIGNS TO ALLOW FOR THE DOWNSTREAM PASSAGE OF SILVER AMERICAN EELS AT HYDROPOWER FACILITIES

by

Tresha Melong

A Thesis Submitted to the Faculty of

Worcester Polytechnic Institute

In Partial Fulfillment of the Requirements for the Degree of

Master of Science

in

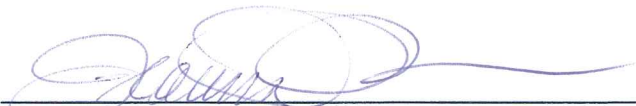Environmental Engineering

By

Tresha Melong

January 2014

Professor Paul Mathisen, Major Advisor

Gregory Allen, Committee Member

Stephen Amaral, Committee Member

Professor Jeanine Plummer, Committee Member

ABSTRACT

Concerns regarding the decreasing population of the American eel (reported by Castonguay *et al.* 1994; Haro *et al.* 2000) have led to design restrictions for hydropower facilities in the Eastern United States. However, the effects of these restrictions on eel passage and their impacts on power generation have not been fully researched. The goal of this study was to evaluate design parameters for bar racks that have potential to prevent entrainment of silver American eels, but also have minimal impacts on power generation. Hydraulic and biological assessments were used to determine the role of bar spacing, rack angle, and approach velocity on head loss across bar racks and the effects of bar spacing and approach velocity on eel bypass efficiency. The hydraulic assessments included computational fluid dynamics (CFD) analyses and laboratory experiments conducted in a re-circulatory flume at Alden Research Laboratory (Alden) in Holden MA. The flume allowed for determination of head losses across bar racks placed at angles of 45 and 90 degrees to the flow direction, with bar spacings of 0.75, 1.0 and 1.5 inches (19, 25 and 38 mm) and approach velocities of 1.5, 2.0 and 2.5 ft/sec (0.46, 0.61 and 0.76 m/s). Biological assessment, supported by funding from the Electric Power Research Institute (EPRI), used the same flume and included experiments with a 90 degree rack angle, bar spacings of 0.75 and 1.0 inches (19 and 25 mm), and approach velocities of 1.5 and 2.0 ft/sec (0.46 and 0.61 m/s). Bypass efficiencies, defined by the percentage of eels moving through the bypass, were evaluated for eels using three 2-hour replicate trials with nighttime releases of 30 eels per trial. Eel behavior in the vicinity of the racks was observed to the extent possible using a DIDSON acoustic camera. Experiments for the 90 degree configuration showed that the guidance efficiencies for the 0.75 inch (19 mm) spacing were greater than those for the 1.0 inch (25 mm) spacing, while the head losses for the 0.75 inch (19 mm) spacing exceeded the head losses for the 1.0 inch (25 mm) spacing by more than 10 percent. Linear regression analysis indicated that 53 percent of the variations in head width are explained by changes in the length of the eel. Results of the hydraulic evaluations were used to develop a new head loss equation that has a correlation coefficient of 98.6 percent. The results of the hydraulic and biological assessments provide a basis for quantifying the impacts of bar rack design on hydropower operation and downstream passage for American eels.

ACKNOWLEDGEMENTS

EXECUTIVE SUMMARY

Physical barriers such as bar racks prevent marine species from entering the turbines at hydropower facilities. These barriers are sometimes referred to as trash racks due to their dual purpose but with proper design they can be effective in the safe downstream passage of many fish species. Among these species are the American eels, for which downstream passage has become a major issue due to the significant decline in their population. This decline has occurred due to the migration and life cycle of the eels, as their spawning habits take them from the Sargasso Sea via the Gulf Stream to the freshwater streams and estuarine habitats of the United States. During downstream passage the silver American eels are in the peak of their maturity with the females growing up to 5 feet (1.5 m) in length. Their size increases their mortality rate when they pass through the turbines because they have a greater chance of being struck by the blades and high approach velocities can cause impingement on the bar racks at the water intakes. Their population decline, documented by Castonguay *et al*. (1994), has resulted in the American eel being currently considered by the U.S. Fish and Wildlife Service to be listed as a Threatened species.

For hydropower facilities, mitigation methods have focused on the design of bar racks to effectively provide safe passage and therefore increase proliferation of the American eel. The U.S. Fish & Wildlife Service (FWS) has prescribed restrictive measures for the downstream passage of the silver American eels to reduce turbine entrainment and mortality (FWS, 2000). These measures include the installation of bar racks with 0.75 inch (19 mm) clear spacing and a reduction of intake approach velocities to 1.5 ft/s (0.46 m/s) or less. However, the costs of implementing these design parameters can be high and significantly reduce the economic viability of smaller hydropower facilities. The use of 0.75 inch (19 mm) bar racks would incur costs associated with installation, operation of a bypass, increased maintenance due to debris and ice removal, and reduced power generation from higher head losses due to narrower spacing and greater debris accumulation.

The objective of this thesis was to evaluate the use of bar racks as an effective physical barrier to prevent the silver American eel from entering the turbine. Additionally, designs were to be tested for minimal operational and engineering impacts on power generation due to head loss. The scope of the research involved two parts: a hydraulic evaluation and a biological assessment. The hydraulic evaluation utilized site assessments to gather information on the specific factors that influence the effectiveness of implemented fish passage designs at hydropower facilities, numerical modeling was completed using Computational Fluid Dynamics (CFD) software to evaluate the hydraulic performance of bar rack designs based on the determined factors for a typical facility and physical modeling to determine the potential hydraulic impacts on the operation of the facility and subsequent power generation. Then, the biological aspect was

completed with live eels to test the guidance efficiency of bar racks with different design parameters and also provide validation for the hydraulic evaluations.

The hydraulic and biological assessments were conducted in a re-circulatory flume of 80 feet in length, 6 feet in width and 7 feet in depth at Alden Research Laboratory (Alden) in Holden MA. The flume allowed for the determination of head losses across bar racks placed at angles of 45 and 90 degrees to the flow direction, with bar spacings of 0.75, 1.0 and 1.5 inches (19, 25 and 38 mm) and approach velocities of 1.5, 2.0 and 2.5 ft/sec (0.46, 0.61 and 0.76 m/s). In addition, application of computational fluid dynamics (CFD) modeling using ANSYS Fluent 14.0 to represent the experimental flow conditions provided insight into the head losses and velocity distributions in the immediate vicinity of the bar racks. For the biological assessment, laboratory testing was conducted in the same flume with live eels, where additional support was provided by the Electric Power Research Institute (EPRI), to determine the fish guidance efficiency of bar racks placed at 90 degrees to the flow direction with bar spacings of 0.75 and 1.0 inches (19 and 25 mm) and approach velocities of 1.5 and 2.0 ft/sec (0.46 and 0.61 m/s). The significance of this research would not only be to incorporate a passage for the eels, but to also include provisions that allow for the passage of other migratory species.

Results indicated that head losses were greater for a 45 degree angled bar rack than a 90 degree rack. Velocity measurements for the upstream cross section of the channel also showed that the flow conditions for the 1.0 and 1.5 inches (25 and 38 mm) clear spacing configurations of the bar racks were similar. Numerical modeling of the physical models proved to be unsuccessful at predicting the head loss that may occur at each condition but predicted accurately the flow patterns approaching the rack which provide insight into where the eels may come into contact with rack. However, a head loss equation developed for this project predicted head loss with a correlation coefficient of 98.6 percent, which was an improvement over previously proposed equations.

Biological testing with live eels, provided results that indicated a clear spacing of 0.75 inches (19 mm) for a 90 degree bar rack with an approach velocity of 1.5 ft/s (0.46 m/s) were be more efficient than the 1.0 inch (25 mm) clear spacing at guiding eels to the bypass. The mean guidance efficiency was 96.1 percent compared to 72.1 percent for the 1.0 inch (25 mm) configuration. Guidance efficiency was found to decrease with an increase in approach velocity and the mean head width of the eels tested with the 0.75 inch (19 mm) spacing rack was lower than that for the 1.0 inch (25 mm) spacing rack. MANOVA analysis showed that head width did not have any significant effect on the length of the eels that did not enter the bypass or pass through the bar rack. However, the clear spacing did have a significant effect on the length and head width of the eels that passed through the rack.

These results provide information that can be helpful in the design and implementation of bar racks at hydropower intakes for the safe downstream passage of the silver American eel. The

proposed head loss equation also provides hydropower operators with a tool that can be easily used to estimate the impacts on power generation for different bar rack designs, which allows for effective decision making specific to each site.

TABLE OF CONTENTS

LIST OF FIGURES

LIST OF TABLES

1.0 INTRODUCTION

Physical barriers such as bar racks are commonly used to prevent marine species from entering the turbines at hydropower facilities. Among these species are the American eels, which have experienced a recent decline in population, as documented by Castonguay et al. (1994). This decline has resulted in the American eel being currently considered by the U.S. Fish and Wildlife Service to be listed as a Threatened species. The decline is believed to be related to the migration and life cycle of the eels, which includes passage from the Sargasso Sea via the Gulf Stream to the freshwater streams and estuarine habitats of the United States. Since this species spawning habits include downstream passage back to the sea, the impacts of hydropower facilities on the downstream passage has become a major concern.

In order to prevent the subsequent further decline in the population of the American eel, the U.S. Fish & Wildlife Service (FWS) has prescribed restrictive measures for the downstream passage of the silver American eels to reduce turbine entrainment and mortality (FWS, 2000). These measures may include shutdown of all units at night for a three month period in the fall when silver eels migrate from freshwater habitats to the marine environment, or installation of bar racks with 0.75 inch (19 mm) clear spacing and a reduction of intake approach velocities to 1.5 ft/s (0.46 m/s) or less. Many projects in the eastern U.S. have opted for the latter and have already installed bar racks at their intakes for anadromous species (e.g., Atlantic salmon, American shad, river herring, etc.) that may provide sufficient protection for American eels. These bar racks typically include 1.0 inch (25 mm) clear spacing, intake approach velocities of 2 ft/s (0.61 m/s) or less, rack angles of 45 degrees to the approach flow, and bypass flow rates of 2 to 5% of project discharge.

However, the smaller clear spacing of 0.75 inch (19 mm) would result in greater head losses and costs associated with increased maintenance (debris and ice removal) and operation of the bypass. Further research would be required to accurately predict the effects on power generation and also the effectiveness of the prescription at providing safe downstream passage for the American eel, because previous research was conducted on silver European eels. Therefore, the effectiveness of these measures and their potential impacts on the hydropower industry is not clear.

This thesis focuses on the use of bar racks as an effective measure to provide safe downstream passage and prevent this catadromous species from entering turbines. The goal was to determine the design parameters for bar racks that will provide safe passage for the American eel, with minimal operational and engineering impacts on power generation at hydropower facilities. Key considerations include whether current bar rack design parameters that already installed at hydropower projects for anadromous species can also be applied for the protection the silver American eel, and whether specifications provided by the FWS would be more effective.

For the purposes of this thesis, the objectives were to use hydraulic and biological assessments to determine the effects of bar rack design on head loss and assess the role of bar spacing on eel passage. For the hydraulic assessment, laboratory experiments were conducted in a re-circulatory flume of dimensions: 80 feet (24.4 m) in length, 6 feet (1.8 m) in width and 7 feet (2.1 m) in depth at Alden Research Laboratory (Alden) in Holden MA. The flume allowed for the determination of head losses across bar racks placed at angles of 45 and 90 degrees to the flow direction, with bar spacings of 0.75, 1.0 and 1.5 inches (19, 25 and 38 mm) 5and approach velocities of 1.5, 2.0 and 2.5 ft/sec (0.46, 0.61 and 0.76 m/s). In addition, application of computational fluid dynamics (CFD) modeling using ANSYS Fluent 14.0 to represent the experimental flow conditions provided insight into the head losses and velocity distributions in the immediate vicinity of the bar racks. For the biological assessment, laboratory testing was conducted in the same flume with live eels, where additional support was provided by the Electric Power Research Institute (EPRI), to determine the fish guidance efficiency of bar racks placed at 90 degrees to the flow direction with bar spacings of 0.75 and 1.0 inches (19 and 25 mm) and approach velocities of 1.5 and 2.0 ft/sec (0.46 and 0.61 m/s). The data gathered from these assessments are intended to provide hydropower operators with the tools and information to determine the impact on power generation and survival rate of the silver American eels depending on the site specifications.

2.0 BACKGROUND

The American eel is a catadromous species that migrates from its fresh water habitats to the sea to spawn; however this vital activity can be blocked or hindered by presence of hydropower facilities. Downstream passage of these species has therefore become a concern due to the size of the eels during migration and their mortality rate if they are forced through the turbine or entrainment on the racks at intakes. This chapter provides background on the migration and life cycle of the American eels, effects of dams on the eel population, and the behavioral response of eels to intake protection devices, specifically bar racks during downstream passage. Then, the applicability of numerical modeling and head loss equations to accurately predict hydraulic performance and effects on power generation are discussed.

2.1 Migration and Life Cycle of American Eels

The American eel (Anguilla rostrata) spawns in the Sargasso Sea, which is approximately two million square miles of warm water located north of the Bahamas and south of Bermuda (Facey et al., 1987; Beak International Inc., 2001). Once the eggs hatch into leptocephali (sing. leptocephalus) larvae, the Gulf Stream transports the eels towards North America's eastern seaboard or further into the North Atlantic region including Greenland and north of Labrador, while they metamorphose into their transparent glass eel phase (Castonguay et al., 1994; Lary and Busch, 1997; EPRI, 1999), shown in Figure 1. However, the American eel is a catadromous species that spends most of its life in fresh or brackish water after being spawned in the ocean and comprises of a single population (panmictic). Migration of the eels to their U.S. freshwater streams and continental habitats usually takes years but during this time the larvae growth reaches up to 2.4 inches (60 millimeters) in length. The eels mature in their estuarine habitats, where over time they grow and change color (Lary and Busch, 1997; Gulf of Maine Council on the Marine Environment, 2007; Van Den Avyle, 1984; U.S. Fish and Wildlife Service, 2011; EPRI, 1999).

The growth phase of the American eel begins with the metamorphosis of the larvae into the notable eel-like form called the glass eels. At this stage, they lack pigmentation as they move towards the coastal areas but once they reach freshwater, they develop pigmentation and are known as elvers. Glass eels are generally 1.8-2.8 inches (45-70 millimeters) long and elvers are 2.6-3.9 inches (65-100 millimeters) long. Yellow eels are the products of the mature elvers and may spend 6-30 years in freshwater and are commonly found in estuaries, rivers and lakes around the Gulf of Maine. Yellow eels may be sexually undifferentiated (gonads contain no definable gamets), hermaphroditic (oogonia and spermatogonia present), or sexually differentiated (females with oogonia; males with spermatagonia present), but none of these stages are capable of reproduction and as such yellow eels are classified as immature (Van Den Avyle, 1984). The final stage of development for the American eel is called the silver eels (up to

5 feet in length for the females; 3 feet for the males). These are the sexually mature yellow eels, which at this stage they have a metallic, blackish-bronze color, and enlarged eyes, fat bodies and thicker skin (Gulf of Maine Council on the Marine Environment, 2007; U.S. Fish and Wildlife Service, 2011).
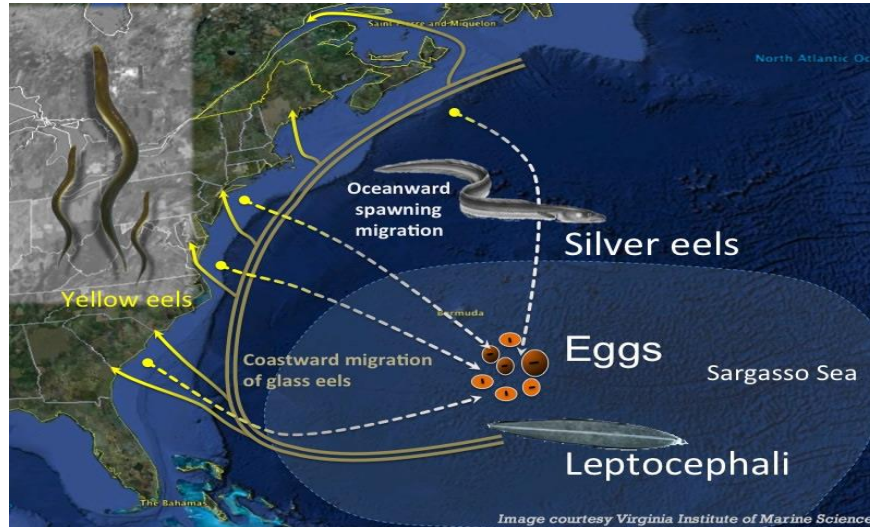
Figure 1 - Life cycle of the American eel (Virginia Institute of Marine Sciences, 2013).

During the metamorphosis of the yellow eel into the silver eel, the digestive tract degenerates indicating that seaward migration for spawning will result in death. The spawning period occurs during the period of February to April (or later) and migration occurs during September to December, where most silver eels descend rivers and streams and begin their journey back to the Sargasso Sea. Migration of the eels for spawning represents the last stage in their life cycle as it only occurs once. This step in their life cycle has however been a challenge for the silver eels due to the installation dams during the 1960s. Eels end up losing their historical freshwater habitats and migration corridors, which results in a decline in the population also caused by mortality in hydropower plant turbines, degradation of current habitat and overharvesting (Gulf of Maine Council on the Marine Environment, 2007; U.S. Fish and Wildlife Service, 2011).

2.2 Decline of the American Eel Population

Dams were originally built on small rivers and tributaries to power grist mills and improve river navigation; however with the rise of the Industrial Revolution in the mid-1800s there was a need for larger industrial mills and other power sources. This demand led to redefining the purpose of dams to provide hydro-mechanical power, which resulted in larger dams and a greater effect on migratory species such as shad. Commercial fishers in the late seventeenth century, who were affected by these dams, raged "shad wars" on the industrialists due to the blockage of the migratory channels (NOAA, 2012). This problem has continued to the present day, where

migratory fish species (such as the American eel) are still affected by these dams and have consequently had severe decline in population over the years.

The increase in hydroelectric dams along the eastern seaboard has led to effects on the proliferation of the American eel directly and indirectly. Modification of habitat is an indirect effect but no less harmful, which results in habitat fragmentation/loss due to blockage and/or impedance of upstream passage and transformation of the riverine system. Direct impacts include the impeding or change in upstream movements of the eel in its early growth stages and the delayed downstream movement which results in increased predation or mortality due to impingement or turbine passage of the mature silver eels (EPRI, 1999; Larinier, 2001). Other factors can be considered such as the overexploitation of the eels in multiple stages of development, micro contaminants and their effects on survival and reproduction, oceanic environmental changes, pre-spawning mortality resulting from bladder worm infections and unregulated commercial harvest of Sargussum in the spawning zone (Beak International Inc., 2001).

The R.H. Saunders dam in Ontario, which was included in the construction of the St. Lawrence Seaway built between 1954 and 1958, can be used as an example of the direct impacts dams have had on the eel population. Its inception was not without opposition as commercial fishers believed that the dam impaired the migration of the American eel to and from Lake Ontario and the upper St. Lawrence River. This concern for eel passage led to the implementation of an eel ladder in 1974, which was equipped in July 1987 with an electronic counter to record total estimates of eels ascending the ladder each year (Marcogliese et al., 1997). The eel ladder also addressed the problem of the clogging of discharge pipes, which resulted in maintenance issues. Figure 2 shows an example of eels using the ladder.

Figure 2 - Upstream migrating American eel (elver) sampled from fish ladder (Photo Credit: Steve Amaral).

Marcogliese et al. (1997) in their study determined whether the recruitment of the eels at the fish ladder in Ontario could be used to predict the abundance of eels in the Lake Ontario and upper St. Lawrence River. Alternative migration routes such as the canal system were accounted for by using long-term data from other sources to standardize the counts at specific intervals each year. The other sources included commercial harvest, commercial electrofishing and research trawls. It was found that there was a similar trend among the four sources, which indicated that the ladder provided a reliable index of eel recruitment. The trend showed dramatic declines over the past decade, which began in 1986 of eel recruitment. From 1975 to 1985, a consistent 600,000 to 1,300,000 eels annually were ascending the ladder. However, in 1986, there was a significant decline to only 200,000 eels. This declining trend remained consistent reaching a low in 1993 of only 8,000 eels ascending the ladder.

Castonguay et al. (1994) reviewed four possible causes of the declining recruitment: habitat change, overfishing, pollution and ecological changes. However, habitat change was found to be the greater issue. The dam was not found to completely hinder upstream migration of the eels to Lake Ontario and the upper St. Lawrence River but there is apparent delay which may have led to increased predation. Downstream migration also proves to be difficult because the turbines of the hydroelectric dam increase the mortality of the migrating adult "silver" eels returning to their spawning site in the Sargasso Sea. Marcogliese et al. (1997) therefore concluded that increased downstream migration or escapement of the adult "silver" eels is pertinent to the survival of the specie and the commercial fishery industry in the upper St. Lawrence River and Lake Ontario.

The potential risk of the American eel going extinct led to a petition being filed in late 2004 with the United States Fish and Wildlife Service (FWS) and the National Marine Fisheries Service (NMFS) to have the American eel listed as a threatened species. The petition was reviewed in 2007 following a series of workshops since 2004 but the American eel was found at the time to not be warranted for protection under the Endangered Species Act. The Service found that declines of eel populations in some areas did not put the overall population in danger of extinction. Subsequently, another petition was filed in 2010 by the Council for Endangered Species Act Reliability, which was found to present substantial information that warranted more extensive status review of the species (FWS, 2011).

2.3 Downstream Fish Passage Facilities and Behavioral Response of Eels

Downstream fish passage facilities normally are typically separated into four categories (EPRI 1986, 1994, 1998, 1999a, 2001). These categories include physical barriers (fixed screens, barrier nets), behavioral barriers (light, sound, electricity), diversion systems (spillways, bypasses, angled screens) and collection systems (surface collectors, traveling screens) (Larinier, 2000; Gosset et al., 2005). Physical barriers prevent fish from entering the turbines by using sufficiently small mesh does not allow passage. In order to avoid impingement, low flow

velocities are required, where flow is adapted to the swimming capacity of the species and stage of maturity (Larinier, 2000; Larinier, 2001). Other physical barriers include bar racks (Figure 4), rotary drum screens, barrier nets and infiltration intakes (EPRI, 1986).

Figure 3 - Bar rack orientation at Cabot Station, Turners Falls (Photo Credit: Steve Amaral, 2012).

Behavioral barriers on the other hand, alter or take advantage of the natural behavior patterns of the fish species to attract or repel them (EPRI, 1986). Examples of these barriers include water bubbles, sound, fixed and moveable chain, attractive or repellent light, electrical and hydrodynamic (louver) screens. Results have shown that the visible chain, light and sound screens would not be applicable due to their specificity (effective only with certain species and sizes). They also have low reliability and are susceptible to local conditions such as water turbidity and hydraulic conditions. The louver screen is similar to the diversion systems but it consists of an array of vertical slats aligned across the intake at a specified angle to the flow. It also guides fish towards a downstream bypass but its efficient is highly dependent on the flow pattern of the canal intake (Larinier, 2000).

Diversion systems provide a route to bypasses at hydroelectric facilities for the fish to return to their natural environment. Angled screens, skimmers, louvers and controlled spillways are some of the systems used to divert fish to bypasses (EPRI, 1986). Most large mainstream dams have spill gates open from the bottom up to allow for water and fish to "spill" underneath, as opposed to small dams that "spill" water over the top. This method has its advantages and disadvantages with regards to different species. It has been found to be the most benign passage route for juvenile salmonids but the elevated dissolved gas downstream can stress or kill other species, reduce swimming performance and resistance to pathogens. There is also the increased predation

due to the increased fish concentration and fish damage caused by turbulence or pressure stresses in high spillway discharge rates (Larinier, 2000).

Modified traveling water screens, fish pumps and Gate well collection nets are examples of collection systems used to bypass turbines by actively collecting the fish and transporting them to their natural habitat. These systems however have two major disadvantages that limit their general applicability at hydro plants. First, capital investment, operation and maintenance costs are high because they involve mechanical operation. Second, these systems are more prone to cause injury to the fish than other systems because of active collection and transport (EPRI, 1986). The presence of physical barriers such as intake screens and trash racks may cause impingement and subsequent suffocation of different species, shown in Figure 4 (Haro et al., 2000). Specifically, eels that unfortunately experience turbine passage are subjected to pressure changes, cavitation, shear stresses and potentially mechanical strike. Damage to the eels may occur during turbine passage and is believed to be primarily attributed to mechanical strike (EPRI, 1999).
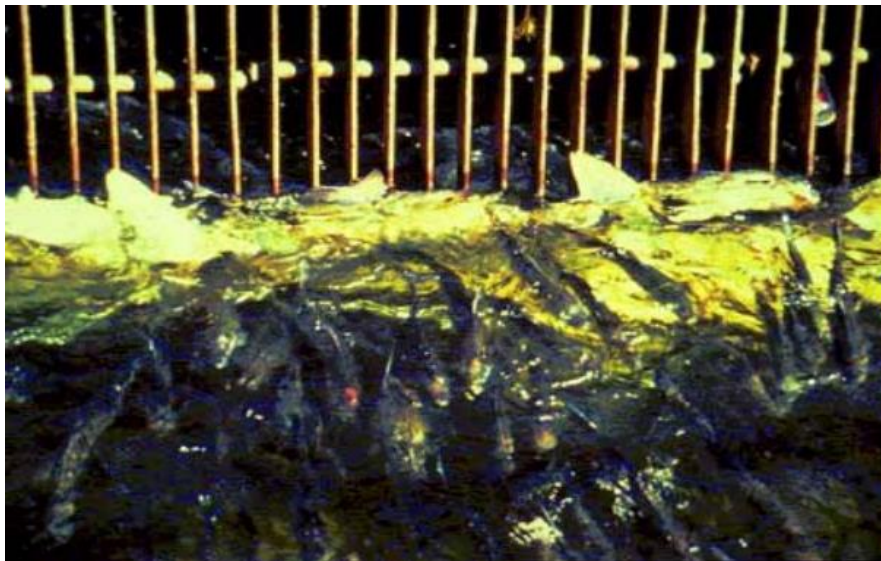
Figure 4 - Impingement of downstream migrating adult American shad on racks at a powerhouse intake. (Larinier, 2001).

However, the mortality rate of eels passing through the turbine may be high, depending upon the characteristics of the turbine and the mode of operation of the plant (Gosset et al., 2005; Durif et al., 2003). The consensus is that small and higher speed turbines do the most damage. For example, measured mortality rates of eels along the East Coast of North America have varied between 20-100% for Kaplan turbines and 6-76% for Francis (Gulf of Maine Council on the Marine Environment, 2007; Haro et al., 2000). Losses in the Francis turbines are affected by hydrodynamic factors such as absolute and relative velocities at the vanes entrance, speed of

revolution and the length of the fish relative to the mean distance between the vanes but the Kaplan is just affected by the mean distance between the blades (EPRI, 1999).

Research has shown that the mortality rates of migrant eels in their silver-phase passing through the turbines are no doubt significant, but the knowledge on the behavior of this specie in response to the downstream passage facilities and its effects are still not fully understood. This is associated with the fact that there is no certainty as to when the migration period of the American eel begins. Haro *et al.* (2000) cites various authors relating their migration period to high or low flow, lunar phase, and water temperature. However, the consensus thus far is that migration occurs during a broad period in fall (approximately September to December) (EPRI, 1999). Telemetry studies have however confirmed that movement occurs primarily at night but at various depths. In order to develop effective intake protection facilities to mitigate the turbine entrainment mortality of the eels, downstream migratory behaviors and responses must be characterized. These parameters affect the effectiveness of bypass entrances and help to determine the applicability of surface versus deep structures and whether the eels search for variable exit hydraulics in the forebay or are they passively entrained through trash racks (Haro et al., 2000).

The behavior of eels has been found to be unlike other downstream migrants, due to their ability to move through canal systems at various depths as opposed to surface-oriented species such as the Atlantic salmon smolts. Eels are described as weak swimmers for their size and at high approach velocities have difficulty avoiding racks or screens. There is lack of literature reporting the detailed in situ observations of the downstream swimming behavior of American eels. However, studies have been conducted with silver phase European eels in an experimental flume that indicate eels have three forms of downstream behavior: passive drift (absence of rheotactic behavior and almost no swimming activity), controlled drift (passive floating but actively conducts position and velocity corrections) and active downstream movement (front part of body slightly raised and rear actively executing swimming movements). The intensity of swimming behavior was found to be related to magnitude of the approach velocity (Haro et al., 2000; EPRI, 2001; Adam et al., 1997).

EPRI (2001) referred to a paper done by Adams, Schwevers and Dumont (1997) which noted that the downstream movement of the eels along the experimental channel always resulted in their collision with objects. No type of response to the barrier occurred until there was physical interaction. The eels exhibited a "startled" response after an intense collision and returned upstream. Flume studies done by Amaral et al. (2002) using American eels had similar observations of eel responses to barriers, which in that case were bar racks and louvers. Brown et al. (2007) also conducted testing on the behavior of downstream migrating eels at dam intakes in New Zealand. The native longfin eels (*Anguilla dieffenbachia*), also a declining population, were used in the study to evaluate the passage routes of the eels using three-dimensional (3D) acoustic

telemetry. Their results were similar to those found in previous studies where no evident trends were found in the determination of passage routes; however combinations of the following searching behaviors were observes before the eels committed to a specific route. These behaviors included: 1) upon encountering the trash rack the eels made a quick, sprint like upstream movement, 2) vertical searching movements, swimming up and down within the water column at or near the trash racks, (3) horizontal searching movements, swimming along the trash racks in a guided movement of the forebay when they encountered the trash racks, and (4) circling movement in small upstream movements at the trash racks and/or throughout the entire forebay.

2.4 Case Studies: Response of Eels to Bar Racks

Russon et al. (2010) researched the response of European eels (Anguilla anguilla) to bar racks at a downstream intake protection facility. The European eel similar to the American eel has had significant decline in its population, which prompted the European Union has passed a legislation that requires member states to meet escapement targets of 40% eel biomass. However, the very same screening systems that have been employed to mitigate fish entrainment by the turbine or divert downstream migrants to bypass facilities can result in mortality. This mortality rate may be due to impingement of the eels on the screens at high velocities, poor design of screens or the weak burst swimming capacity of the eels.

The study by Russon et al. (2010) assessed the behavioral response to the bar racks by using glass-walled recirculatory flume to perform two experiments. These experiments consisted of using racks at different angles on either the horizontal plane relative to the flow or the vertical plane relative to the channel floor. Velocities were chosen based on those typical of hydropower reservoirs. The efficiency of the racks was assumed to increase with low rack angles relative to the flow or the channel flow and low discharge.

Under the experimental conditions created, eels tend to exhibit behavioral avoidance only after encountering the physical structure that increases their risk of impingement at high velocities. This is opposite reaction of the Atlantic and Pacific salmon smolts that have been found to avoid abrupt velocity gradients. There was a clear advantage found in using angled racks, as opposed to those placed vertically and perpendicular to flow. This would provide better guidance efficiency and reduce probability of impingement. The most effective angles found were those <45 degrees on the vertical or horizontal planes, with the probability of impingement higher at more acute angles. The approach velocity at which the eels managed to escape was 0.9 m/s, however further research is necessary.

Similar research was done by Amaral et al. (2001) in an attempt to develop information on the efficiency of fish guidance using angled bar racks and louvers on different riverine fish species including the American eel. An indoor flume was also used in this experiment with estimated

length of 80 feet (24.4 m), width of 6 feet (1.7 m) and depth of 7 feet (2.1 m). The flume was readily adaptable to test different rack angles, slat orientations, bar spacings, water velocities and bypass configurations. The rack angles tested were 45 and 15 degrees, with the flow rate ranging from approximately 28.2 cfs (0.8 m^3/s) (approach velocity of 0.98 ft/s (0.3 m/s)) to 88.3 cfs (2.5 m^3/s) (approach velocity of 2.95 ft/s (0.9 m/s)). The water depth was maintained between 5.4 and 5.6 feet (1.65 and 1.72 m). The bar slat spacings were 1.0 and 2.0 inches (25 and 50 mm) for the bar rack configuration and 2 inches (50 mm) for the louver array. The evaluation was completed over a time period of two years, with the American eel demonstrating the highest guidance efficiencies of the tested species at the 45 degree structures but increased substantially for the tests with the 15 degree structures.

The important parameters that were found to influence the guidance efficiency included slat orientation, array angle, slat spacing, approach velocity, the use of a solid bottom overlay, and fish species and size. The consensus found was that the 15 degree structures had higher guidance efficiency than the 45 degree structures and guidance efficiency decreased with increasing approach velocity. Field testing was recommended in order to verify these results and determine the design parameters that will be critical for future applications.

These case studies therefore provide a platform for the experimental conditions required to design a suitable intake structure to aid in the safe downstream passage of the American eel. There will be further research into the use of angled bar racks but emphasis will be placed on the spacing of the bars. The following sections provide background on the numerical modeling of the bar racks and the use of head loss equations to predict the hydraulic performance of the intake structures and their subsequent effect on power generation.

2.5 Numerical Methods of Modeling Physical Barriers

Numerical modeling is a powerful tool used to visualize the dynamic behavior of physical systems. Computer simulations such as the Computational Fluid Dynamics (CFD) model are effective in simulating the hydraulic patterns that occur at the intake structures for the safe passage of the eels. However, before the CFD model can be used, preliminary calculations are required for better applicability. Anderson (2009) highlights in his attempt to define computational fluid dynamics that there are three fundamental principles that govern the physical aspects of fluid flow, which are the conservation of mass, Newton's second law and the conservation of energy. These fundamental principles can be represented by mathematical equations but computational fluid dynamics (CFD) replaces these equations with numbers so that a solution can readily be ascertained. The CFD models help to predict the efficiency of the bar racks at preventing the eels from being entrained and also head loss that occur at different spacings without physical tests

2.5.1 Governing Equations

The governing Navier –Stokes equations for the unsteady, incompressible and turbulent fluid flow in a Cartesian co-ordinate system, the continuity equation and the equations of the *k-e* turbulence model (Montazeri-Namin et al., 2012; Christakis et al., 2002) are shown as follows:

Navier –Stokes equation:

$$\rho \frac{\partial u^i}{\partial t} + \rho u^j \frac{\partial u^i}{\partial x^j} = -\frac{\partial p}{\partial x^i} + \frac{\partial}{\partial x^j}\left[\mu\left(\frac{\partial u^i}{\partial x^j} + \frac{\partial u^j}{\partial x^i}\right)\right] + \frac{\partial \tau^{ij}}{\partial x^j} + \rho g^i \qquad \textbf{(Equation 1)}$$

Continuity equation:

$$\frac{\partial u^i}{\partial x^i} = 0 \qquad \textbf{(Equation 2)}$$

where u^i, p, ρ and l are the mean fluid velocity components, pressure, density and molecular viscosity of the fluid flow, respectively. τ^{ij} is known as the Reynolds stress tensor, which represents the effects of the turbulent fluctuations in the fluid flow.

As far as predicting the free surface by implementing the VOF method (Hirt and Nichols, 1981), the volume fraction of the water, F, has been introduced in a computational cell and is defined as follows:

$$F = \frac{\delta\Omega_{water}}{\delta\Omega_{cell}} \qquad \textbf{(Equation 3)}$$

where $\delta\Omega_{cell}$ is the volume of the computational cell and $\delta\Omega_{water}$ is the fraction of the volume of the cell filled with water. Therefore, we have F = 1 when the cell is full of water, F = 0 when the cell is full of air and 0 < F < 1 when the cell contains a free surface.

k equation:

$$\frac{\partial(\rho k)}{\partial t} + \frac{\partial(\rho u_i k)}{\partial x_i} = \frac{\partial}{\partial x_i}\left[\left(\mu + \frac{u_t}{\sigma_k}\right)\frac{\partial k}{\partial x_i}\right] + G - \rho\varepsilon \qquad \textbf{(Equation 4)}$$

ε equation:

$$\frac{\partial(\rho\varepsilon)}{\partial t} + \frac{\partial(\rho u_i \varepsilon)}{\partial x_i} = \frac{\partial}{\partial x_i}\left[\left(\mu + \frac{u_t}{\sigma_\varepsilon}\right)\frac{\partial\varepsilon}{\partial x_i}\right] + C_{1\varepsilon}\frac{\varepsilon}{k}G - C_{2\varepsilon}\rho\frac{\varepsilon^2}{k} \qquad \textbf{(Equation 5)}$$

where ρ = volume fraction average density; t = time; u_i = velocity component in x_i coordinate (*i* = 1,2,3); μ = volume fraction average molecular viscosity; $C_{1\varepsilon}$ = 1.44; $C_{2\varepsilon}$ = 1.92 (constants of the ε equation); and G = generation of turbulent kinetic energy which can be given as:

12

$$G = \mu_t \left(\frac{\partial u_i}{\partial x_j} + \frac{\partial u_j}{\partial x_i} \right) \frac{\partial u_i}{\partial x_j} \qquad \text{(Equation 6)}$$

where μ_t = turbulent viscosity and it can be calculated as:

$$\mu_t = \rho C_\mu \frac{k^2}{\varepsilon} \qquad \text{(Equation 7)}$$

where C_μ = 0.09 (experimental constant); σ_k =1 (turbulence Prandtl numbers of k); and σ_ε = 1.33 (turbulence Prandtl numbers of ε).

2.5.2 Multiphase Modeling

The volume of fluid (VOF) model is used to simulate the free surface profile associated with open channel flows. The existence of the free surface between the moving water and the atmospheric air above it indicates that the flow is governed by the forces of gravity and inertia. The VOF method relies on the fact that the two fluids (water and air) are immiscible and uses a single set of momentum equations to track the change in volume fractions of each fluid throughout the computational domain. The sum of the fractions of water and air is 1 in each computational cell, as shown in the following mathematical formulation (Montazeri-Namin et al., 2012).

$$\alpha_w + \alpha_a = 1 \qquad \text{(Equation 8)}$$

According to the law of mass conservation of air and water, the subsequent differential equation of volume fraction of water shown below can be solved to determine the interface between water and air.

$$\frac{\partial \alpha_w}{\partial t} + u_i \frac{\partial \alpha_w}{\partial x_i} = 0 \qquad \text{(Equation 9)}$$

Basically, the VOF method follows regions rather than surfaces with minimum storage requirements. The VOF method would therefore not be a logical choice for problems with intersecting surfaces. It is applicable to three-dimensional computations, with the advantage of its conservative use of stored information. Therefore, the VOF method provides a simple and economical way to track free boundaries in two- or three-dimensional meshes. However, if the surface boundary does not remain fixed in the fluid, then Equation 9 must be modified (Hirt and Nichols, 1981; Christakis et al., 2002).

2.5.3 Bar Rack Head Loss Calculations

An important issue for hydroelectric plant operators is the impact of the head losses produced by the physical barriers on power generation. Several equations have been proposed to aide in the assessment of head losses due to physical barriers such as angled trash racks or bar racks. The first equation to come to mind is the Kirschmer equation (1926), however this equation which

accounts for the bar shape factor K_F, angle α, bar thickness b, and bar spacing e was originally proposed only for vertical or inclined trash racks (angled to the channel floor). The equation was therefore useless for application to angled trash racks (angled to the channel wall). Mosonyi (1966) rectified this discrepancy by modifying Kirschmer's equation to include angled trash racks between 90 and 30 degrees. The Kirschmer-Mosonyi equation (Eq. 10) utilizes most of Kirshmer's factors but includes a multiplicative term $K_{K.-M.}$. Mosonyi provides tabulated values of this factor, which depends on the ratio of bar spacing to thickness (e/b) and the angle α of the approach flow.

$$K_{Kirschmer-Mosonyi} = K_F \left(\frac{b}{e}\right)^{\frac{4}{3}} K_{K.-M,}$$ **(Equation 10)**

Meusburger (2002) also referred to Kirschmer (1926) for his equation, by using the bar shape factor K_F. His proposed equation (Eq. 11) accounted for blockage ratio O_g and rack angle α. However, the blockage ratio only considers the blockage resulting from the screen (the bars, spacers, diagonal brace and the screen supports) that lie between 10 and 40% for power stations in Switzerland. Blockage caused by debris, which is relevant for head loss and typical for most hydropower facilities, has been disregarded and would result in a factor of loss approximately 110% higher than it would be based on these correlations.

$$K_{Meusburger} = K_F \left(\frac{O_g}{1-O_g}\right)^{1.5} \left(\frac{\alpha}{90°}\right) O_g^{-1.4\tan(90°-\alpha)}$$ **(Equation 11)**

Clark *et al*. (2010) conducted experiments on trash racks in an open channel flow and submerged conditions using piezometer taps. Their proposed head loss equation (Eq. 12) accounts for blockage ratio, approach flow angle and bar shape. They concluded that using non-rectangular bars reduced head loss and the water surface disturbance from open channel experiments are negligible. However, although the equation is simpler it only focuses on set parameters of 0.17 and 0.039 feet (0.053 and 0.012 m) for clear spacing and bar thickness, respectively during the experiments with angled trash racks. The only changing factor was the angle α which was between 90 and 60 degrees, so it is not applicable for different values of e and b.

$$K_{Clark} = 7.43\eta[1 + 2.44\tan^2(90° - \alpha)]O_g^2$$ **(Equation 12)**

According to Raynal *et al.* (2013), Zimmermann (1969) conducted testing for his equation in a straight channel with the trash rack perpendicular to the channel and the bars would rotate between angles 90 and 45 degrees, similar to louvers. This method was notably different from that of Meusburger (2002) and Clark *et al.* who used specific flume configurations with oblique approach flows, which is not representative of a typical hydropower plant due to the alignment of the flow with bars. Zimmermann's equation (Eq. 13) accounts for ratio between clear spacing and bar thickness (b/e) and also bar thickness and bar depth $+(b/p)$.

$$K_{Zimmerman} = 3.87 \tan^{7/4}(90° - \alpha) + K_F \left(\frac{b}{p}\right)^{4/3} + \frac{K_F}{\sin^3(\alpha)}\left[\left(\frac{b}{e}\right)^{4/3} - \left(\frac{b}{p}\right)^{4/3}\right]$$

(Equation 13)

Idel'chik (1966) and Spangler (1929) formulated of values showing the relationships for various approach flows, bar shapes and clear spacings. Idel'chik (1969) focused on two conditions, where the approach flow is straight ($\alpha = 0$) or oblique ($\alpha > 0$). However, Spangler (1929) concentrated on the relationship between the angle of approach and the bar shape.

Raynal *et al.* (2013) is the newest addition to the proposed head loss coefficient equations, where experiments were conducted in a straight flume with trash racks of rectangular and hydrodynamic bars. The Raynal et al. equation (Eq. 14) accounted for three parameters: blockage ratio O_g, bar shape and the ratio of bar thickness and bar depth (b/p) that would have an effect on the rack angle α. The study only focused on bar shape and blockage ratio, as the bar thickness and depth were fixed at $p = 1.6$ inches (40 mm) and $b = 0.2$ inches (5 mm). Their equation was similar to Meusburger (2002), where the K_i depends on the bar shape and K_α depends on the blockage ratio, angle of the rack and bar shape. Several limitations make this equation only applicable for blockage ratios between 36 and 60%, rack angles between 90 and 30 degrees, rectangular or profiled bars with horizontal spacers and (b/p) ratio close to 0.125.

$$K_{Raynal} = K_i \left(\frac{O_g}{1-O_g}\right)^M K_\alpha; \ K_\alpha(K_F, O_g, \alpha) = 1 + k_i \left(\frac{90°-\alpha}{90°}\right)^{2.35} \left(\frac{1-O_g}{O_g}\right)^3$$

(Equation 14)

However, all these equations are based on the principle of conservation of energy demonstrated by the Bernoulli's energy equation (Eq. 15) (Chow, 1959). The mean velocities (V_1 and V_2) and water depths upstream and downstream (y_1 and y_2) could be readily measured in flume testing, which was the option for most authors. Upstream and downstream mean velocities are quite important for calculating head losses, since angled racks have higher losses which alters the flow through the rack and causes water-depth measurements to experience greater errors (Raynal *et al.* 2013).

$$y_1 + \frac{V_1^2}{2g} = y_2 + \frac{V_2^2}{2g} + \Delta H \qquad \text{(Equation 15)}$$

Therefore, head loss due to the rack ΔH depends on the head loss coefficient of resistance K_g and the upstream velocity head (Eq. 16) (Chow, 1959; Idel'chik, 1966; Raynal *et al.* 2013).

$$\Delta H = K_g \frac{V_1^2}{2g} \qquad \text{(Equation 16)}$$

2.6 Summary

Decline in the population of the American eel has forced the U.S. Fish and Wildlife Service (FWS) to prescribe smaller spacings and lower intake approach velocities for dams on the eastern seaboard. Protection of this species during their downstream migration has become imperative, which has led to research on the design of the bar racks at the dam intakes to prevent entrance to the turbine or impingement. These bar racks are essentially physical barriers that must be designed with the consideration of spacing, approach flow and array angle. The effectiveness of these designs can be evaluated using physical models and telemetry studies. Numerical modeling was also introduced as a method of predicting hydraulic performance and head loss equations have been developed by previous researchers to provide operators with a means of calculating the effect on power generation at different design conditions. Additional hydraulic and biological analyses to assess the effectiveness of impacts of bar rack design on head loss and eel passage are described in the subsequent chapters of this thesis.

3.0 METHODOLOGY

The goal of this research was to evaluate design parameters for bar racks that would provide safe passage for the American eels at hydropower dam facilities and also have minimal operational and engineering impacts on power generation. The scope of the research involved two parts: a hydraulic evaluation and a biological assessment. The hydraulic evaluation utilized site assessments to gain actual conditions at a hydropower facility, numerical modeling and laboratory evaluations to determine the potential hydraulic impacts on the operation of the facility and subsequent power generation. Then the biological aspect was completed with live eels to test the guidance efficiency of the bar rack at different design parameters and also provide validation for the hydraulic evaluations. This chapter provides the methods used to achieve the goal of this thesis.

3.1 Hydraulic Evaluation

Restrictive measures such as the bar racks have been prescribed by the U.S. Fish & Wildlife Service (FWS) to reduce turbine entrainment and mortality of the American eels. These intake structures are intended to guide the eels to bypass facilities to ensure their safe downstream passage. The installation the bar racks have specific parameters required by the FWS that include 0.75 inch (19 mm) clear spacing and a reduction of the intake approach velocity of no greater than 1.5 ft/s (0.46 m/s). However, the effects of reducing the clear spacing and the approach velocity on the operation of the hydropower project have not been previously evaluated. Also, minimal research has been completed in regards to the American eel, so specific changes in head loss associated with the reduced bar spacing still cannot be accurately predicted. Therefore, the effectiveness of these measures and their potential impacts on the hydropower industry are still unclear. In order to test these theories, the following objectives were completed. First, site assessments were conducted to gather information on the specific factors that influence the effectiveness of implemented fish passage designs at hydropower facilities. Then, numerical modeling was completed using Computational Fluid Dynamics (CFD) software to evaluate the hydraulic performance of bar rack designs based on the determined factors for a standard facility. Lastly, physical modeling was conducted as a means of comparison and validation of the proposed bar rack designs and a new head loss equation was developed based on the results.

3.1.1 Site Assessments

The first objective was to determine the specific factors that influence the effectiveness of the implemented fish passage facilities at hydropower facilities. This objective was achieved by conducting site assessments, which involved visiting hydropower facilities to conduct visual inspections and interviews or informal surveys.

3.1.1.1 Visual Inspection

Hydropower facilities were chosen based on their implemented fish passage facilities. Some of these facilities included the Holyoke Project (Hadley Falls Station and Holyoke Canal), Cabot Station, Turners Falls Project (Connecticut River) and the Woronoco Hydro, Westfield River. Inspected facilities were focused in the New England area due to proximity and existing implementation of the prescribed bar racks required by the U.S. Fish & Wildlife Services (FWS). Inspection involved photographs being taken and discussions with the operators to get their insight on the fish passage design and its impact on the operation of the facility.

3.1.1.2 Hydropower Facilities Survey

Interviews or informal surveys were conducted with operators or staff at hydropower facilities that have incorporated fish passage designs to enable the safe passage of the American eel. The facilities visited or contacted were mainly in the New England area. The questions focused on the effectiveness of the FWS bar rack design prescriptions and the subsequent impacts on the operation of the hydropower facility. The list of interview questions is shown in Appendix A.

3.1.2 Physical Modeling

The laboratory testing was conducted in a re-circulatory flume with a length of 80 feet (24.4 m), a width of 6 feet (1.8 m) and a depth of 7 feet (2.1 m) at Alden Research Laboratory (Alden), as shown in Figure 5. Fabrication of infrastructure and actual experiments were completed during the period of March 2013 to May 2013. The flow rate was controlled by adjusting a variable speed pump. The water level was modified by adjusting the total water volume in the flume.
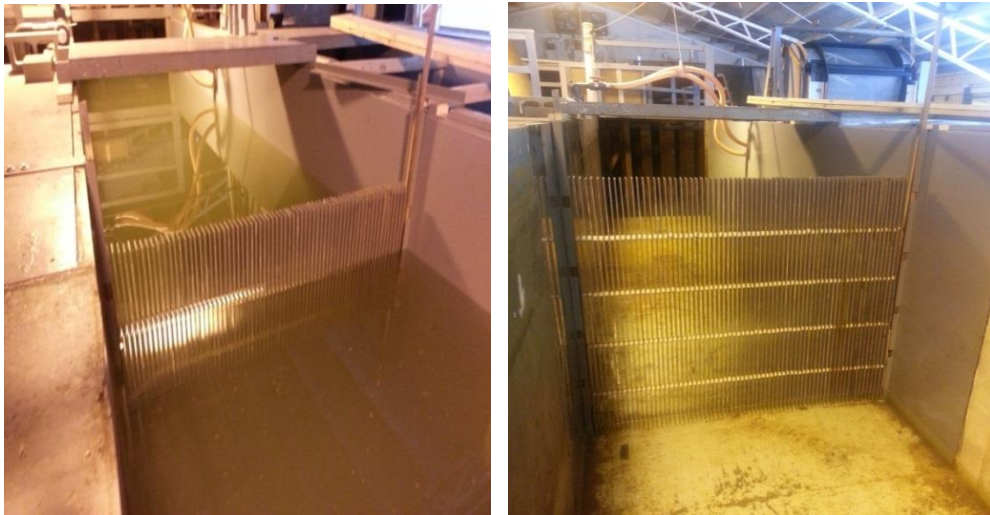
Figure 5 - Flume used for laboratory evaluations with 90 degree bar rack.

The flume layout (plan view) of the configurations of the 90 and 45 degree angle bar racks in the channel are shown in Figure 6. The rack height was approximately 6 feet and at the entrance to the channel there are fixed screen that straightens the flow as it approaches the rack. Velocity measurements were taken 6.6 feet (2.0 m) upstream and 3.9 feet (1.2 m) downstream from the center of the rack.

Initial tests were completed to ensure the apparatus would be able to provide the experimental conditions that represent ideal flow conditions approaching a hydropower facility. Tracer analysis using dyes was conducted to ensure plug flow conditions or laminar flow of constant velocity approaching the bar racks and also to ascertain flow patterns at the bar racks.
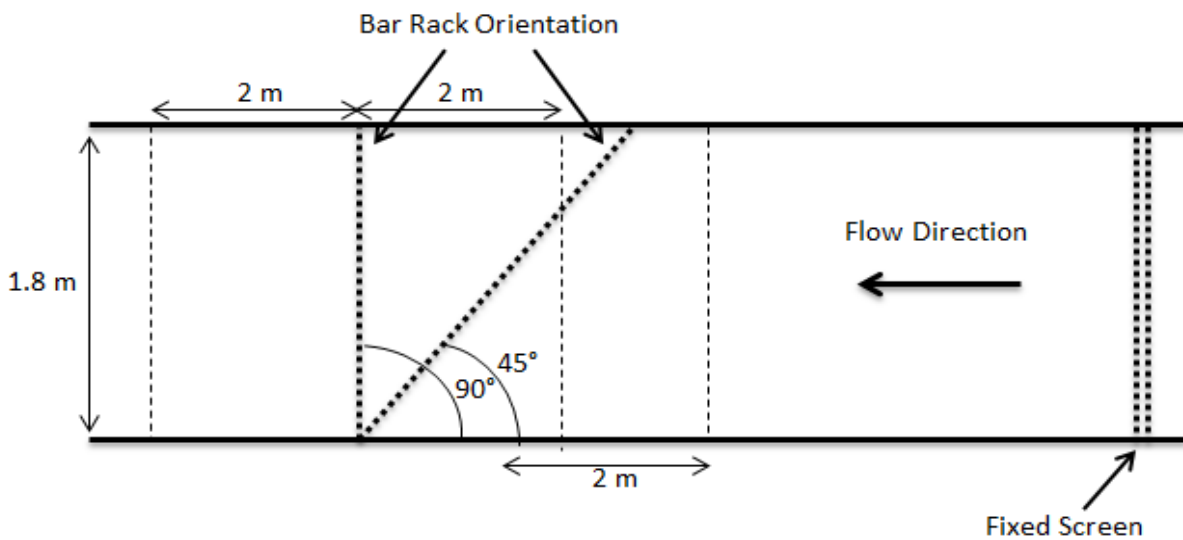
Figure 6 - Plan view of flume layout.

Experiments were conducted using steel slats with dimensions of 3 inches (76.2 mm) in length and 0.25 inches (6.3 mm) in width. The steel slats were separated by spacers and held together by four horizontal cross members. Spacers of different sizes were used to create the three clear bar spacings selected for testing (0.75, 1.00, and 1.50 inches (19, 25 and 38 mm)). These bar racks were placed vertically in the flume at angles of 90 and 45 degrees for each evaluation.

The bar rack angles and approach velocities 1.5, 2.0 and 2.5 ft/s (0.46, 0.61 and 0.75 m/s) were alternated between trials, while the depth of 1.5 meters (5 feet) was maintained. Approach velocities 6.6 feet (2.0 m) upstream and 3.9 feet (1.2 m) downstream of the bar racks were measured using a SONTEK Acoustic Doppler Velocimeter (ADV) (Figure 7) at nine points within the cross section of the flow in the flume.

Figure 7 - SONTEK Acoustic Doppler Velocimeter.

The velocity measurements were recorded using the ADV data acquisition system, version ADF 4.0 and the data files were displayed using the HorizonADV software. The approach velocities were selected to match those found at typical hydroelectric facilities. Pressure change was measured by installing pressure taps in the flume floor connected to a manometer board or differential pressure transducers (Figure 8).

Figure 8 - Manometer board and Amprobe 34XR-A True-rms Digital Multimeter.

Debris loading was evaluated by using barriers to block flow through sections of the bar racks and head loss was measured. Wooden planks were used as the barriers in a grid that was designed to rest against the rack with the pressure from the approaching flow to keep it in place, as shown in Figure 9. Debris loading was conducted for 20, 40 and 60 percent blockage ratios.

Blockage ratios (O_g) were calculated by determining the difference between the total open area of the wooden barrier and the blocked area bar rack and then calculating the ratio of the area blocked by debris to the open area of the remaining bar rack. Equations 17 and 18 show the variables considered: blockage ratio of the bars and spacers (O_b) and blockage ratio of the debris loading (O_d)

$$O_b = N_b * b * l + N_b * e * h \qquad \text{(Equation 17)}$$

$$N_b = \frac{l * w}{(b + e) * l}$$

$$O_d = [(L * W) - (N_B * b * L + N_B * e * h)] - \left[s\big((l * w) - O_b\big)\right] \quad \text{(Equation 18)}$$

$$N_B = \frac{L * W}{(b + e) * L}$$

where $N_b, b, l, e, h, w, L, W, s$ and N_B are the number of bars within one open grid of the debris loading, the bar thickness, the height of the each immersed grid, the clear spacing between each bar, the diameter of the spacers, the width of each open grid, the height of the immersed bar rack at each angle to the flow, the width of the bar rack across the channel, the number of open grids of the debris loading and the number of bars within the immersed bar rack spanning the channel, respectively.

Figure 9 - Debris loading testing completed using wooden planks against the bar rack.

3.1.3 New Proposed Head Loss Equation

Based on the data gathered from the physical modeling, a new head loss equation was developed to provide hydropower plant operators with an easier method of predicting the impact on power generation at different bar rack design parameters. The assumptions for this equation are as follows:

- Head loss (H_L) is proportional to the number of bars that the flow must pass by or alternatively, the number of openings that the flow must pass through
- Length of the bar rack (L) is proportional to the number of bars/number of openings. For a given alignment of the rack, the length is given by:

$$\cos \theta = \frac{W}{L} \ or \ L = \frac{W}{\cos \theta} \qquad \text{(Equation 19)}$$

The number of bars in the rack is estimated by:

$$N_{bar} = \frac{L}{b+e} \qquad \text{(Equation 20)}$$

      where:
      W = width of the channel (feet)
      N_{bar} = number of bars
      θ = array angle
      b = thickness of each bar
      e = width of the each spacing

If $\theta = 0$, then $\cos \theta = 1$ and W=L

Head loss (H_L) can then be approximated as:

$$H_L = H_{L_{bend,up}} + H_{L_{cont}} + H_{L_{exp}} + H_{L_{bend,down}} \qquad \text{(Equation 21)}$$

      where:
      $h_{L_{bend,up}}$ = head loss at upstream bend
      $h_{L_{bend,down}}$ = head loss at downstream bend
      $h_{L_{cont}}$ = head loss at contraction as flow approaches rack
      $h_{L_{exp}}$ = head loss at expansion as flow leaves rack

Since it is advantageous to define the losses in terms of the velocity at the rack, the equation is expressed in terms of V_{rack} (velocity between the bars) instead of V_{up} (velocity upstream), which gives the expression:

$$V_{up} * A_{up} = V_{rack} * A_{rack} \qquad \text{(Equation 22)}$$

Given:

$$A_{up} = W * H_{up} \qquad \text{(Equation 23)}$$

$$A_{rack} = \frac{e}{b+e} * L * H_{rack} \qquad \text{(Equation 24)}$$

Variations in H_{up} and H_{rack} are neglected. Equations 22 and 23 are then substituted into equation 21:

$$V_{up} * W * H_{up} = V_{rack} * \frac{e}{b+e} * L * H_{rack} \qquad \text{(Equation 25)}$$

$$V_{up} = V_{rack} * \frac{L}{W} * \frac{e}{b+e} \qquad \text{(Equation 26)}$$

However from equation 19, we get:

$$V_{up} = V_{rack} * \frac{1}{\cos\theta} * \frac{e}{b+e} \qquad \text{(Equation 27)}$$

where:
V_{up} = Upstream velocity (ft/s)
A_{up} = Area of upstream channel (ft^2)
V_{rack} = Average velocity between the bars (ft/s)
A_{rack} = Area of total openings in bar rack (ft^2)
H_{up} = Depth of water upstream (ft)
H_{rack} = Depth of water at rack face (ft)

Consideration is also required for what happens if the rack is blocked. This percentage blockage (O_g) would reduce the area of the rack:

$$O_g = \frac{A_{blocked}}{A_{total}} = \frac{1 - A_{open}}{A_{total}} \qquad \text{(Equation 28)}$$

If there is no blockage equation 25 would apply but if there is blockage:

$$A_{open} = A_{rack} = \left(\frac{e}{b+e} * L * H_{rack} \right) * (1 - O_g) \qquad \text{(Equation 29)}$$

Then:

$$V_{up} * W * H_{up} = V_{rack} * \frac{e}{b+e} * L * H_{rack} * (1 - O_g) \qquad \text{(Equation 30)}$$

Neglecting variations between the H_{up} and H_{rack}:

$$V_{up} = V_{rack} * \frac{1}{\cos\theta} * \frac{e}{b+e} * (1 - O_g) \qquad \textbf{(Equation 31)}$$

$$V_{rack} = V_{up} * \cos\theta * \frac{b+e}{e} * \left(\frac{1}{1-O_g}\right) \qquad \textbf{(Equation 32)}$$

The head loss equation can be formulated considering the minor loss coefficients. It is expected that the head loss expression is in the form (recall Eq. 21):

$$H_L = H_{L_{bend,up}} + H_{L_{cont}} + H_{L_{exp}} + H_{L_{bend,down}}$$

However, head loss is expressed as the product of a constant (k_α) and the velocity head $\left(\frac{V^2}{2g}\right)$ as shown in Eq. 33:

$$H_{L_\alpha} = k_\alpha * \frac{V^2}{2g} \qquad \textbf{(Equation 33)}$$

where k_α depends the specific minor loss being considered. In this case, coefficient can be specified for the upstream bend $(k_{bend,up})$, downstream bend $(k_{bend,down})$, the entrance at the bar rack (k_{cont}), and the exit from the bar rack (k_{exp}). The velocity head may depend on upstream velocity (V_{up}) or the velocity through the rack (V_{rack}) (Eq. 32), depending on how the loss is interpreted. In this case, the head loss equation takes the form:

$$H_L = \left(k_{bend,up} + k_{bend,down} + k_{cont} + k_{exp}\right) * \frac{V^2}{2g}; \text{ with } V = V_{up} \text{ or } V_{rack} \quad \textbf{(Equation 34)}$$
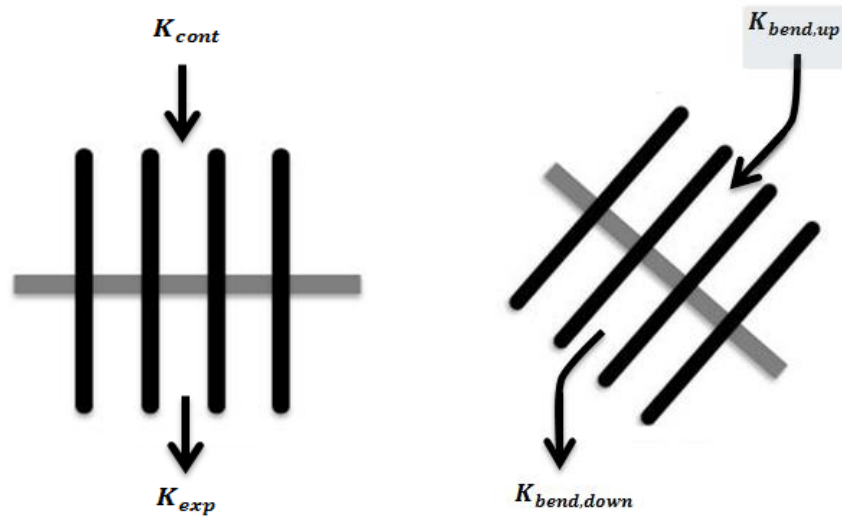
Figure 10 - Bar rack configurations for the 90 (left) and 45 (right) degree structures with minor loss coefficients associated with approaching flow.

24

Figure 10 shows the 90 and 45 degree bar rack structures and the approach flow minor loss coefficients. For the 90 degree bar rack, k_{cont} and k_{exp} depend on the velocity between the bars (V_{rack}), but for the 45 degree structure, $k_{bend,up}$ and $k_{bend,down}$ depend on both velocity upstream (V_{up}) and the velocity between the bars.

The equation can then be written as:

$$H_L = \left[(k_{bend,up} + k_{bend,down}) * \frac{V_{up}^2}{2g}\right]$$
$$+ \left[\left((k_{bend,up} + k_{bend,down}) + (k_{cont} + k_{exp})\right) * \frac{V_{rack}^2}{2g}\right]$$

(Equation 35)

In terms of V_{up}:

$$H_L = \left[(k_{cont} + k_{exp}) + (k_{bend,up} + k_{bend,down}) + \left((k_{bend,up} + k_{bend,down}) *\right.\right.$$
$$\left.\left.\left(\frac{1}{\cos\theta} * \frac{e}{b+e} * (1 - O_g)\right)^2\right)\right] * \left[\frac{\left(V_{up}*\cos\theta*\frac{b+e}{e}*\left(\frac{1}{1-O_g}\right)\right)^2}{2g}\right]$$

(Equation 36)

where: k_{cont} and k_{exp} are both 0.2; $k_{bend,up}$ and $k_{bend,down}$ are both 0.65. The correlation coefficient, calculated for all the measured head-loss coefficients and those predicted by Eq. (33), was approximately 98.6%. The proposed equation is applicable to bar racks inserted in a straight channel, with blockage ratio Og between 36 and 60%, angle from wall α between 90° (perpendicular to flow) and 30°, and for rectangular bars with horizontal spacers.

3.1.4 Numerical Modeling

The second objective was to evaluate the prescribed bar rack design parameters using Computational Fluid Dynamics (CFD) to model the hydraulic performance. In order to evaluate the hydrodynamics that may occur at the bar racks, simulations were completed using 18 unsteady, free-surface, three-dimensional CFD code that solved the Reynolds-averaged Navier- 19 Stokes equations in conjunction with a two-equation turbulence model.
These simulations were completed using ANSYS FLUENT 14.0, a commercial software package, to characterize the flow patterns that occur at the bar racks. The numerical model configuration was used to simulate the actual conditions in the experimental setup for each condition evaluated during the physical laboratory.

3.1.4.1 Model Geometry

A 3D model of the re-circulatory flume that was used to complete the hydraulic testing was developed using the ANSYS Workbench 14.0 DesignModeler. The model was developed based on the same scale as the experimental flume with the dimensions of 80 feet (24.4 m) in length by 6 feet (1.8 m) in width by 7 feet (2.1 m) in depth. Figure 11 shows the CFD models of the flume with 90 and 45 degree bar rack orientations.
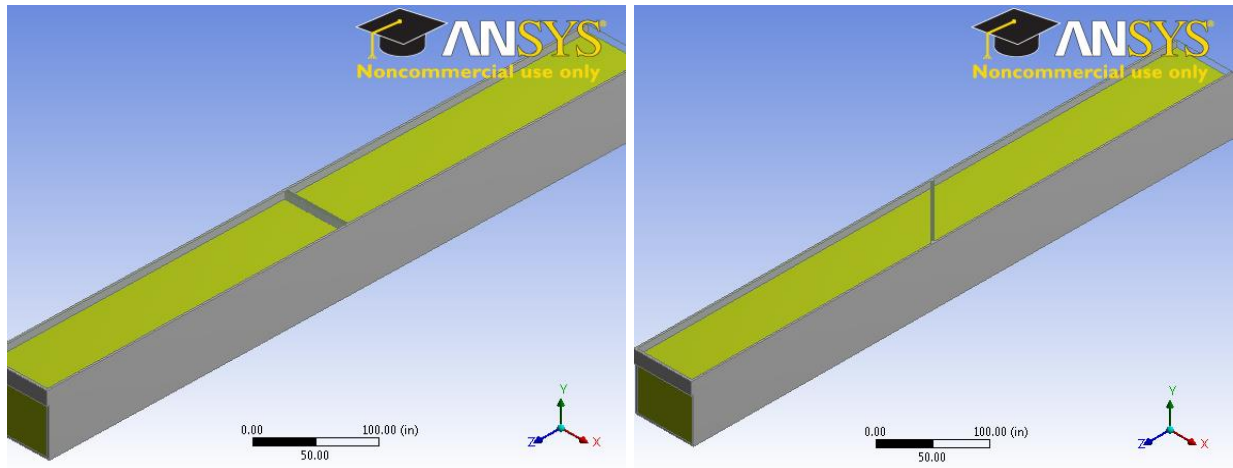
Figure 11 - CFD model of flume showing 90 and 45 degree bar rack orientation.

The bar racks were modeled using a rectangular EXTRUDED base with a width of 0.25 inch (6.3 mm) and 3 inches (76.2 mm) length at spacings of 0.75, 1.0 and 1.5 inches (19, 25 and 38 mm) per orientation (Figure 12). Dimensions were chosen such that the origin was located in the middle of the channel at half of the depth, with the flow in the negative z-axis direction and the y-axis was aligned with the positive vertical direction. The sketch of the channel cross section was done in the x-y plane, the rectangular sketches of the bars in the z-x plane and the circular sketches (diameter of 1 in.) for cross bars of the rack in the z-y plane. The channel was created using the SWEEP function along a path the length of the flume.

Since the CFD analysis was an open-channel flow problem, the FILL tool was used to simulate fluid within the channel after the frame was established. The FILL was achieved by using the cavity function by selecting all the surfaces the water or air would come into contact with when it was filled. After the fill was completed, the fluid was divided into 2 bodies using the slice by plane operation. This operation was done in order to improve the meshing and post- processing for the liquid and air regions in the CFD analysis. The slice plane was added by creating a new plane from the z-x plane with the offset of 2 feet (0.61 m) in the z-direction from the origin. This plane represented the approximate level of the water free surface.
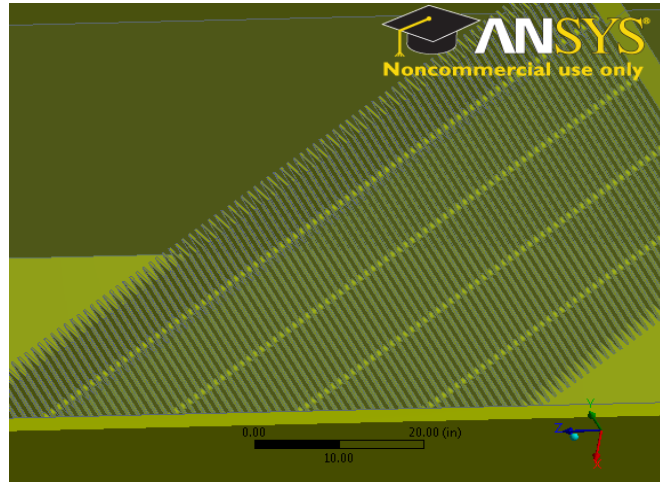
Figure 12 - CFD model showing the extruded bar rack at 45 degrees to the flow.

3.1.4.2 Mesh Generation

The ANSYS Workbench 14.0 Meshing software was used to generate the meshing required for CFD analysis. An automatic patch conforming algorithm was chosen for mesh control with the preference of the tetrahedron method. The advanced size function was used based on proximity and curvature, with the relevance center set to medium. The remaining size settings of smoothing, transition, and span angle center were set to medium, slow and fine, respectively. The default settings were retained for the curvature normal angle, proximity accuracy, number of cells across gap, minimum and maximum size of elements and faces, and growth rate. Body sizing method was also used with an element size of 2.5 inches (63.5 mm) and a chosen soft behavior, with default settings for curvature normal angle and growth rate (Figure 13).
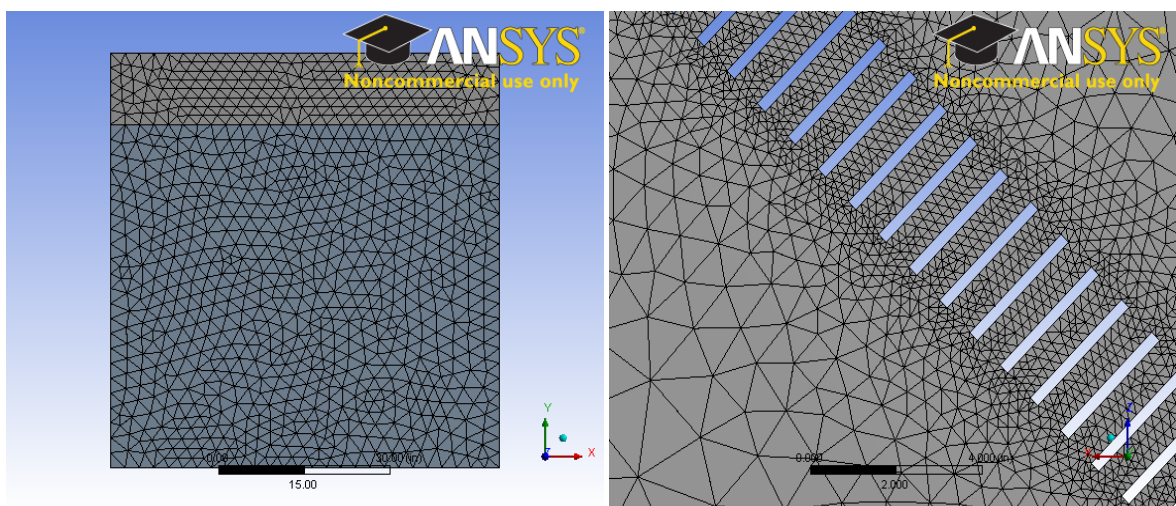
Figure 13 - Meshing of an inlet face and between bars showing effect of body sizing.

The resulting mesh for the flume with a 45 degree bar rack orientation consisted of 4,532,547 nodes and 23,951,281 elements, with a minimum skewness of 1.24E-05 and a maximum skewness of approximately 0.85. There was a minimum aspect ratio of 1.15 and a maximum of 15.48. Four named selections were created to define boundary conditions in the Fluent solver. The inlet and outlet were created for each of the liquid and air domains. The bodies of air and water were also named to distinguish the fluid characteristics.

3.1.4.3 Fluent Solver Setup

ANSYS Fluent 14.0 was used to perform the CFD analysis of the multiphase flow with free surface. A transient simulation was performed using the pressure-based solver and gravitational acceleration set to -32.2 ft/s^2 (-9.81 m/s^2) in the y-direction. The units were set to inches for length, ft/s for velocity and dyn/cm for surface tension. The volume of fluid (VOF) model was used to track the interface between the phases, with the open channel flow option enabled. The open channel flow option has been found to be an effective method for multiphase flows when the free surface is to tracked (Hirt and Nichols, 1981). The volume fraction was calculated using the explicit scheme with the implicit body force disabled. The turbulence model chosen was the realizable k-ε model with standard wall functions.

Water was added from the fluent database as an addition to the materials air and aluminum. For the primary phase, air was chosen due to the fact that the velocity measurements were to be performed using water as the working fluid in the flume evaluations. Water was chosen as the secondary phase, due to it having a greater density and weight than air which is important for the open channel flow option in the VOF model (ANSYS Inc., 2011). A constant surface tension coefficient of 73.5 dyn/cm was applied in the phase interaction setting in order to accurately model the interface between the two phases. The standard operating pressure of 101, 325 Pa was applied and a specified operating density of 1.225 kg/m^3.

The next step was to address the boundary conditions. This step is one of the most important factors in a successful CFD analysis, and is also one of the more challenging since there can be different approaches. In this case, the challenge was the appropriate treatment of the free surface. For the purposes of this research, the free surface was defined using the default setting of an interface, rather than representing it as a symmetry surface. For both the water and air inlets, instead of classifying them as velocity inlets, pressure inlet boundary conditions with the open channel option selected were chosen. The water was chosen as the secondary phase for the inlet. The free surface level was specified as 24 inches with the bottom level at -36 inches, which is the bottom of the channel or flume.

Pressure outlet boundary conditions with the open channel option were also used for the outlets. The turbulence settings were set to be the same as those for the inlet, with the backflow direction

specified to be normal to the boundary. Also, the same settings were used in the open channel settings with regard to the free surface and bottom levels. In the pressure outlet boundary condition, no velocity specification was required.

For the outlets, a pressure outlet boundary condition with the open channel option was used. The same turbulence settings as the inlets were used, with the backflow direction specified to be normal to the boundary. Also, the same settings were used in the open channel settings with regard to the free surface and bottom levels. In the pressure outlet boundary condition, no velocity specification is required.

3.1.4.4 Fluent Solution Methods

The PRESTO scheme was used for spatial discretization of pressure with the PISO scheme for pressure and velocity coupling. First order upwind schemes were used for momentum, turbulent kinetic energy, and turbulent dissipation rate. The geo-construct scheme was chosen for volume fraction, and a first order implicit scheme was used for the transient formulation. The solution controls or under-relaxation factors for pressure, density, body forces, momentum, turbulent kinetic energy, turbulent dissipation rate, and turbulent viscosity were 0.3, 0.5, 0.5, 0.7, 0.8, 0.8, and 1, respectively.

First the calculation was initialized by filling the entire domain with the air phase; then the water phase was patched into the appropriate cells which lie below the specified free surface level. The initial velocity of 1.5, 2.0 or 2.5 ft/s (0.46, 0.61 and 0.76 ft/s) was specified. A transient simulation was specified using a fixed time step size of 1 second, maximum iterations of 20 and an upper limit of 10 time steps.

3.2 Biological Assessment

The objective of the biological assessment was to evaluate the efficiency clear spacing alternatives for bar rack and to identify optimum bar rack configurations that can effectively accommodate safe downstream passage for eels at dams. Accordingly, a flume study was proposed to determine the fish guidance efficiency for silver American eels associated with several bar rack spacings and approach velocities of interest, as well as the effect of rack angle. The data gathered from this study is intended allow project owners and resource agencies to make informed decisions that weigh biological and cost considerations associated with the implementation of downstream passage facilities for silver eels.

3.2.1 Flume Design and Construction

The same testing flume at Alden Research Laboratory (Alden) for the hydraulic modeling was used to conduct fish guidance tests with silver American eels. This flume was used for a previous EPRI study (EPRI, 2001) that investigated fish guidance efficiency of angled bar racks and louvers with eight species of fish (including American eel). The flume is 80 feet (24.4 m) in length, 6 feet (1.8 m) in width and 7 feet (2.1 m) in depth, with the capability to operate at flow rates up to 100 cfs (2.8 m³/s) and velocities up to 3 ft/s (0.91 m/s) at full depth. Water was re-circulated through the closed loop system for desired velocities using a bow thruster and motor. The flume was able to be adapted to test different rack angles, bar angles, bar spacings, water velocities, and bypass configurations. Holding facilities suitable for simultaneous housing of multiple fish species were located in the same building as the test flume.

The approximate design of the test facility that was used for the bar rack evaluations with American eel is presented in Figure 14, where the bar rack was set at an angle of 90 degrees to the flow. The major components of the facility include an upstream fixed isolation screen, a bottom release pipe, the bar rack structures, an entrainment net and pen downstream of the bar rack and a bypass with an inclined screen leading to a collection box.
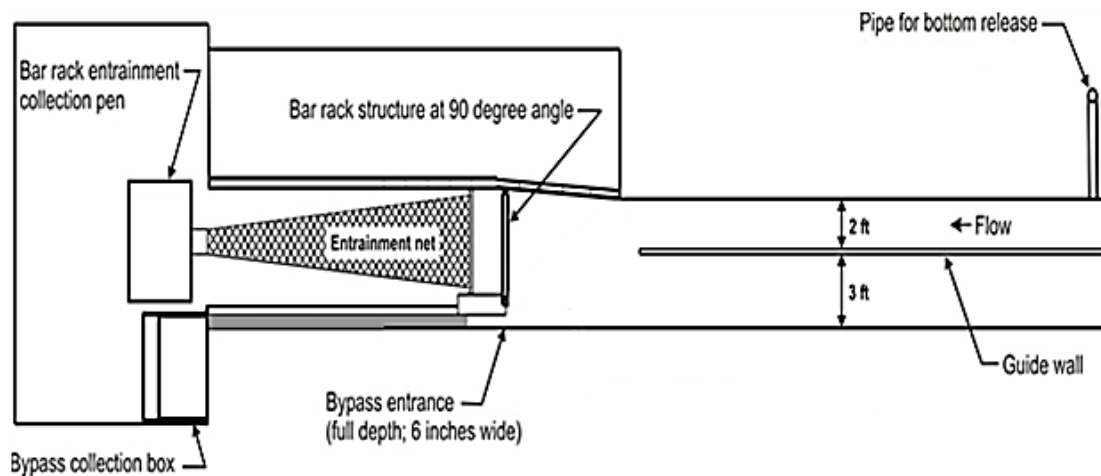
Figure 14 - Schematic of the test flume configuration proposed for the evaluation of bar rack structures with American eel (Adapted from EPRI, 2001).

Due to the extensive requirements and limited available funds for the biological testing, the scope was limited to two clear bar spacings (0.75 and 1.0 inches (19 and 25 mm)) and only one structural angle (90 degrees). The bar racks were constructed with steel slats separated by spacers and held together by four horizontal cross members. The 90 degree bar rack was approximately 5 feet (1.5 m) in length. One end of the bar rack structure terminated at a bypass entrance, which was configured to extend the full depth of the water column and was 6 inches (152.4 mm) wide. The bypass received approximately 11 percent of the flume flow (4.1 and 5.5

cfs (0.12 and 0.15 m^3/s), depending on approach velocities of 1.5 and 2.0 ft/s (0.46 and 0.61 m/s)). A wedge-wire screen angled at 16 degrees from the bottom passed most of the bypass flow while guiding eels to the bypass collection box. The collection system for fish entrained through the bar racks consisted of an entrainment net with a steel frame seated in a slot about 1.6 feet (0.5 m) from the downstream end of the rack. The entrainment net tapered about 19.5 feet (5.9 m) in length to a funnel that guided eels into a collection box.

Eels were transported from the holding facilities in buckets (3 to 4 eels in each container) to the flume. Each bucket was emptied into a release pipe that has an outlet near the floor of the flume and a plunger was used to inject them into the flume. A guide wall was installed upstream to increase the potential for eels to interact with the side of the bar rack opposite the bypass for the 90 degree structure. The guide wall prevented eels from crossing to the opposite side of the flume immediately after release, thereby preventing them from following the far wall directly into the bypass without interacting with the bar rack first.

The collection systems were designed to allow continuous removal of collected eels without altering the model test condition. Eels were dip-netted from both collection areas at specified time intervals after each test release. At the completion of each test, an isolation screen was used to keep eels from moving upstream out of the bypass or through the bar rack. The isolation screen consisted of a wooden frame with a 0.25 inch (6 mm) wire mesh that was lowered by hand and seated in front of the rack.

3.2.2 Test Fish Acquisition and Holding Facilities

Silver American eels were purchased from a commercial fisherman in Maine who uses fyke nets located at lake outlets to capture them during the fall outmigration. The target size range for test fish was 24 to 36 inches (609.6 to 914.4 mm). All the eels were held in a 5,500-gallon (20,819.8 liters) re-circulating holding facility. This facility consisted of eight circular tanks which drain into one of two sump tanks. Water from the sump tanks is returned to the holding tanks after passing through bag filters, an activated charcoal filter, an ultraviolet light sterilizer, and a bio filter.

Water quality parameters (i.e., ammonia, dissolved oxygen, temperature, pH, and salinity) were monitored daily. Daily water quality conditions for the test flume are presented in Table 1. Salinity was maintained between about 1 and 2 ppt. to reduce stress and the potential for fungus. DO levels were monitored throughout testing and never fell below 6 ppm. Water temperatures ranged from 17.6 to 19.9 degrees Celsius.

Table 1 - Flume water quality data

Date	Time	Temp. (°C)	D.O. (ppm)	pH	Salinity (ppt.)	Note
9.18.2013	13:15	18.5	8.97	8.09	1.23	Flume running
9.20.2013	07:44	19.1	9.01	8.01	1.24	Flume running
9.23.2013	14:26	19.9	8.50	8.13	1.24	Flume off
9.24.2013	08:20	19.0	6.41	8.13	1.24	Flume off
9.25.2013	10:20	18.4	10.29	8.33	1.25	Flume off
9.27.2013	08:05	17.6	8.25	8.21	1.17	Flume off
9.30.2013	09:00	17.6	7.60	8.00	1.15	Flume off
10.01.2013	10:15	18.0	9.00	8.26	1.16	Flume off

3.2.3 Experimental Procedures

Silver American eels were released upstream of the bar rack for each set of test conditions (bar spacing and approach velocity). Guidance efficiency was evaluated by collecting them from each downstream location (bypass or entrainment net) during and at the end of each trial and also and upstream of the bar rack at the end of some trials. Three trials with a total of 30 eels each were conducted for each set of test conditions. Test conditions included bar rack structure angle to flow: 90 degrees, approach flow velocities: 1.5 and 2.0 ft/s (0.46 and 0.61 m/s) and clear bar spacing: 0.75 and 1.00 inches (19 and 25 mm).

A total of 12 trials were conducted for the evaluation of guidance efficiency (1 structure angle, 2 velocities, 2 bar spacings and 3 replicate trials). Approximately 30 eels were released per trial, with a total of 90 eels for evaluation at each set of test conditions. All trials were conducted after dusk without any artificial lighting, because during downstream migration silver American eels are most active at night. Hence, a DIDSON (Dual-Frequency Identification Sonar) camera was used to observe eel behavior in the vicinity of the bar rack and bypass. The DIDSON is an imaging sonar camera that produces near video-quality images by using high frequency sound waves. Day time observations were also completed using underwater cameras placed on both sides of the channel and focused on the area in front of the rack. The duration of each trial was about two hours, after which eels were collected from the bypass collection box, the bar rack entrainment net pen, and in the flume area upstream of the rack and bypass.

All eels included in the evaluation of guidance efficiency were naïve (i.e., not re-used in multiple trials). The collection systems were designed to allow removal of bypassed and entrained fish at intervals of 30 minutes during each trial. At the completion of each trial, an isolation screen was used to keep eels from moving upstream out of the bypass or through the bar rack. The collected

eels were placed into separate labeled containers based on their collection location at the end of each trial. The number of eels recovered from the bypass and bar rack entrainment net was recorded at each interval and the total number recovered from both locations was used in the calculation of guidance efficiency.

The length of each eel was measured by using a measuring board, with the measurement taken from the tip of their mouth to the end of their tail to the nearest millimeters (mm). The 1-meter long board enabled the accurate measurement of the eels due to its v-shaped design. The head width of each eel was also measured using a caliper to the nearest millimeters (mm). The eels were immobilized by using ice baths after they were removed from the flume, measured and then returned to the holding system for recovery.

3.2.4 Data Analysis

Fish guidance efficiency (FGE) was quantitatively evaluated for each set of test parameters using the combined data from all three trials with the following equation:

$$FGE = B \div (B + E)$$
(Equation 37)

Where B is the number of eels collected from the bypass and E is the number of eels entrained through the bar racks. Confidence intervals (95%) (Eq. 38) were calculated for each estimate of fish guidance efficiency and statistical comparisons were made among the test conditions to identify any significant differences. The FGE data was recorded and compared with results from previous experiments designed to test hydraulic impacts of bar screens (e.g. head losses).

$$95\% \ Confidence \ Interval = \bar{X} \pm Z * \frac{\sigma}{\sqrt{n}}$$
(Equation 38)

Where $\bar{X}$ is the sample mean, Z is the value from the standard normal distribution for the selected confidence level (at 95% confidence level, $Z = 1.96$), σ is the standard deviation and n is the sample size.

Additionally, a one-way multivariate analysis of variance (one-way MANOVA) test was completed using the FGE data to determine if there were statistically significant differences in the guidance efficiencies with changing fixed factors. The fixed factors included approach velocity (1.50 and 2.00 ft/s (0.46 and 0.61 m/s)) and slat spacing (0.75 and 1.00 inches (19 and 25 mm)) and the dependent variables included the location of the eels at the end of the trials (bypass, entrained or upstream) and the length and width of the eels found at each location. This test was completed using the Statistical Package for Social Science (SPSS) 19.0 software using a 95 percent confidence interval (alpha = 0.05) and a p-value less than 0.05 considered to be statistically significant. Furthermore, the Student Newman-Keuls Post Hoc ANOVA analysis

was used to find the FGE results and the pair of fixed factors that were significantly different from each other. This analysis allowed for the determination of the most effective conditions that would provide greater fish guidance efficiency for the safe passage of the silver American eel.

3.3 Evaluation of Design Parameters

Bar racks are essentially physical barriers that prevent the silver American eel from entering the turbines. However, a simple rack without specific design parameters would not be effective at mitigating the mortality rate of the eels due to the potential for impingement at a high approach velocity. The main goal of this thesis was to compare the results for different design conditions (approach velocity, bar clear spacing and array angle to the flow) using physical and biological modeling to assess the advantages and disadvantages of each. Based on this analysis, recommendations were made with regards to the most effective design of the bar rack that would result in greater fish guidance efficiency and subsequently safe passage for the silver American eel. The hydraulic and biological assessments determined the criteria for the evaluation of the design conditions, where velocity profiles, CFD analyses, head loss measurements, fish guidance efficiencies and visual observations were considered.

The velocity profiles from the hydraulic tests show the vulnerability of the eels to impingement at different approach velocities. CFD contour plots highlight the transport channels and contact regions of the eels with the bar rack. Fish guidance efficiencies and visual observations refer to the effectiveness of the bar rack at getting the eels to the bypass, while head loss analysis focuses on impacts to power generation at each condition.

4.0 RESULTS AND ANALYSES

A full understanding of the requirements for ensuring downstream passage of silver American eels at hydropower facilities requires an understanding of the impacts of bar rack design on eel passage and head loss. This chapter presents the results from hydraulic evaluations and biological assessments that can provide this information. These data were used to assess the hydraulic performance and effectiveness of the bar rack designs at protecting the eels from entrainment.

4.1 Hydraulic Evaluations

Velocity and head-loss data were collected for eighteen (18) bar rack design conditions by measuring the profiles of the water channel approaching and leaving the bar rack, and using pressure taps on the channel floor to monitor the difference in head before and after the rack. The velocity profiles, CFD models and head loss results are presented in the following sections.

4.1.1 Velocity Profiles at each Slat Spacing

Profiles of the cross section of the channel upstream of the bar rack were found by measuring velocity at nine points within the channel using an Acoustic Doppler Velocimeter (ADV). These nine points provide a representation of the conditions of the velocity distribution in the channel immediately upstream of the bar rack (flow as it is affected by depth and the channel walls and floor). Figure 15 shows the velocity profiles that occur as flow approaches a bar rack with (a) a 0.75 inch (19 mm), (b) 1.0 inch (25 mm) and 1.5-inches (38 mm) spacing for the 45 and 90 degree array angles.

(a)

(b)

(c)
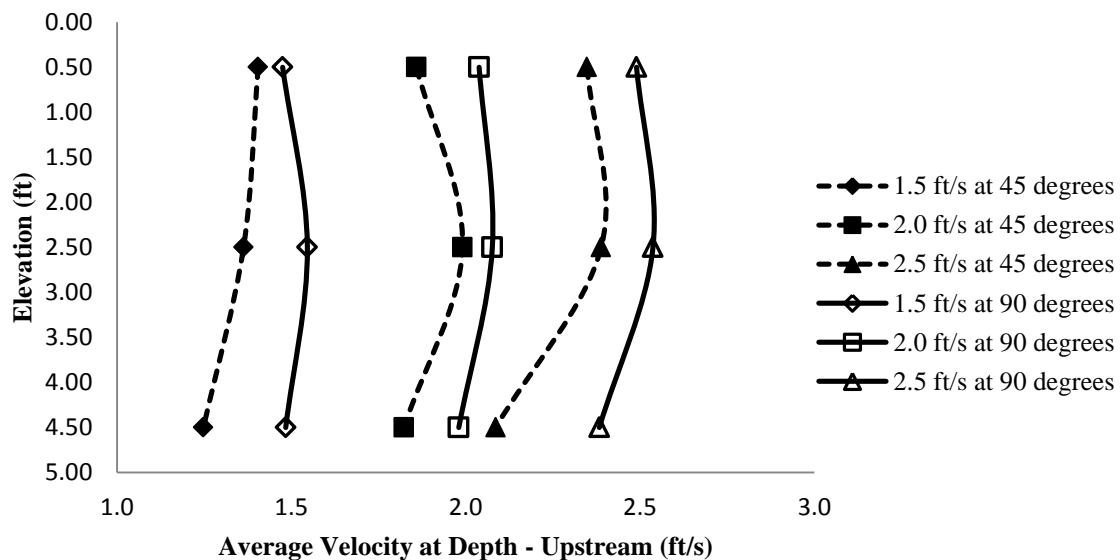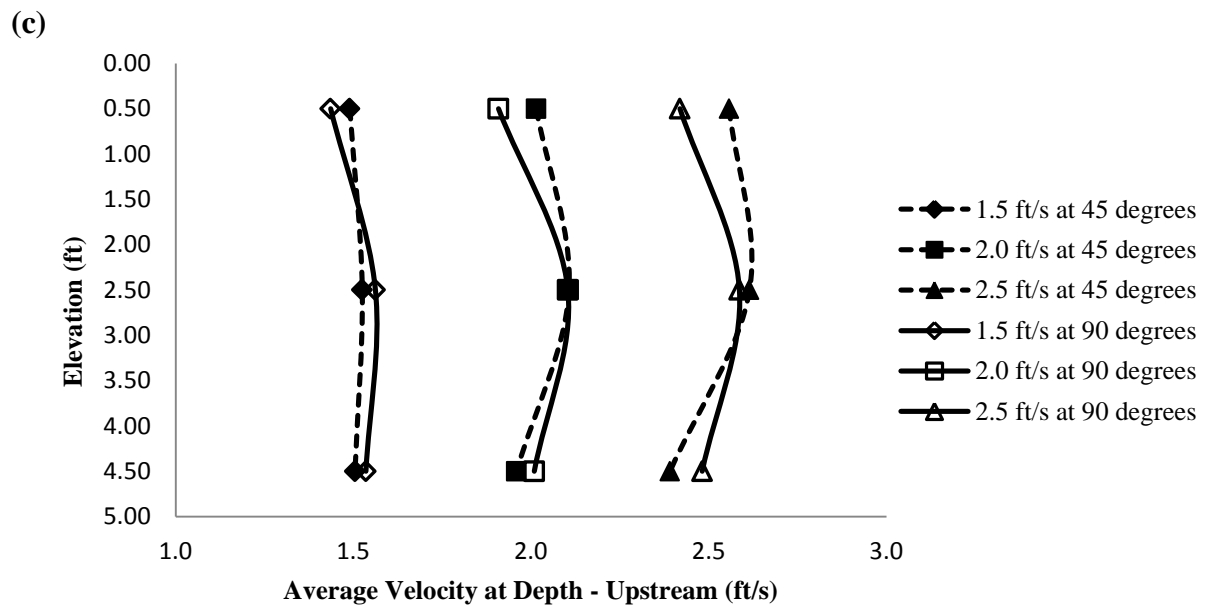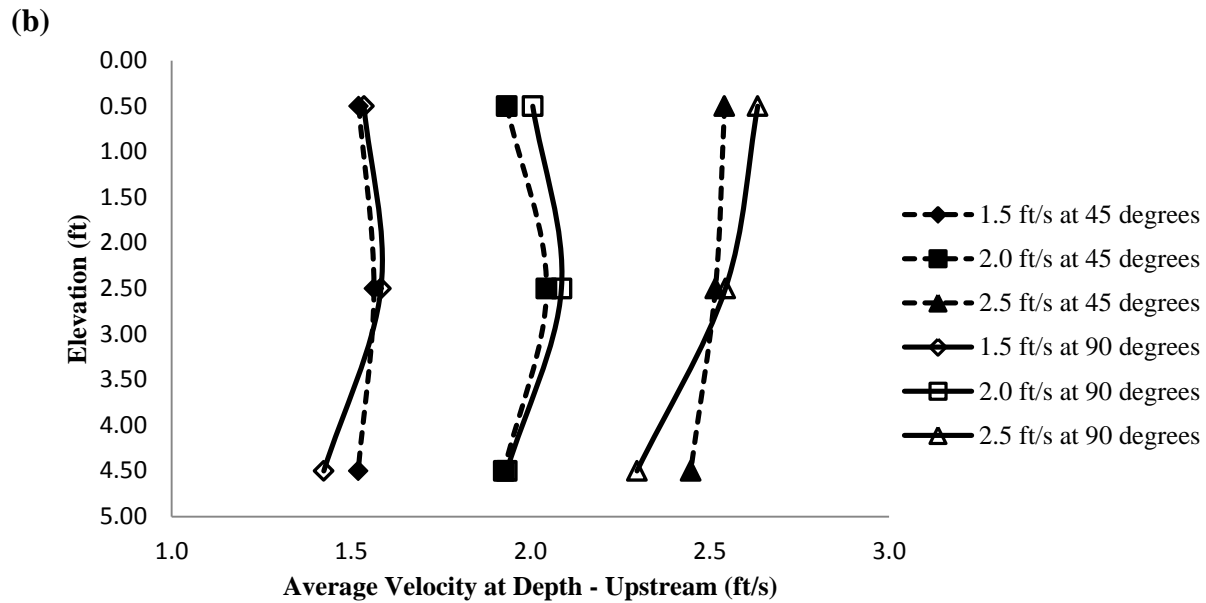
Figure 15 - Velocity profile comparison for 45 and 90 degree orientation bar racks with (a) 0.75 inch (19 mm), (b) 1.0 inch (25 mm) and 1.5 inches (38 mm) spacing.

For the 0.75 inch (19 mm) spacing, the velocity approaching the 45 degree array is lower than that approaching the 90 degree array. This difference is likely a result of the operational conditions in the flume, which differ to some extent since the head losses for the 45 degree bar rack configurations are greater than those for the 90 degree orientations. For bar racks with 1.0 and 1.5 inches (25 and 38 mm) clear spacing, shown in Figures 15 (b) and (c), respectively, the profiles for the 45 and 90 degree bar rack angles are nearly identical, which indicates the flow approaching these racks are uniform.

4.1.2 Velocity Profiles at each Array Angle

The previous section focused on the effect of clear spacing of each bar rack on the velocity profiles approaching the rack. Velocity measurements taken at three points in the depth of the flume for each condition at each array angle also show additional trends. Figure 16 illustrates the relationship between clear spacing and approach velocity for the 45 degree rack. The velocity measurements were normalized by dividing each value by the average approach velocity to minimize the effects of outliers in the data set.

For the 45 degree rack (Figure 16), the higher velocities of 2.0 and 2.5 ft/s at all clear spacings were similar except that of the 1.0-inch spacing at 2.5 ft/s. At the higher velocities for the 0.75, 1.0 and 1.5 inches (19, 25 and 38 mm) spacing, the profile illustrated that there were greater flows occurring in the middle of the channel with the lowest occurring at the bottom of the channel. Lower velocity measures would be expected at the bottom of the channel due to an increase in friction. However, the difference in trend that is indicated by the 1.0 inch (25 mm) spacing at an approach velocity of 2.5 ft/s (0.76 m/s) is quite an interesting anomaly, which is also observed for the 90 degree rack (Figure 17). Approach velocity of 1.5 ft/s (0.46 m/s) also provided a more uniform flow profile for all spacings of the rack, except the 0.75 inch (19 mm) where greater flows were measured at the surface and lower at the bottom of the channel.
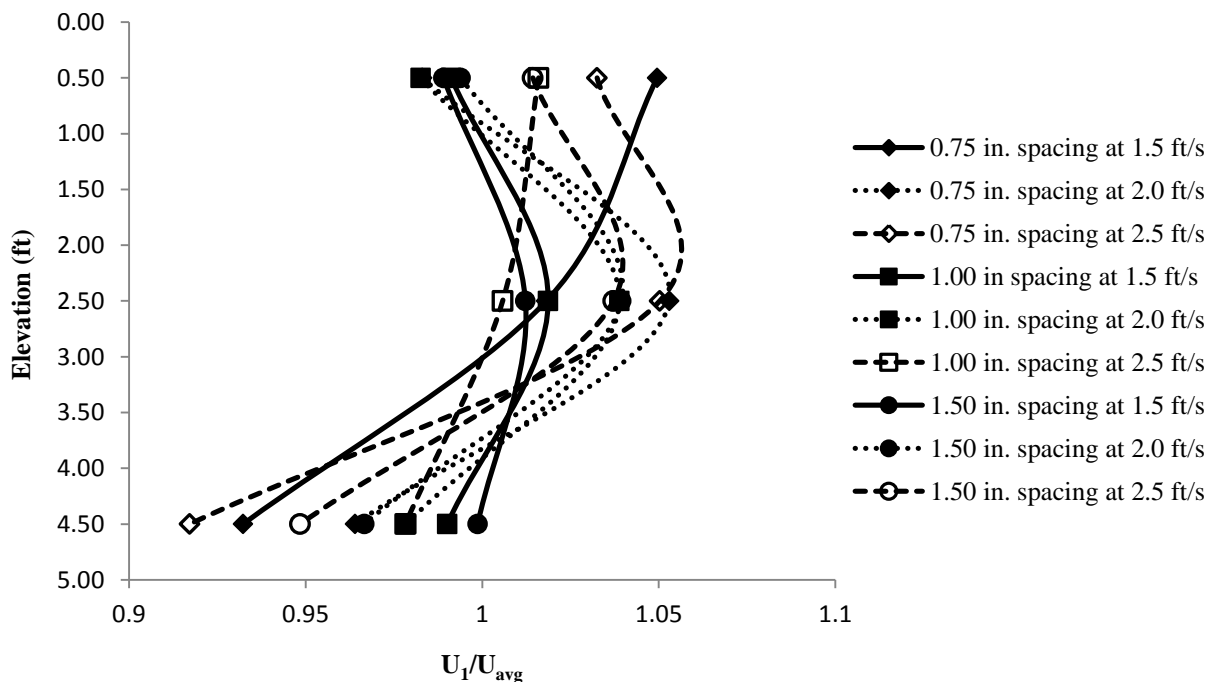
Figure 16 - Velocity profile comparison (normalized streamwise U1/Uavg) for 45 degree orientation upstream of the bar rack.

The anomalies found for the 1.0 inch (25 mm) spacing at 2.5 ft/s (0.75 m/s) approach velocity may have been exaggerated by the scale of the plots and do not necessarily indicate a consistent occurrence. In general, the characteristics for the velocity profiles for the 45 and 90 degree bar racks are uniform with consistent the highest approach velocities occurring in the middle of the channel.
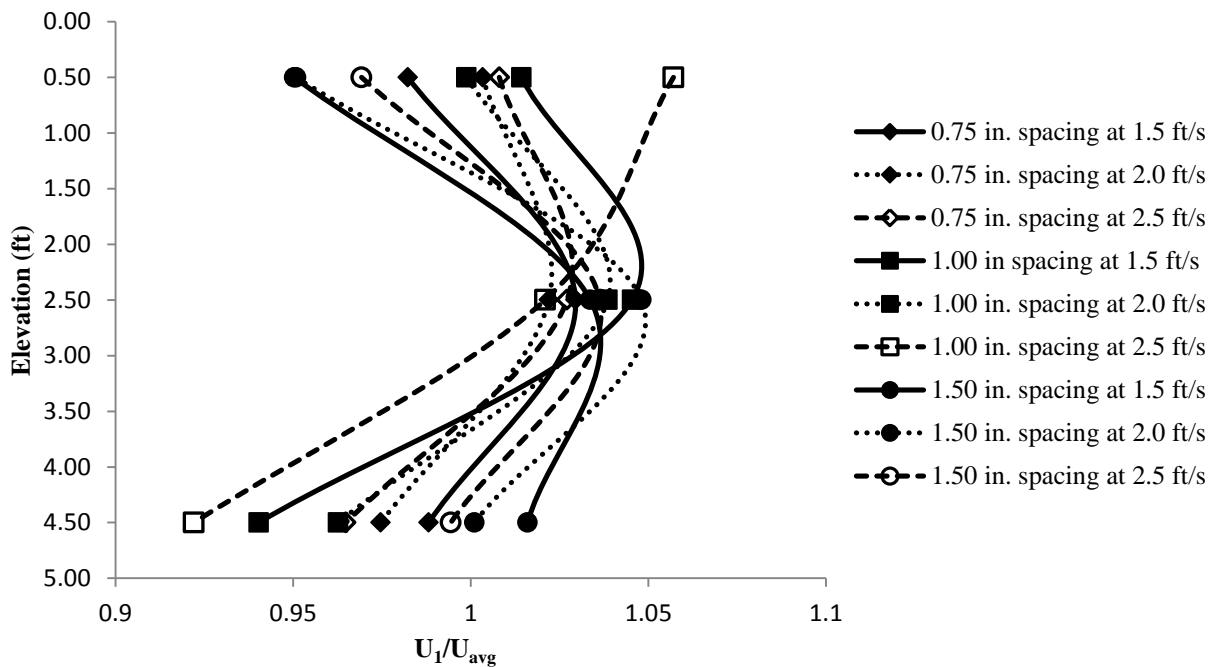
Figure 17 - Velocity profile comparison (normalized streamwise U1/Uavg) for 90 degree orientation upstream of the bar rack.

However, these velocity measurements are based on the average velocity at each depth that may be significantly different from the contour profiles at a plan view. Further analysis using numerical modeling would provide the flow changes along the width of the channel that may provide an explanation for the discrepancies.

4.2 Bar Rack Head Loss Coefficients

Head loss resulting from the resistance of the bar racks at the intakes have been a concern of hydropower operators since more stringent prescriptions have been mandated by the U.S. Fish and Wildlife Services. This section presents the results of the head losses gathered from the physical models and those predicted by calculations using previously proposed equations. A newly developed head loss equation is also presented for comparison.

4.2.1 Physical Model Head Loss

A SONTEK Acoustic Doppler Velocimeter (ADV) was used to measure approach velocities 6.6 feet upstream (2.0 m) and 3.9 feet (1.2 m) downstream of the bar rack. The average velocity upstream (V_1) and downstream (V_2) were used to calculate the change in velocity head. Pressure taps in the floor of the flume were attached to a manometer board which provided the change in water depths across the rack from upstream (H_1) to downstream (H_2). Data gathered from physical models is presented in Appendix C. Head loss was calculated by accounting for the mean velocities and the change in water depths. Equation 15 (which was previously provided in Chapter 2, the background chapter) was used to calculate the head loss from the data gathered during the laboratory tests.
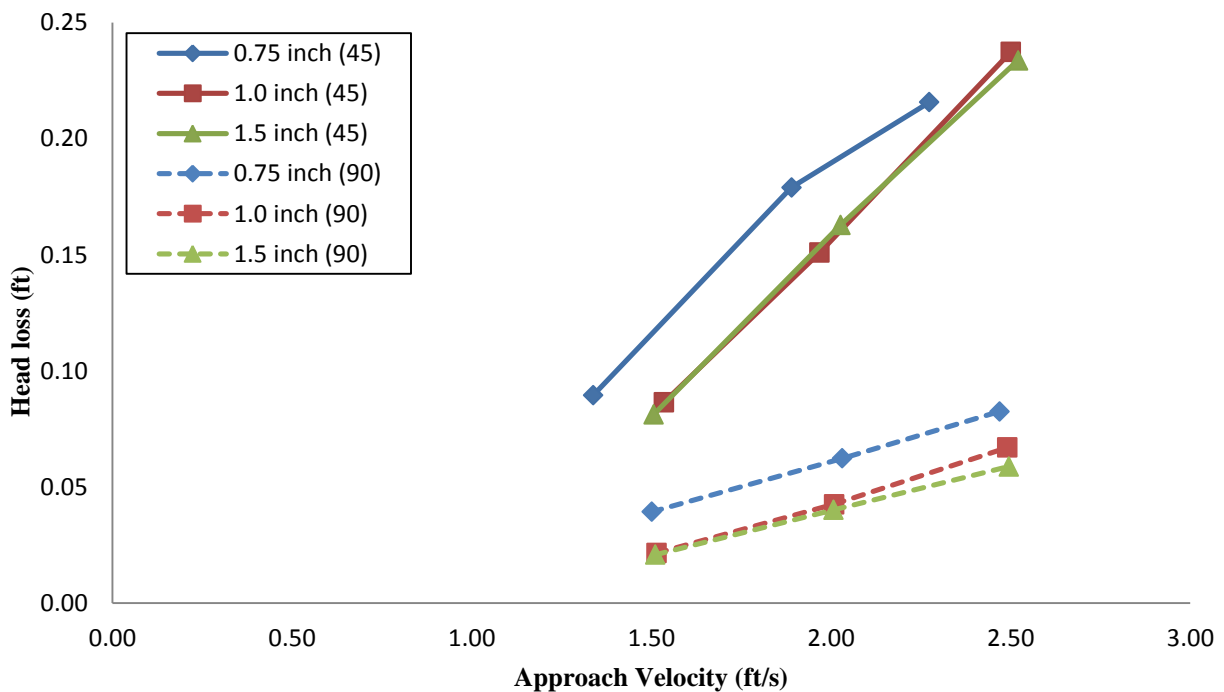
Figure 18 - Comparison of head loss results for 45 and 90 degree angled bar rack to the flow.

Figure 18 shows the results for the calculated head losses based on the data for the 45 and 90 degree angled racks. For equivalent approach velocities, the 45 degree bar rack resulted in greater head losses than the 90 degree rack. The results for the clear spacings of 1.0 and 1.5 inches (25 and 38 mm) at 45 and 90 degree angled racks have similar results and in some instances are identical. This trend likely indicates that the difference in head loss between these two cases is relatively small. The 0.75 inch (19 mm) clear spacing displays a large difference in head loss compared to the other configurations.

4.2.2 Applicability of Head Loss Equations

The head loss measured from the physical modeling and those predicted by Kirschmer-Mosonyi (1966), Zimmermann (1969), Idel'chik (1979), Meusburger (2002), Clark *et al.* (2010) and Raynal *et al.* (2013) are compared for the three different spacings and approach velocities in Figures 19 and 20. Figure 19 shows the results for the 90 degree bar rack and Figure 20 shows the results for the 45 degree bar rack. For essentially all conditions and parameters, the results predicted by the previously developed equations were not consistent with the measured head losses. Review of the results in Figures 19 and 20 indicates the following observations and considerations:

- Head losses given by the Clark *et al.* (2010) equation are far lower than the measured values for the 45 and 90 degree bar racks.
- Zimmermann's (1969) equation gives head loss results that are far greater at both array angles. For the 45 and 90 degree angle bar rack, the head loss results were an average 4 and 0.10 feet (1.2 and 0.003 m), respectively (Appendix F). The results from Zimmermann's equation were omitted from Figure 22 due to the scale of the other results. Consequently, according to Raynal *et al.* (2013), the Zimmermann equation would not be applicable to angled bar racks as it is adapted to 90 degree configurations to the flow but it may be suitable for louvers (bar racks with angled bars).
- Head losses given by the Kirschmer-Mosonyi (1966) and Meusburger (2002) equations are rather close for the 45 degree orientation but are still far lower than the measured values.
- Clark *et al.* (2010) and Meusburger (2002) produce rather identical results for the 90 degree bar rack, but are far lower than the measured values.
- Raynal *et al.* (2013) although recent, also falls out of range as it is far too high for the 45 degree bar rack (Appendix F) and far too low for the 90 degree bar rack; similar to Zimmermann it was ommitted from Figure 24.
- Idel'chik's (1976) equation is the only one that shows consistency with the measured head loss from the experimental data. However, it underestimates by 25-65% for both array angles which may be due to the fact that the channel alignment with the flow approaching the bar rack.

Similar to Raynal *et al.* (2013) argument, the difference in the equations lies in the configuration of the channel and the bar racks. For this investigation, the bar racks were inserted inside a straight channel opposed to Idel'chik (1976) method where the array angle remained fixed but the approaching channel was changed to the investigating angle, and may explain the discrepancies in results.

(a)

(b)

(c)
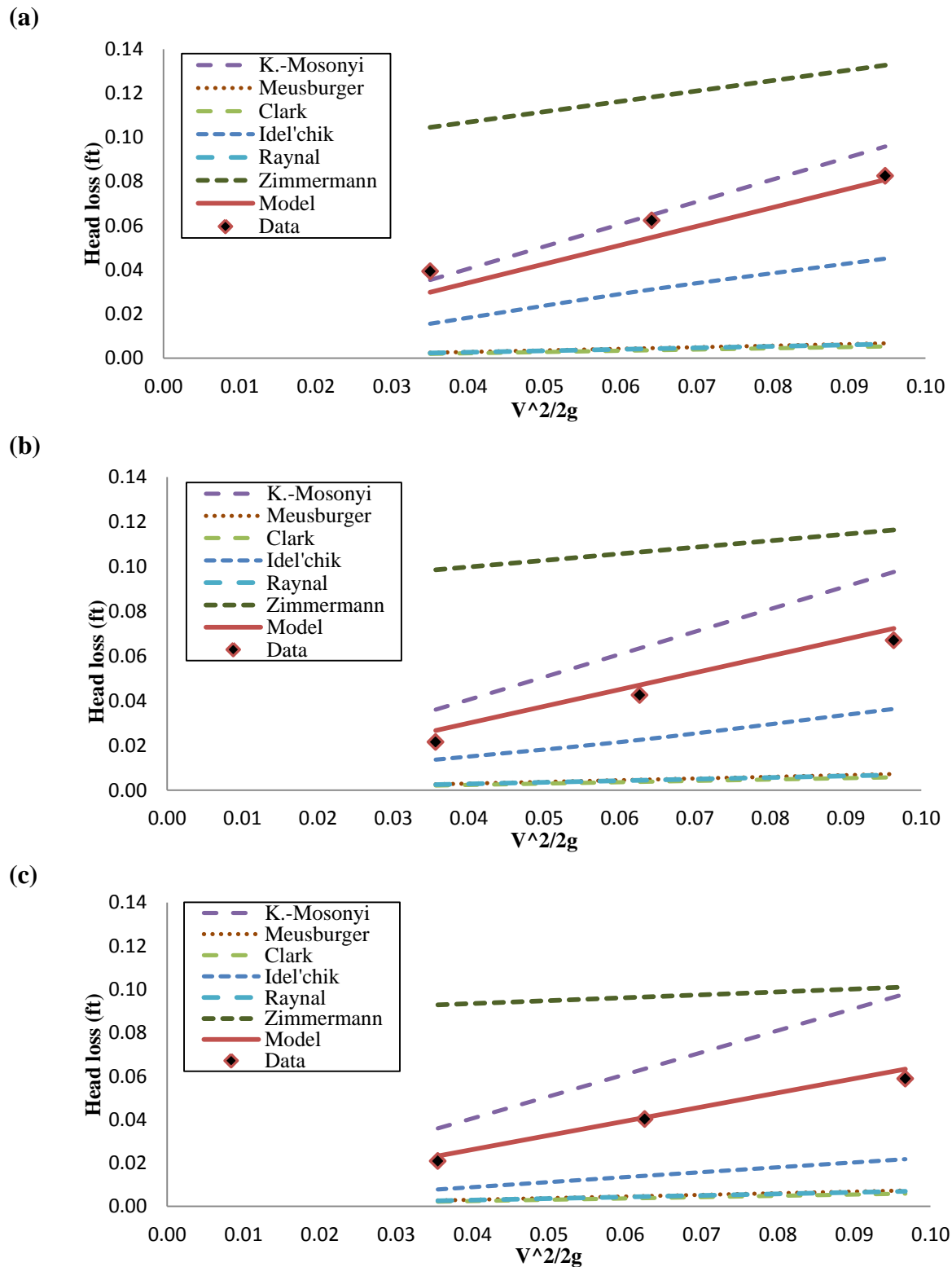
Figure 19 - Comparison of head loss coefficients for 90 degree bar rack with (a) 0.75 (19), (b) 1.0 (25) and (c) 1.50 inch (38 mm) spacing.
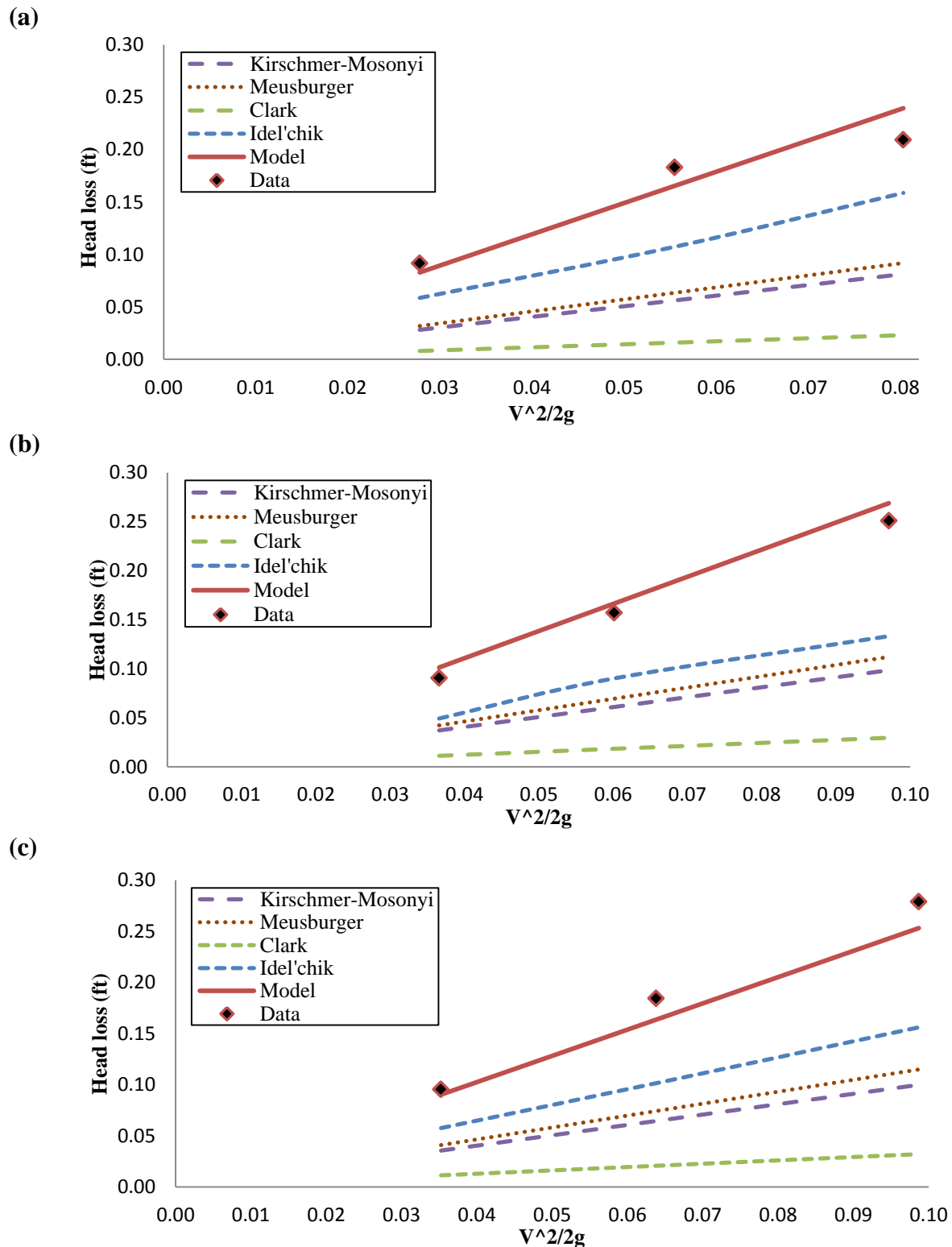
Figure 20 - Comparison of head loss coefficients for 45 degree bar rack with (a) 0.75 (19), (b) 1.0 (25) and (c) 1.50 inch (38 mm) spacing.

However, when analyzing these models commonalities occur in variables that are considered for each equation, including bar shape, blockage ratio O_g and the array angle α. These variables were considered for the formulation of the new head loss model (Equation 36 presented in Chapter 3) that was also presented in Figures 19 and 20.

4.2.3 Debris Loading

Physical modeling was completed in the same flume to evaluate the effects of debris blockage on the head loss. Debris loading was simulated by wooden planks in a uniform grid for blockage ratios of 20, 40 and 60 percent. Results indicated that with increased blockage and approach velocity, there were corresponding increases in head loss as would be expected (Appendix D).

(a)

(b)
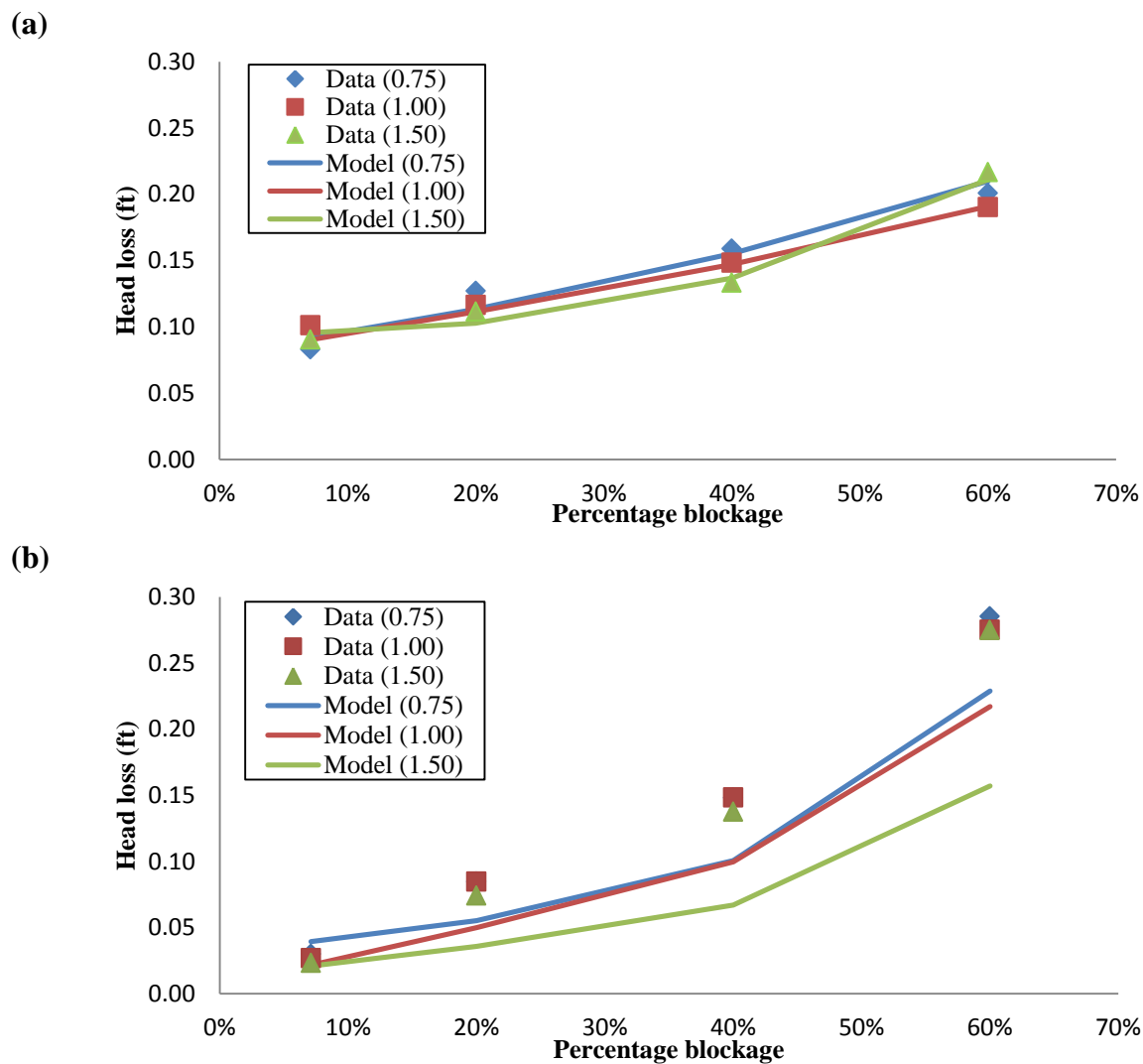
Figure 21 - Comparison of head loss for (a) 45 and (b) 90 degree bar racks at an approach velocity of 1.5 ft/s (0.46 m/s).

However, for increasing approach velocity and blockage ratio, the head losses for the 90 degree bar rack were greater than the head losses for the 45 degree rack. This result contradicted the hydraulic tests completed without blockage, for which the head loss associated with the 45 degree rack exceeded those of the 90 degree rack. Figure 21 shows the comparison between the 45 and 90 degree rack at an approach velocity of 1.5 ft/s (0.46 m/s) for each blockage ratio.

(a)

(b)
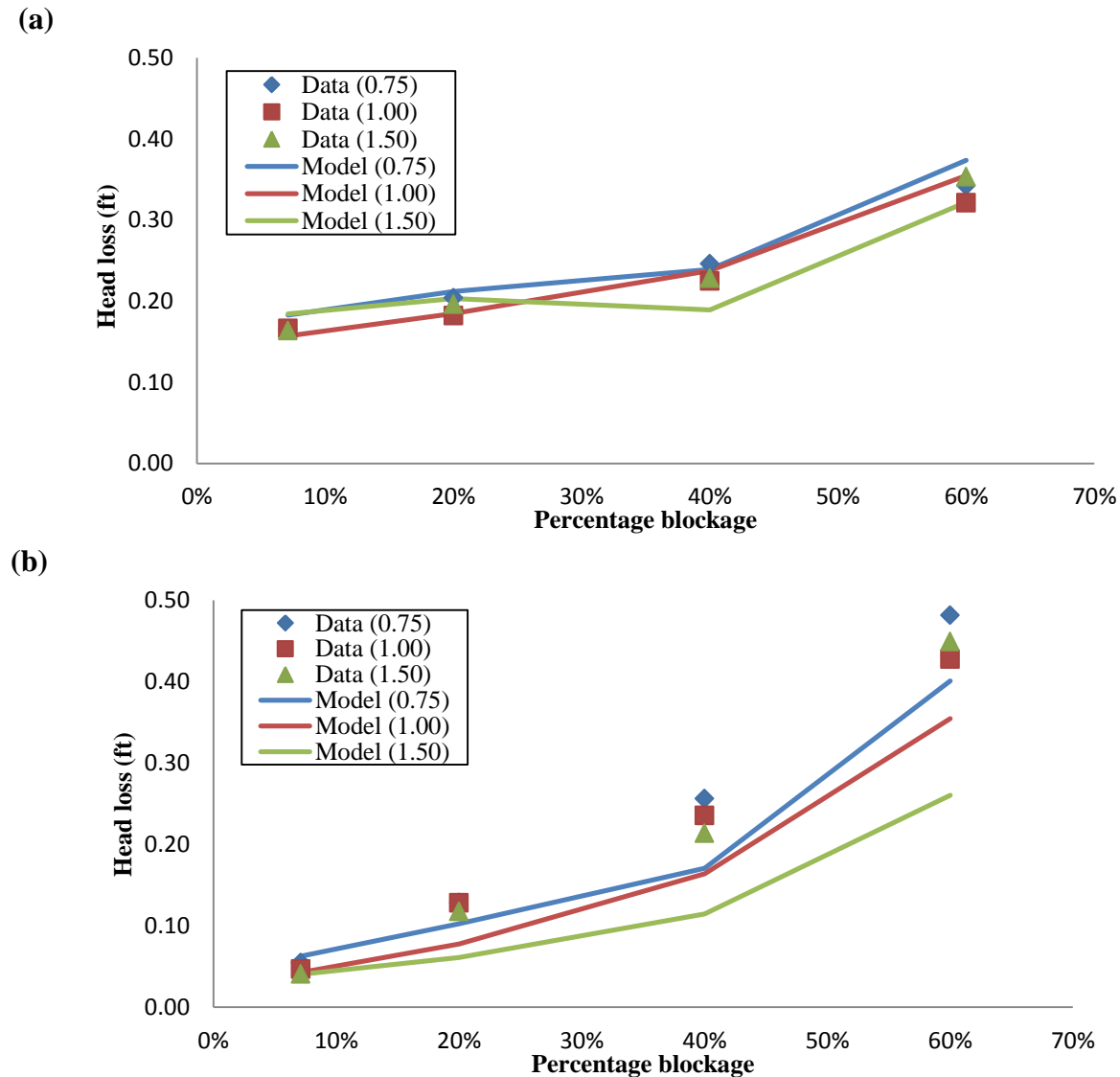
Figure 22 - Comparison of head loss for (a) 45 and (b) 90 degree bar racks at an approach velocity of 2.0 ft/s (0.61 m/s).

The debris loading data were used as a verification and applicability test for the new proposed head loss equation. For the 45 degree angled bar rack data, the equation's predictions closely matched the measured head losses, with a correlation coefficient of 98.6 percent. However, for the 90 degree rack the predictions were approximately an average range of 18 to 27 percent less

than the measured head losses with blockage and the correlation coefficient was 96.4 percent. Figure 22 shows the comparison between the 45 and 90 degree rack at an approach velocity of 2.0 ft/s (0.61 m/s) for each blockage ratio.

(a)

(b)
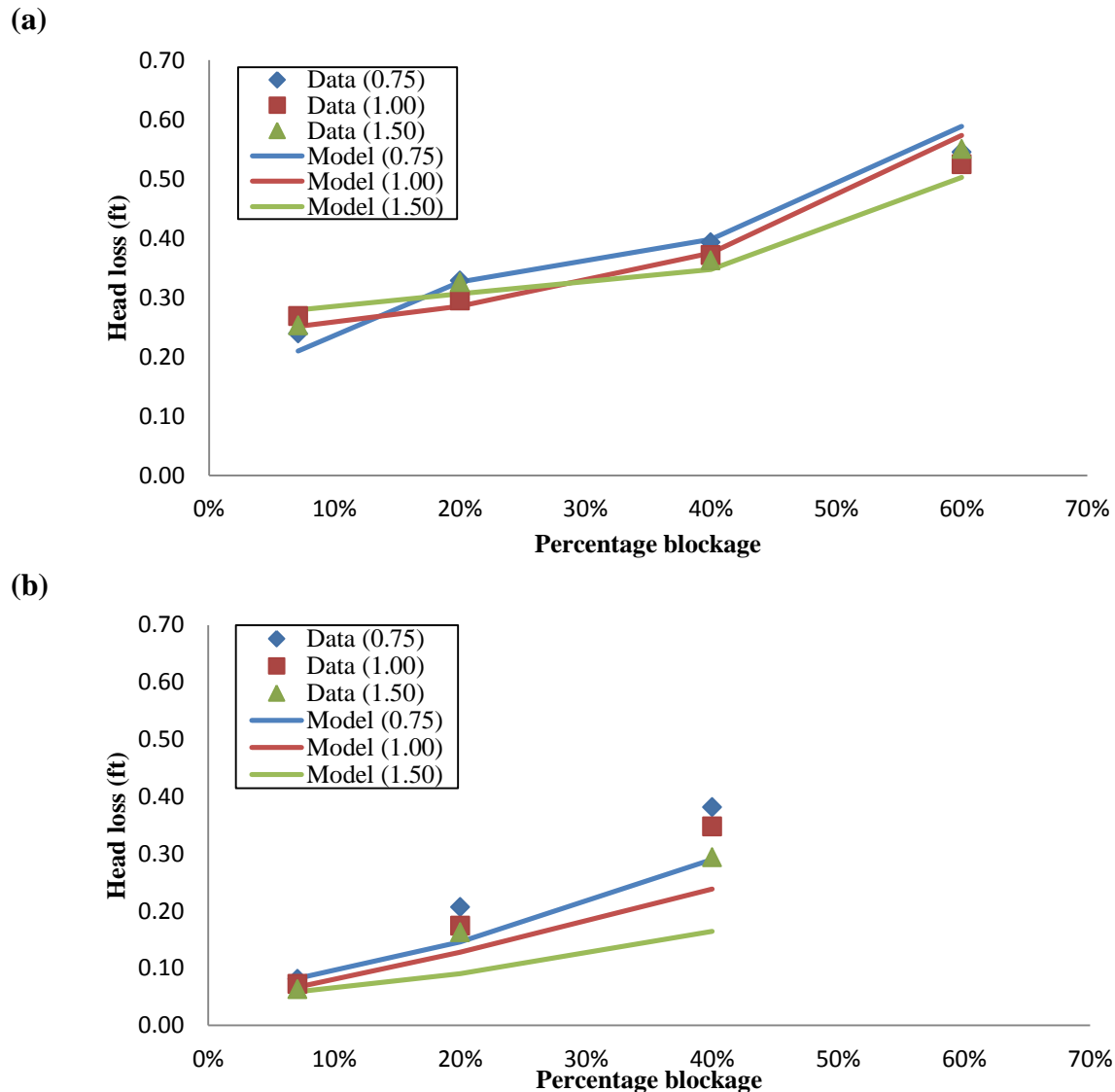
Figure 23 - Comparison of head loss for (a) 45 and (b) 90 degree bar racks at an approach velocity of 2.5 ft/s (0.76 m/s).

Figure 23 (b) shows the results for the 90 degree bar rack at an approach velocity of 2.5 ft/s (0.76 m/s). The data for the 60 percent blockage ratio could not be obtained because the increased pressure force on the rack due to high approach velocity caused it to distort in shape. This bending would have eventually resulted in a toppling of the rack which would have caused substantial damage and safety hazards.

The debris loading evaluations showed that under blockage conditions, the 90 degree bar rack generates greater head loss than the 45 degree rack and is susceptible to overtopping with increased approach velocities and blockage ratios. The new head loss equation can be applied for conditions with blockage ratios 0 to 60 percent for 45 degree racks and 0 to 20 percent for 90 degree racks.

4.3 CFD Models

Computational Fluid Dynamics (CFD) was used to model the hydraulic performance of bar rack designs at different specified parameters. The commercial software package, ANSYS FLUENT 14.0, was used to complete eighteen simulations. These simulations characterized the flow patterns that occur at the bar racks with specified approach velocity (1.5, 2.0 and 2.5 ft/s (0.46, 0.61 and 0.76 m/s)), slat spacing (0.75, 1.0 and 1.5 inches (19, 25 and 38 mm)) and array angle (45 and 90 degrees). The numerical model simulated the actual conditions and geometry (1:1 ratio) of the experimental flume used in the laboratory evaluation.

4.3.1 Contour Plots

Figure 24 shows the contour plots simulated by the numerical modeling software, ANSYS Fluent 14.0, for a 45 and 90 degree angled bar rack with 0.75 inch (19 mm) spacing at an approach velocity of 2.5 ft/s (0.76 m/s), respectively. The contour plots for the remaining 16 simulations are shown in Appendix B. Contour plots were assessed at an elevation of 3 feet (0.91 m). For the 90 degree angled bar rack, the velocity contours (z-component) are uniform on their approach and exit from the rack.

Velocity is shown to decrease to approximately 1.7 ft/s (0.52 m/s) when the flow is in contact with the rack. This result is similar to the trend shown in Figure 15 of the previous section, where was consistent at all conditions but the 1.0 inch (25 mm) spacing at 2.5 ft/s (0.76 m/s). The maximum velocity measurement of 3.0 ft/s (0.91 m/s) was indicated to occur between the bars and is evenly distributed across the rack.

On the other hand, the 45 degree bar rack has a non-uniform flow approaching the rack. The higher velocity contours approaching the rack occurred on the left side of the channel, but upon contact decreased to approximate/y 1.5 ft/s (0.46 m/s). Figure 25 shows that the highest velocity occurs at the ends of the rack along the channel walls.

(a)

(b)
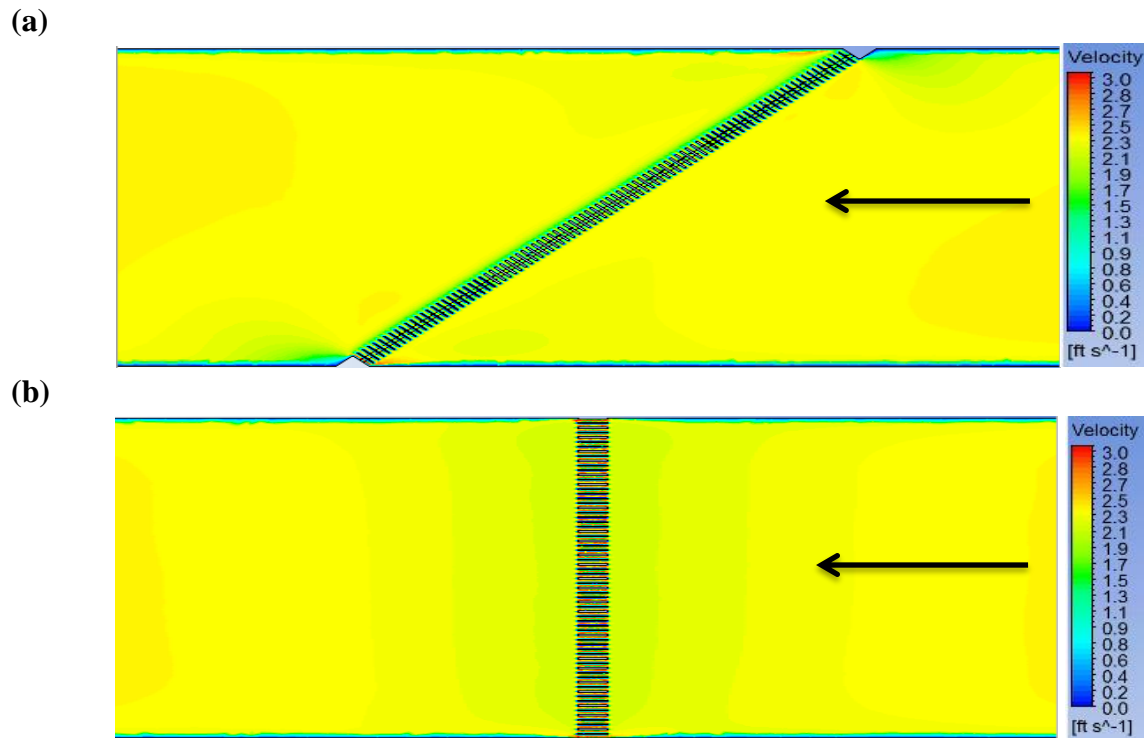
Figure 24 - Simulated velocity contours of flow through the flume (elevation 3 feet (0.91 m)) at an approach velocity of 2.5 ft/s (0.76 m/s) with a bar rack of 0.75 inches (19 mm) at (a) 45 and (b) 90 degrees.

The contour plot for the 45 degree bar rack also shows the flow pattern approaching the rack. Higher velocities occur in the middle of the channel, which differ from the velocities that occur in the 90-degree rack due to the flow direction change that results from the 45-degree rack. This direction variability (or meandering) is more prominent for lower approach velocities, as shown in Figure 25.
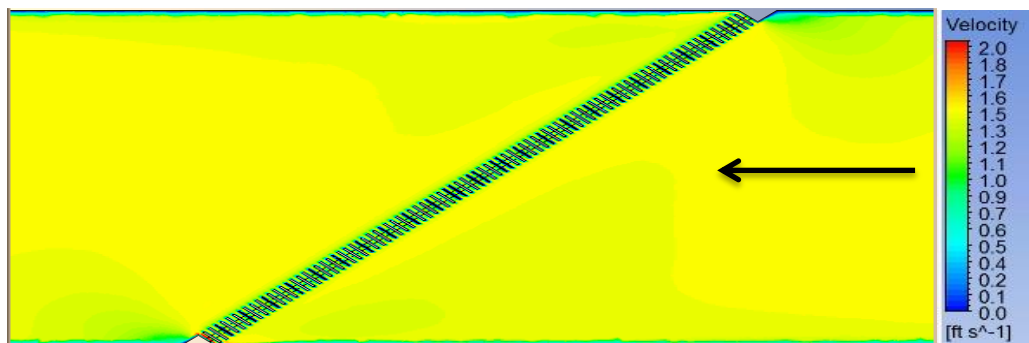
Figure 25 - Simulated velocity contours of flow through the flume at 1.5 ft/s (0.46 m/s) with a bar rack of 0.75 inch (19 mm) spacing at 45 degrees.

This change in direction of the approaching flow is likely responsible for the difference in velocity profile shown in Figure 15 of the previous section. The lower approach velocity of 1.5 ft/s (0.46 m/s) has a more uniform profile than the higher velocity of 2.5 ft/s (0.76 m/s). The higher approach velocity has a greater mid-depth velocity, because the bend disappears as the channel is straightened.

4.3.2 CFD Predicted Head Loss Comparisons

The summary of the head loss results predicted by the CFD software is presented in Table 2. The predicted head loss results produced by the ANSYS Fluent 14.0 software were gathered from the CFD-Post application. The difference in the height of the water before and after the rack was predicted by using the function calculator to estimate the pressure change in pounds per square inch (psi) then converting to feet of water.

Table 2 - Summary of predicted head loss results from numerical modeling software

Spacing	45 degrees			90 degrees		
	Approach Velocity	Measured Head loss (feet)	Predicted Head loss (feet)	Approach Velocity	Measured Head loss (feet)	Predicted Head loss (feet)
	1.34	0.089	0.084	1.501	0.039	0.081
0.75	1.89	0.179	0.085	2.031	0.062	0.072
	2.27	0.216	0.168	2.470	0.082	0.161
	1.54	0.086	0.069	1.514	0.022	0.128
1.00	1.97	0.151	0.009	2.009	0.043	0.028
	2.50	0.237	0.064	2.491	0.067	-0.017
	1.51	0.081	0.037	1.511	0.021	0.035
1.50	2.03	0.163	0.035	2.007	0.040	0.004
	2.52	0.234	0.042	2.496	0.059	-0.071

The results shown in Table 2 show that the numerical model predicted the head loss to be less than that measured with the physical model for the 45 degree bar rack but greater than for the 90 degree rack up to 2.0 ft/s (0.61 m/s) for the 0.75 and 1.0 inch (19 and 25 mm) bar spacing. Major discrepancies such as the results for the 90 degree bar rack with 1.0 and 1.50 inches (25 and 38 mm) spacing presented negative head losses at the largest approach velocity of approximately

2.5 ft/s (0.76 m/s), which indicated that the water level leaving the rack was greater than the water level approaching the rack. Figure 22 shows 'jump-like' hydraulic feature that occurs after the rack for the 1.0 and 1.50 inches (25 and 38 mm) spacing at an approach velocity of 2.5 ft/s (0.76 m/s), which might explain the negative head loss obtained when evaluating the results of the software. Additional research is recommended to provide a more detailed evaluation of the simulations and head loss evaluations for these simulations.
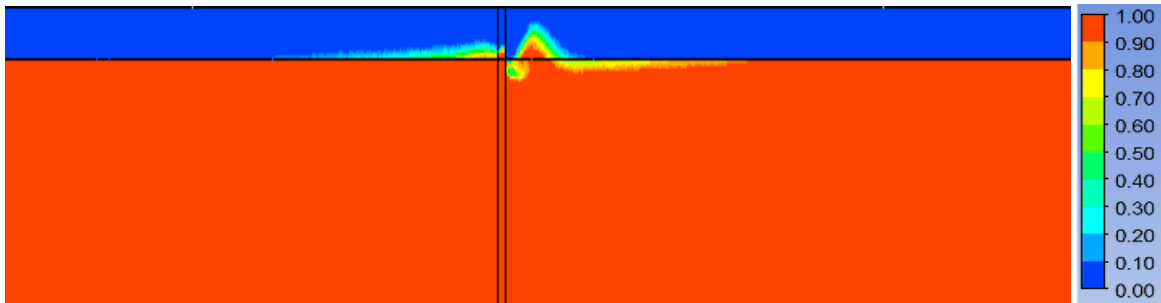
Figure 26 - Volume fraction contour plot showing 'jump-like' hydraulic feature after the bar rack for a 90 degree bar rack with clear spacing of 1.5 inches at 2.5 ft/s (0.75 m/s).

4.4 Biological Assessment

The purpose of the biological assessment was to evaluate the effectiveness of bar racks in bypassing the silver American eel such that they enter bypass channels without being entrained during downstream migration. The bar racks with commonly used clear spacings were evaluated for water velocities that typically occur at hydropower intakes. This section presents the results from live eel testing with bar rack design parameters of two clear spacings: 0.75 and 1.0 inches (19 and 25 mm), approach velocity conditions: 1.5 and 2.0 ft/s (0.46 and 0.61 m/s) and bar rack angle: 90 degrees.

4.4.1 Fish Guidance Efficiencies

Table 3 shows the summary of the results per trial and the average guidance efficiency. The efficiency of the bar rack at guiding the eels to the bypass involved consideration of the approach velocity and clear spacing of the bar rack. For an approach velocity of 1.5 ft/s (0.46 m/s), the results indicated that the 90 degree angle bar rack with 0.75 inch (19 mm) clear spacing produced the highest fish guidance efficiency (FGE). For the approach velocity of 2.0 ft/s (0.61 m/s), the bar rack with a spacing of 0.75 inch (19 mm) spacing also had the highest efficiency rate.

Table 3 - Summary of results from silver American eel guidance trials with bar racks angled 90 degrees to the approach flow

Approach Velocity (ft/s)	Total Number of fish released	Mean Length (inches)	Mean Head Width (inches)	Number of fish entrained	Number of fish bypassed	Total recovered down-stream	Percent recovery down-stream	Mean % Guidance efficiency (±95% CI)
0.75 inch spacing								
1.5	91	29.5	0.89	3	74	77	84.6	**96.1 (7.8)**
2.0	82	29.0	0.85	8	66	74	90.2	**89.2 (9.0)**
1.0 inch spacing								
1.5	90	29.2	0.97	19	49	68	75.6	**72.1 (0.0)**
2.0	90	30.0	0.94	20	47	67	74.4	**70.1 (16.9)**

To further clarify the results, Figure 27 represents the mean percentage guidance efficiencies for each paired parameter. The results for the bar rack configuration of 1.0 inch (25 mm) clear spacing at 1.5 ft/s (0.46 m/s) approach velocity shows a guidance efficiency of 72.1% for all trials. Error bars for 95% confidence intervals indicate that there is a significant difference between the mean FGE for the 0.75 and 1.0 inches (19 and 25 mm) clear spacing bar rack for approach velocities of 1.5 ft/s (0.46 m/s).
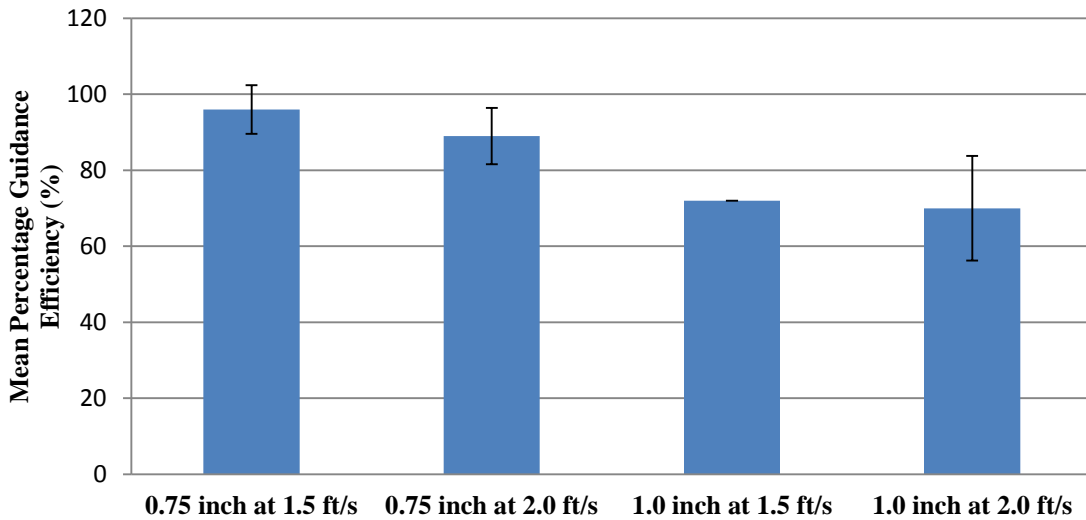
Figure 27 - Mean Percentage Fish Guidance efficiency at the different conditions of clear spacing and approach velocity.

At the higher approach velocity, the FGE decreased slightly. This difference in FGE for the two velocities at each condition was found to be related to the length of the eels but not for all recovery locations.

To help interpret the FGE results, information on mean length and head width was considered. First, Figure 28 shows a comparison between the mean length, approach velocity and clear spacing for the various locations. The error bars for 95% confidence intervals shown in Figure 28 all overlap and return t-test p-values less than 0.05, which indicate there are significant differences in lengths between conditions or locations. In general, the larger eels were found upstream with the greatest mean length of 31 inches (762 mm) found at a 1.0 inch (25 mm) clear spacing and an approach velocity of 2.0 ft/s (0.61 m/s). For the 0.75 inch (19 mm) clear spacing, the length of the eels being entrained was lower for the higher approach velocity. In contrast, for the 1.0 inch (25 mm) clear spacing, the mean lengths of the eels being entrained and also entering the bypass were both higher for the higher approach velocity. Overall, the differences in mean length do not appear to be statistically significant and the differences in FGE cannot be related to differences in eel length.
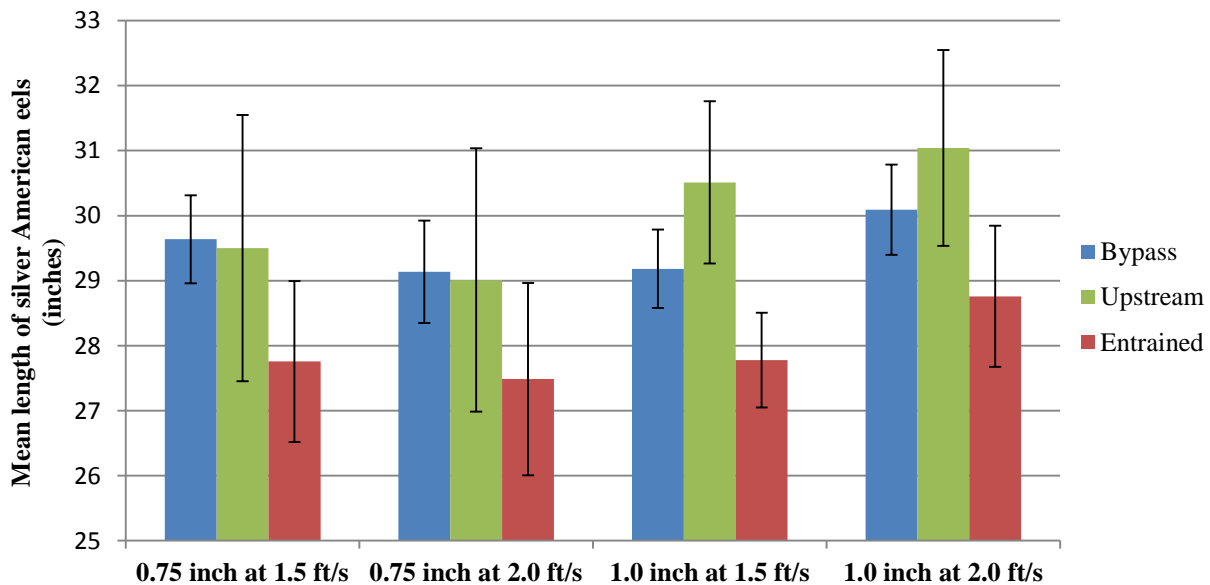
Figure 28 - Mean length, approach velocity and clear spacing for different locations, with error bars showing 95% confidence intervals.

Figure 29 shows the comparison between the mean head width, approach velocity and clear spacing for the various locations. In this figure, the mean head widths of the eels entrained in the 1.0 inch (25 mm) bar rack were less than the width of the clear spacing, as opposed to the 0.75 inch (19 mm) bar rack for which the mean head widths were greater than the width of the clear

spacing. For the entrained eels, the mean head width for the higher approach velocity was greater than that for the lower approach velocity.
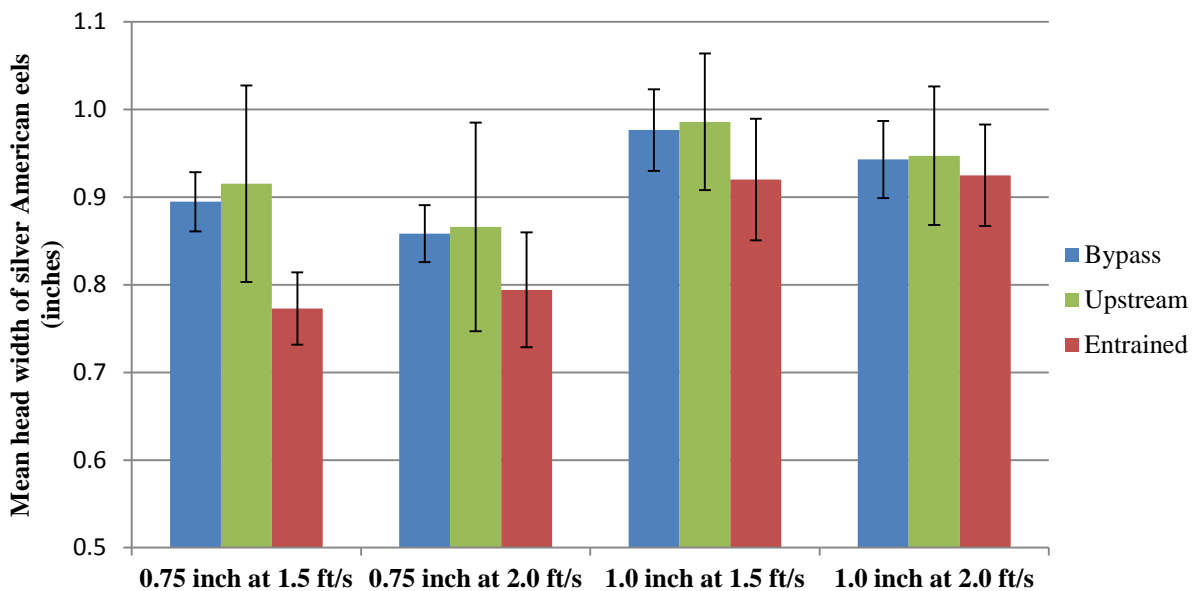
Figure 29 - Mean head width, approach velocity and clear spacing according to location with error bars showing 95% confidence intervals.

Mean head widths of the eels found in all locations for the 1.0 inch (25 mm) clear spacing bar rack were also larger than those for the 0.75 inch (19 mm) bar rack. The ANOVA analysis (using a 95% confidence level, where alpha = 0.05) confirms that there is a statistically significant difference for the head width of the eels for the 0.75 and 1.0 in trials (with an $F_{(1, 341)} = 15.83$, $p = 0.0005$, as shown in Appendix E). It is recognized that this is likely a result of the population that was used in the trial, although it is emphasized that all eels were chosen randomly for each trial. On the other hand, the mean head width appeared to be consistent for each of the three sampling locations (i.e. upstream, bypassed and entrained). The difference in head widths may have also increased the effect of clear spacing on the measured FGE, which may indicate that using a smaller bar spacing is overrated. While more detailed analysis of the results is needed to fully discern the role of length and head width, the results provide helpful insight into the impacts of bar spacing on eel entrainment. More detailed information on the overall sample population is provided in the next section.

An analysis of variance (ANOVA) test was also completed to determine if there were statistically significant differences in length and head width of the eels based on the clear spacings. The test was conducted using a 95 percent confidence level (alpha = 0.05) and the results showed that there was a statistically significant difference between the two independent parameters based on the clear spacing of the bars ($F_{(2, 340)} = 9.54$, $p = 0.0005$; Wilk's lambda

= 0.947) (Appendix E). This difference was illustrated in Figures 27 and 28, where the 1 inch (25 mm) clear spacing bar rack had the greater means in both length and head widths of the eels.

4.4.2 Sample Population

For the biological assessment, a total of 353 silver American eels were used to evaluate the guidance efficiency of each 90 degree bar rack based on the design parameters of clear spacing and approach velocity. The mean length of eels tested was 29.4 inches (746.8 mm), with approximately 3 percent of the test fish having lengths greater or less than the target range of 24 to 36 inches (609.6 to 914.4 mm) (Figure 30). Simple linear regression analysis was used to show the correlation between the length and head width of the eels. The regression equation: $y = 0.0402x - 0.2706$, shows that for every additional 1 inch change in length there is a change in head width of -0.2304 inches (-5.8522 mm). The R^2 value of 0.5271 indicates that about 53 percent of the variation in head width about its mean is explained by variations in the length of the eels. Therefore, the estimated head width of an eel with a length of 30 inches (762 mm) is 0.93 inches (23.6 mm) with a 95 percent confidence interval of 0.92 to 0.94 inches (23.4 to 23.9 mm).
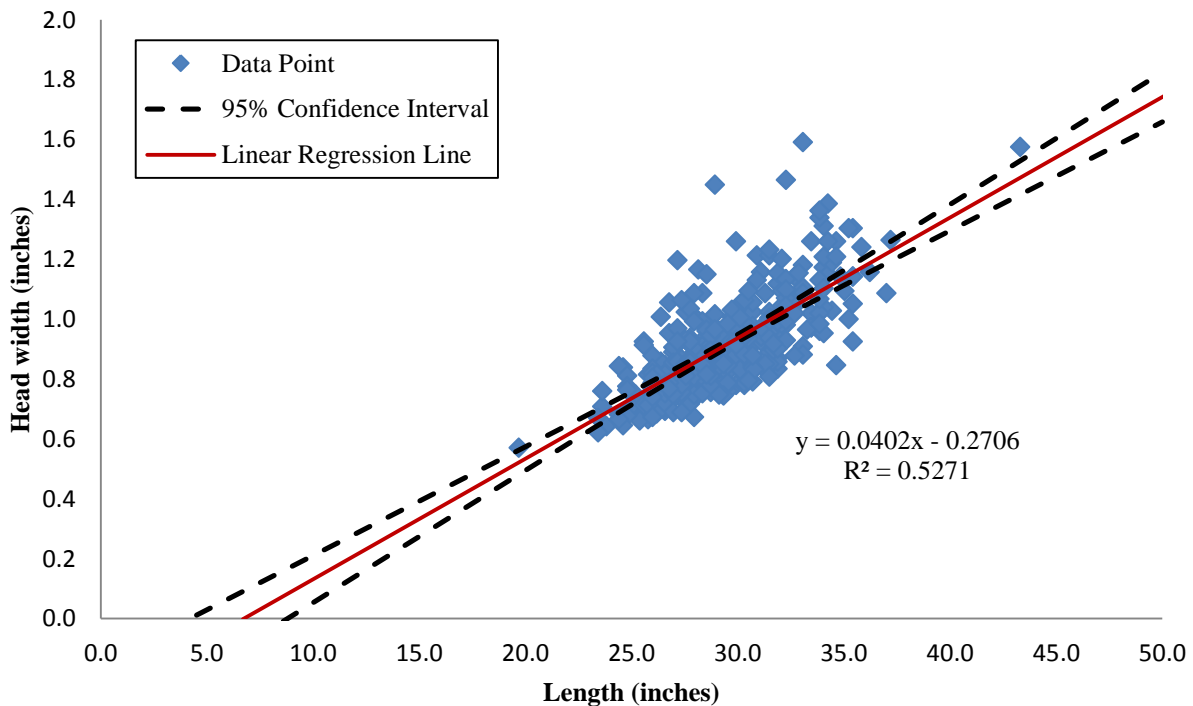
Figure 30 - Linear regression analysis with 95% Confidence interval.

Figure 31 shows the 95 percent predicted interval for the eel population. This interval provides an indication of the range in head widths that might be expected based on the mean length of the eels during downstream migration. For example, for eels with a mean length of 30 inches (762

mm), the estimated head width would be between 0.72 and 1.16 inches (18.3 and 29.5 mm). In general, for experiments with the 0.75-inch (19 mm) rack, eels with lengths less than 20 inches (500 mm) could potentially be entrained, while eels greater than 31 inches (780 mm) would likely not be entrained. For the experiments with the 1.0-inch (25 mm) rack, it was found that eels with lengths less than 26 inches (660 mm) could potentially be entrained, while eels greater than 39 inches (983 mm) would likely not be entrained.
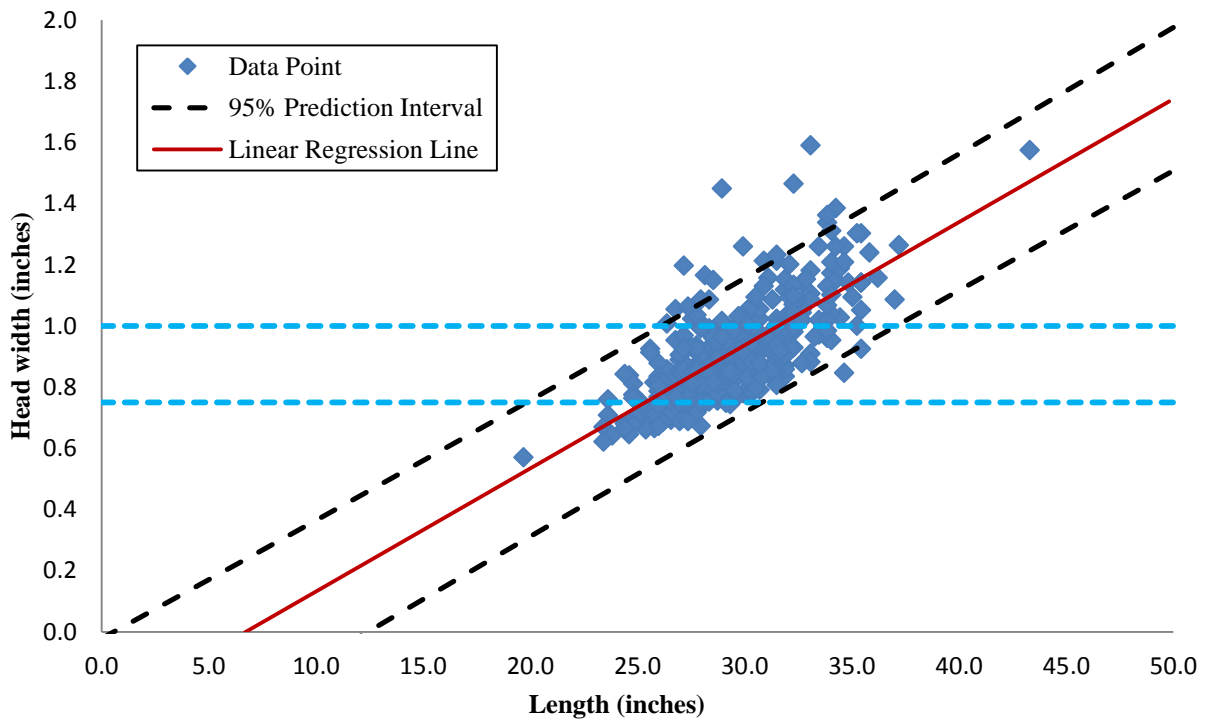
Figure 31 - Linear regression analysis with 95% Prediction interval (Blue dashed lines indicate the clear spacing of the bar racks: 0.75 and 1.0 inches (19 and 25 mm)).

4.4.3 Visual Observations

Visual observations of the eels approaching the bar rack at night time (using the DIDSON camera) revealed that they stayed in close contact with the flume floor and walls but also utilized the entire channel during downstream movement. Due to their drifting ability, they were observed to usually strike the bar rack head first. However, after contact with the rack the eels would immediately swim back upstream or moved perpendicularly to the flow along the bottom of the rack until they moved into the slats or found the entrance to the bypass. A number of eels, during night time observations were found to approach the bar rack tail first, as they were carried by the current of the flow downstream, but upon contact would swim with effort back upstream.

Figure 32 shows the sonar image produced by the DIDSON camera of the eels as they approach the bar rack, where in this particular capture the eels are swimming back upstream after being obstructed by the bar rack. The bypass is shown on the left side of the image with the wedge-wire screen.
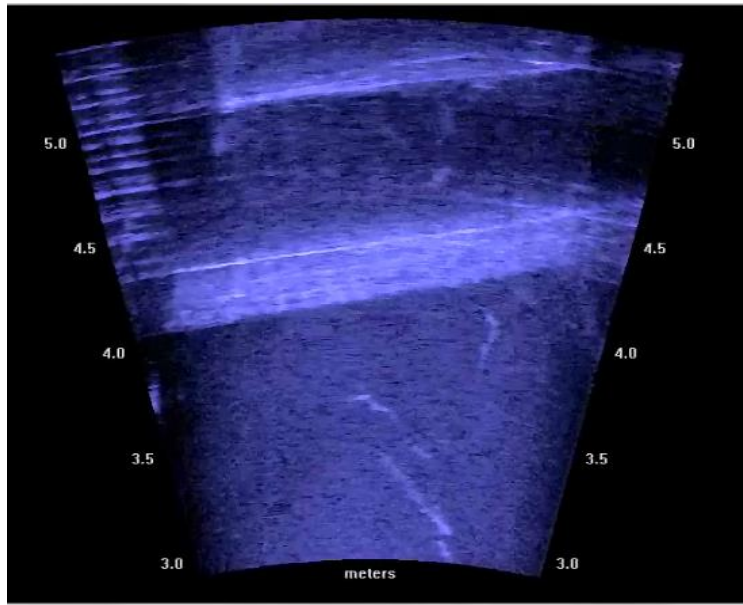
Figure 32 - DIDSON sonar image of eels approaching the bar rack.

Similar behavior was observed during the day time, where the eels would stay in close contact with flume floor and walls and would immediately swim upstream after hitting the rack. However, during the day time majority of the eels remained upstream after they were released and during downstream movement would not utilize the entire channel but remained closer to the walls. Downstream movement dramatically decreased during the day time and less eels were observed to come into contact with the bar rack.

5.0 DISCUSSION AND CONCLUSIONS

This chapter provides an overview of the results presented in the previous chapter. Conclusions are based on the data gathered from the hydraulic and biological assessments. Recommendations for future study are presented and a new head loss equation has been proposed for the convenience of hydropower operators.

5.1 Hydraulic Assessments

The hydraulic aspect of this thesis focused on evaluating design parameters for bar racks that have been prescribed by the US Fish and Wildlife Service (FWS) (including a 0.75 inch (19 mm) clear spacing and 1.5 ft/s (0.46 m/s) approach velocity) and others that have been previously implemented by hydropower operators. Physical modeling tests were conducted for bar racks with 0.75, 1.0 and 1.5 inches (19, 25 and 38 mm) clear spacing, approach velocities of 1.5, 2.0 and 2.5 ft/s (0.46, 0.61 and 0.76 m/s), and structural angles to the flow of 45 and 90 degrees. During the flume testing head loss was measured and hydraulic performance was observed. Numerical models using ANSYS Fluent 14.0 software were also used as a prediction model and a new head loss equation was developed based on the data from the physical testing. The data were found to support the following conclusions:

- Velocity profiles upstream of the 90 and 45 degree bar rack structures do not indicate any major differences in flow approaching the rack at different bar spacings, confirming that experimental conditions were appropriate for assessing head losses
- Head losses for the 45 degree racks were higher than the head losses for the racks angled at 90 degrees
- Numerical models predicted flow patterns more accurately than head loss measurements
- CFD models showed the change in direction of flow approaching a 45 degree bar rack structure compared to the uniform flow approaching the 90 degree rack
- A new proposed head loss equation produced results comparable to those measured by physical modeling

5.2 Biological Assessments

For the biological assessments in this research, downstream passage for the silver American eel was assessed by conducting tests with live eels and recording guidance efficiency as well as eel length and head width data. The scope for the biological assessments included a 90 degree bar rack structure, two configurations (0.75 and 1.0 inches (19 and 25 mm)) and two approach velocities (1.5 and 2.0 ft/s (0.46 and 0.61 mm)). The results are summarized in Section 4.4.

Overall, the results indicate that guidance efficiencies are closely related to the head width in relation to clear spacing of the bar rack openings. Analysis of averages for all data indicated that the guidance efficiencies for the 1.5 ft/s (0.46 m/s) approach velocity were slightly higher than those 2.0 ft/s (0.61 m/s) approach velocity. However, these differences were not statistically significant. In addition, the average guidance efficiency for the 0.75 inch (19 mm) clear spacing was higher than that of the 1.0 inch (25 mm) spacing. However, differences in mean head widths of the eels used for the 0.75 inch (19 mm) and 1.00 inch (25 mm) trials likely affect these results. More specifically, the mean head width of the eels tested with the 0.75 inch (19 mm) spacing rack was lower than that for the 1.0 inch (25 mm) spacing rack. Therefore, the average guidance efficiencies for the 0.75 and 1.00 inch spacing, as presented in this thesis, do not provide a full indication of the relative advantage of the two alternatives for design. Comparisons between guidance efficiencies for specific head width and length ranges can provide more insight into the role of bar spacing. Analysis of these differences and specific considerations regarding head width can be found in EPRI publication (in press).

Visual observations of the behavior and response of the eels to the bar rack provide some insight into their behavior. First, observed eel behavior in this facility was generally similar for day and night time, because the eels tended to remain close to the walls and floor of the flume despite the time of day. However, during night time testing, eels were observed to use the entire channel rather than only the walls (day time observations) for downstream movement. In addition, at higher approach velocities, a greater number of eels interacted with the bar rack during the night as opposed to the daytime observations. The eels were found to drift with the flow during downstream passage but upon contact with the rack (generally head first), they were observed to immediately swim back upstream or move perpendicularly to the flow at the bottom of the rack until they went through the bars or found the bypass. These observations are similar to those found by previous researchers (Adams et al. 1997; EPRI, 2001; Amaral et al. 2003; Brown et al. 2007; Russon et al. 2010) during their behavioral studies of the silver American eel. Therefore, these results further prove the consistency of the behavioral response of eels to downstream fish facilities.

5.3 Recommendations for Further Research

The results from this study provide a basis for assessing the impacts that bar rack design will have on eel passage and head loss at hydropower intakes. Additional research would provide further information to define design requirements for bar racks. For example, the physical modeling tests were conducted under ideal laboratory conditions using a standard bar rack design with relatively short lengths and shallow depths for bar racks and a full-depth bypass. It cannot be fully certain that the guidance efficiency estimates for these conditions would be the same as those that would be found for field applications. As such, further validation of the head loss equations for field conditions and for other blockage scenarios would be valuable. In addition,

the biological testing only included the 90-degree racks. Additional testing with the 45-degree racks would be useful. Additional field tests would help to verify these laboratory results and to determine which design parameters (e.g. clear spacing, approach velocity and head width) will be most important to future applications. Finally, research into the numerical modeling of bar racks open channel should also be considered for more accurate predictions of head loss. The Volume of Fluid (VOF) operator was used for this analysis but due to time limitation a complete research into other methods could not be completed. Additional research addressing the applicability of CFD could provide flexibility in the development of alternative designs for specific conditions. The research completed in conjunction with this thesis provides a basis for these additional investigations.

REFERENCES

Adam, B.; Schwevers, U.; Dumont, U. Behavioral survey of eels (Anguilla anguilla) migrating downstream under laboratory conditions. Verlag Natur & Wissenschaft. 1997, 16, 1-63.

Amaral, S.V.; McMahon, B.J.; Black, J.L.; Winchell, F.C. Fish guidance efficiency of angled bar racks and louvers. *Proceedings of Water Power*. 2001. HCI Publications.

Amaral, S. V.; Winchell, F. C.; McMahon, B. J.; Dixon, D. A. 2003. Evaluation of angled bar racks and louvers for guiding silver phase American eels. *American Fisheries Society Symposium 33:367-376.* 2003.

Anderson, J.D. Computational fluid dynamics. *Governing Equations of Fluid Dynamics.* J.F. Wendt (Ed.). 2009, Part I, 15-51.

ANSYS, Inc. *ANSYS Fluent User's Guide, 14.0,* 2011.

Beak International Inc. *The decline of the American eel (Anguilla rostrata) in the Lake Ontario/St. Lawrence River ecosystem: A modeling approach to identification of data gaps and research priorities.* Lake Ontario Committee: Great Lakes Fishery Commission Ann Arbor, Michigan. 2001, 1-70.

Brown, L.; Boubee, J.; Haro, A. Behavior and fate of downstream migrating eels at hydroelectric power station intakes. *6th International Symposium on Ecohydraulics,* Christchurch, NZ. 2007

Carr, J. W.; Whoriskey, F. G. Migration of silver American eels past a hydroelectric dam and through a coastal zone. *Fisheries Management and Ecology*. 2008, 15, 393-400.

Castonguay, M.; Hodson, P.V.; Couillard, C.M.; Eckersley, M.J.; Dutil, J-D.; Verreault, G. Why is recruitment of the American eel, Anguilla rostrata, declining in the St. Lawrence River and Gulf? *Canadian Journal of Fisheries and Aquatic Sciences.* 1994, 51, 479-488.

Christakis, N.; Croft, T. N.; Patel, M. K. A new unstructured algorithm based on the Volume of Fluid method for tracking material interfaces in a finite-volume framework. R. Herbin; D. Kroner (Eds). *Finite Volumes for Complex Applications III (Third International Symposium on Finite Volumes for Complex Applications, Porquerolles, France)*. Hermes Penton Ltd. London UK. 2002, 487-494.

Clark, S.P.; Tsikata, J.M.; Haresign, M. Experimental study of energy loss through submerged trashracks. *J. Hydraulic Res.* 2010, 48(1), 113–118.

Chow, V.T. Open-channel hydraulics. McGraw-Hill: New York, 1959.

Durif C.; Elie P.; Gosset C.; Rives J.; Travade F. Behavioral study of downstream migrating eels by radio-telemetry at a small hydroelectric power plant. D. A. Dixon (Ed). *Biology, Management and Protection of Catadromous Eels*. American Fisheries Society, Bethesda. 2003, 33, 343-356.

Electric Power Research Institute (EPRI). Assessment of downstream migrant fish protection technologies for hydroelectric application. Prepared by Stone & Webster Engineering Corporation, EPRI Report No. AP-4711, EPRI: Palo Alto, CA, 1986.

Electric Power Research Institute (EPRI). Research Update on Fish Protection Technologies for Water Intakes. Prepared by Stone & Webster Engineering Corporation, EPRI Report No. TR-104122, EPRI: Palo Alto, CA, 1994.

Electric Power Research Institute (EPRI). Fish Protection at Cooling Water Intakes. Prepared by Alden Research Laboratory, Inc., EPRI Report No. TR-114013. EPRI: Palo Alto, CA, 1998.

Electric Power Research Institute (EPRI). Review of Downstream Fish Passage and Protection Technology Evaluations and Effectiveness. Prepared by Alden Research Laboratory, Inc., EPRI Report No. TR-111517, EPRI: Palo Alto, CA, 1999a.

Electric Power Research Institute (EPRI). American Eel (Anguilla rostrata) scoping study: A literature and data review of life history, stock status, population dynamics, and hydroelectric impacts. TR-111873, EPRI: Palo Alto, CA, 1999b.

Electric Power Research Institute (EPRI). Technical Evaluation of the Utility of Intake Approach Velocity as an Indicator of Potential Adverse Environmental Impact Under Clean Water Act Section 316(b). Prepared by Oak Ridge National Laboratory, EPRI Report No. 1000731. EPRI: Palo Alto, CA, 2000.

Electric Power Research Institute (EPRI). Review and documentation of research technologies on passage and protection of downstream migrating catadromous eels at hydroelectric facilities. 1000730. EPRI: Palo Alto, CA, 2001.

Electric Power Research Institute (EPRI). Evaluation of Angled Bar Racks and Louvers for Guiding Fish at Water Intakes. TR-1005193, EPRI: Palo Alto, CA. 2001.

Electric Power Research Institute (EPRI), Evaluation of bar rack designs for protecting silver American eels at Hydropower Intakes, EPRI: Palo Alto, CA, in press.

Facey, D.E.; Van Den Avyle, M. J. Species profiles: life histories and environmental requirements of coastal fishes and invertebrates (North Atlantic) −American eel. US Fish Wildl. Ser. Biological Report 82(11.74) U.S. Army Corps of Engineers, TR EL-82-4. 1987, 28 pp.

Gosset, C.; Travade, F.; Durif, C.; Rives, J.; Elie, P. Tests of two types of bypass for downstream migration of eels at a small hydroelectric power plant. *River Research and Applications.* 2005, 21, 1095–1105.

Gulf of Maine Council on the Marine Environment. *American Eels: Restoring a Vanishing Resource in the Gulf of Maine*. [online], 2007. Science Translation Project of the Gulf of Maine Council.

Haro, A.; Richkus, W.; Whalen, K.; Hoar, A.; Busch, W-D.; Lary, S.; Brush, T.; Dixon, D. Population Decline of the American Eel: Implications for Research and Management. *Fisheries*. 2000, 25(9), 7-16.

Haro, A.; Castro-Santos, T.; Boubée, J. Behavior and passage of silver-phase American eels, Anguilla rostrata (LeSueur) at a small hydroelectric facility. *Dana*. 2000, 12, 41-50.

Hirt, C.W.; Nichols, B.D., Volume of Fluid (VOF) method for the dynamics of free boundaries. *Journal of Computational Physics*. 1981, 39, 201-225.

Idel'chik, I.E.; Barouch, A. *Handbook of Hydraulic Resistance: Coefficients of Local Resistance and of Friction (spravochnik Po Gidravlicheskim Soprotivleniyam, Koeffitsienty Mestnykh Soprotivlenii I Soprotivleniya Treniya)*. National technical information service: Springfield, 1966.

Kamula, R. *Flow over weirs with application to fish passage facilities*. Oulu University Press. Academic Dissertation. 2001, 113 pp.

Khan, L. A Three-Dimensional Computational Fluid Dynamics (CFD) Model Analysis of Free Surface Hydrodynamics and Fish Passage Energetics in a Vertical-Slot Fishway. *North American Journal of Fisheries Management.* 2006, 26(2), 255-267.

Kirschmer, O. Untersuchungen über den Gefällsverlust an Rechen, vol. 1. Mitteilungen des hydraulischen Instituts der TH München. Munich, Germany, 1926.

Larinier, M. Dams and fish migration. *Dams, Ecosystem Functions and Environmental Restoration, Thematic Review II.1 prepared as an input to the World Commission on Dams.* G. Berkamp; M. McCartney; P. Dugan; J. McNeely; M. Acreman. (Eds.). [online], 2000, 1-30.

Larinier, M. Dams, fish and fisheries. Opportunities, challenges and conflict resolution. *FAO Fisheries Technical Paper*. No. 419. G. Marmulla. (Ed.) Rome, FAO. 2001. 166 p.

Lary S.J.; Busch, W.D.N. American Eel, Anguilla rostrata, in Lake Ontario and its tributaries: distribution, abundance, essential habitat and restoration requirements. *Administrative Report No. 97-01*. US. Department of the Interior, Fish and Wildlife Service, Lower Great Lakes Fishery Resources Office: Amherst, NY, 1997, 27 pp.

Ma, L.; Ashworth, P.J.; Best, J.L.; Elliott, L.; Ingham, D.B.; Whitcombe, L.J. Computational fluid dynamics and the physical modeling of an upland urban river. *Geomorphology*. 2002, 44(3-4), 375-391

Marcogliese, L.A.; Casselman, J.M.; Hodson, P.V. *Dramatic Declines in Recruitment of American Eel (Anguilla Rostrata) Entering Lake Ontario - Long Term Trends, Causes and Effects.* Plenary presentation at the 3rd National EMAN Meeting: Saskatoon, Saskatchewan, January 22, 1997.

Meusburger, H. Energieverluste an Einlaufrechen von Flusskraftwerken. *PhD thesis*. Bau-Ing., ETH-Zürich, 2002. http://e-collection.library.ethz.ch/view/eth:26261.

Montazeri-Namin, M.; Ghazanfari-Hashemi, R. S.; Ghaeini-Hessaroeyeh, M. *3D Numerical Simulation of Supercritical Flow in Bends of Channel.* International Conference on Mechanical, Automotive and Materials Engineering (ICMAME): Dubai, 2012, 167-171.

Raynal, S.; Courret, D.; Chatellier, L.; Larinier, M.; David, L. An experimental study on fish-friendly trashracks – Part 2. Angled trashracks *J. Hydraulic Res.* 2013, 51(1), 67-75.

Richmond, M.C.; Carlson, T.J.; Serkowski, J.A.; Cook, C.B.; Duncan, J.P.; Perkins, W.A. *Characterizing the Fish Passage Environment at The Dalles Dam Spillway: 2001-2004.* PNNL-16521, Pacific Northwest National Laboratory: Richland, WA, 2007.

Roberson, J.A.; Cassidy, J.J.; Chaudhry, M.H. *Hydraulic Engineering* (2nd ed.). John Wiley & Sons: New York, NY, 1998.

Russon, I. J.; Kemp, P. S.; Calles, O. Response of downstream migrating adult European eels (Anguilla anguilla) to bar racks under experimental conditions. *Ecology of Freshwater Fish*. 2010, 19, 197-205.

Schilt, C.R. Developing fish passage and protection at hydropower dams. *Applied Animal Behavior Science*. 2007, 104 (3-4), 295-325.

Spangler, J. Investigations of loss through trash racks inclined obliquely to the stream flow. *Hydraulic of the laboratory practice*, ASME, New York, 1929, 461–470.

U.S. Fish and Wildlife Service. *Existing Hydroprojects with Operating Fish Passage Facilities in FWS Region 5*. Draft. January 2000.

U.S. Fish and Wildlife Service. The American eel. *News release, 2011: American Eel May Warrant Protection Under the Endangered Species Act*. [online], 2011.

Van Den Avyle, M. J. Species profiles: life histories and environmental requirements of coastal fishes and invertebrates (South Atlantic) – American eel. U.S. Fish Wildl. Serv. FWS/OBS-82/11.24. U.S. Army Corps of Engineers, lR EL-82-4, 1984, 20 pp.

Virginia Institute of Marine Sciences. *American Eel Monitoring Program: Life History*. http://www.vims.edu/research/departments/fisheries/programs/eel_survey/life_history/index. php (accessed March 4, 2013).

Yang, H.; Haynes, M.; Winzenread, S.; Okada, K. *The History of Dams*. [online], 1999.

Zimmermann, J. Widerstand schräg angeströmter Rechengitter. Universität Fridericana Karlsruhe, Theodor-Rhebock-Flußbaulaboratorium, Mitteilungen Heft 157. 1969.

APPENDIX A: OPERATOR INTERVIEW QUESTIONS

1. Name of site (project):_____
2. Name of river or upstream water body: _____
3. Type of development:
   _____ hydro   _____ steam electric
   _____ potable water supply   _____ other (specify)
   _____ irrigation
4. Name of owner: _____
   Address: _____

   _____
5. Name of survey respondent: _____
6. Flow rate through development: _____cfs
7. Head: _____ ft
8. Capacity of development: _____mw (if applicable)
9. Is fish passage facility...?
   _____proposed
   _____existing
   _____not required
   _____future unspecified requirement
10. How long has this facility been in operation? _____
11. Type of passage facility (check more than one, if applicable)
    _____angled screen
    _____inclined screen
    _____angled louver
    _____drum screen
    _____bar rack
    _____vertical traveling screen
    _____bypass
    _____physical collection
    _____spillway
    _____pipeline
    _____other (specify) _____
12. What fish species are commonly found in this area?

    _____
13. List names and size and/or life stages of species to be protected:

Name	Size and/or Life stage

14. Period and seasons of operation

      _____daytime   _____all seasons

      _____nighttime   _____limited periods of the year

      _____24 hours

15. Is the facility equally effective under all flow conditions, seasons or time of day?

    _____

    _____

16. Published or unpublished references, notes, data, etc. On facility design, operation and cost (please list and if possible, send copies).

    _____

    _____

17. Further contacts for additional information

    _____

    _____

18. Has the facility been reliable or effective from an engineering standpoint? If not please indicate types of operational problems.

    _____

    _____

19. What are the impacts of the fish passage facilities on the operation of the facility?

    headloss _____ft

    lost power _____kw-hrs/yr

    power downtime _____hrs/yr

20. Please identify systems/components requiring maintenance and the frequency and duration of such activities.

    _____

    _____

21. Please describe any unexpected problems (e.g. Deris loading) and solutions to these problems.

    _____

    _____

22. Additional comments

    _____

APPENDIX B: CFD VELOCITY CONTOUR PLOTS
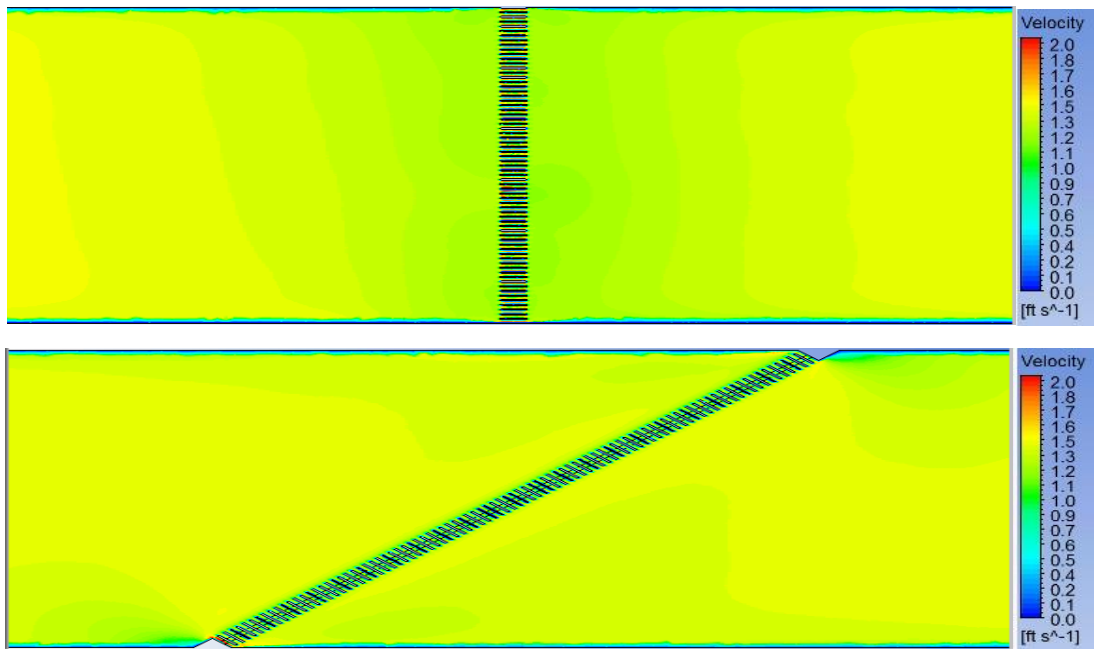
Figure B-1 - Simulated velocity contours of flow through the flume at 1.5 ft/s with a bar rack of 0.75 in. spacing at 90 and 45 degrees.
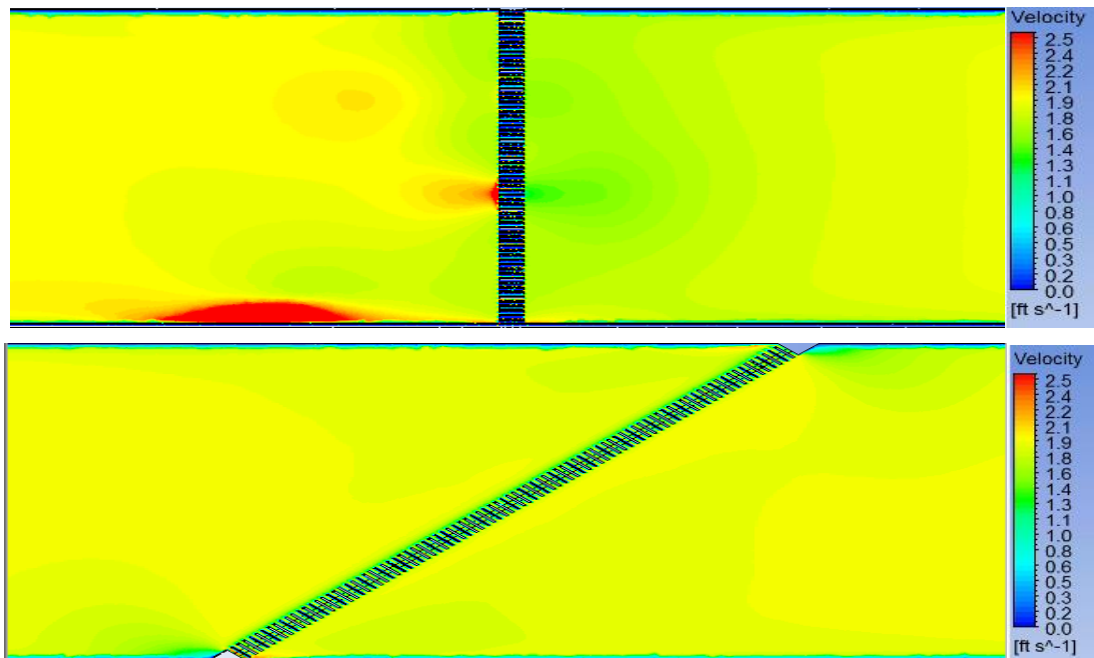
Figure B-2 - Simulated velocity contours of flow through the flume at 2.0 ft/s with a bar rack of 0.75 in. spacing at 90 and 45 degrees.
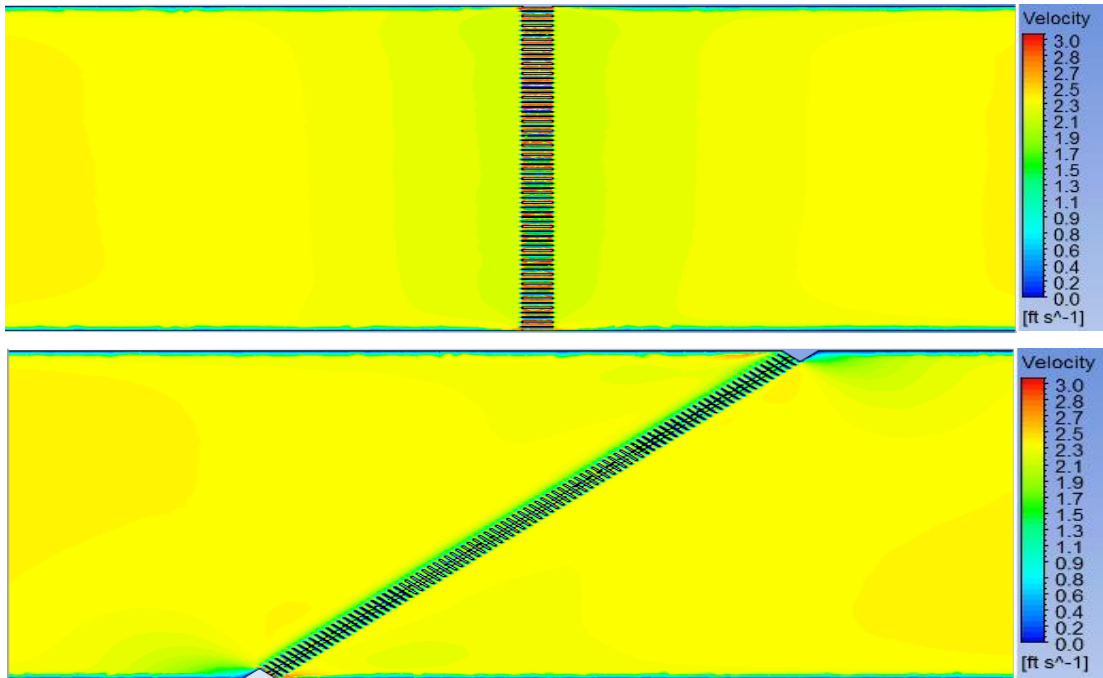
Figure B-3 - Simulated velocity contours of flow through the flume at 2.5 ft/s with a bar rack of 0.75 in. spacing at 90 and 45 degrees.
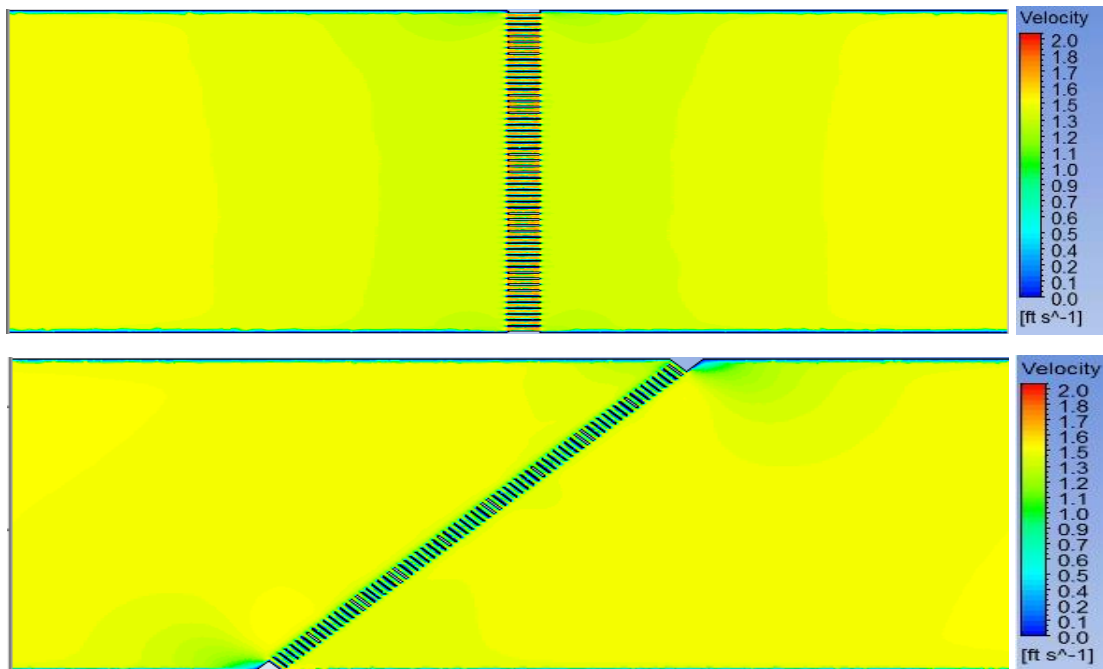
Figure B-4 - Simulated velocity contours of flow through the flume at 1.5 ft/s with a bar rack of 1.00 in. spacing at 90 and 45 degrees.
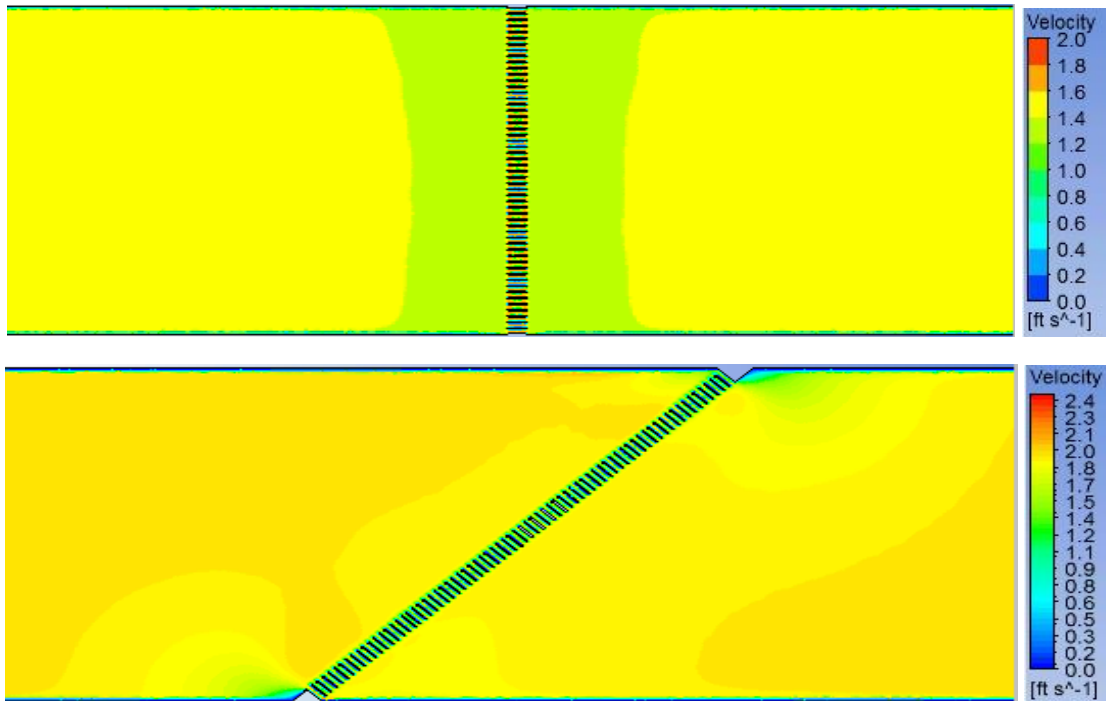
Figure B-5 - Simulated velocity contours of flow through the flume at 2.0 ft/s with a bar rack of 1.00 in. spacing at 90 and 45 degrees.
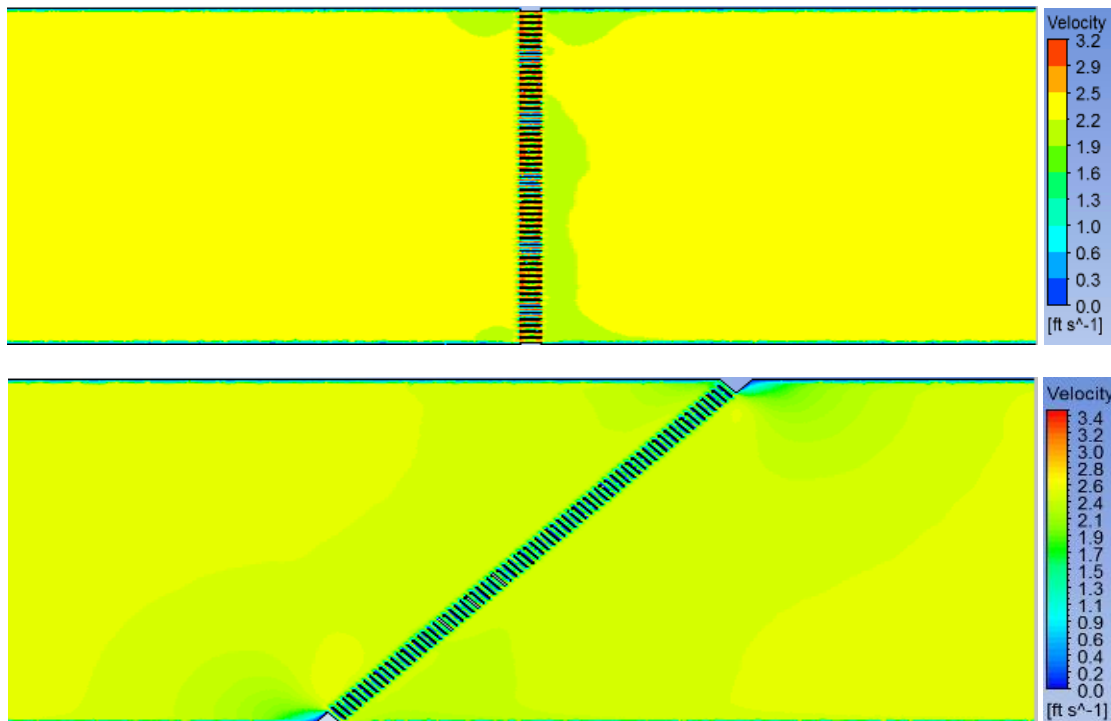
Figure B-6 - Simulated velocity contours of flow through the flume at 2.5 ft/s with a bar rack of 1.00 in. spacing at 90 and 45 degrees.
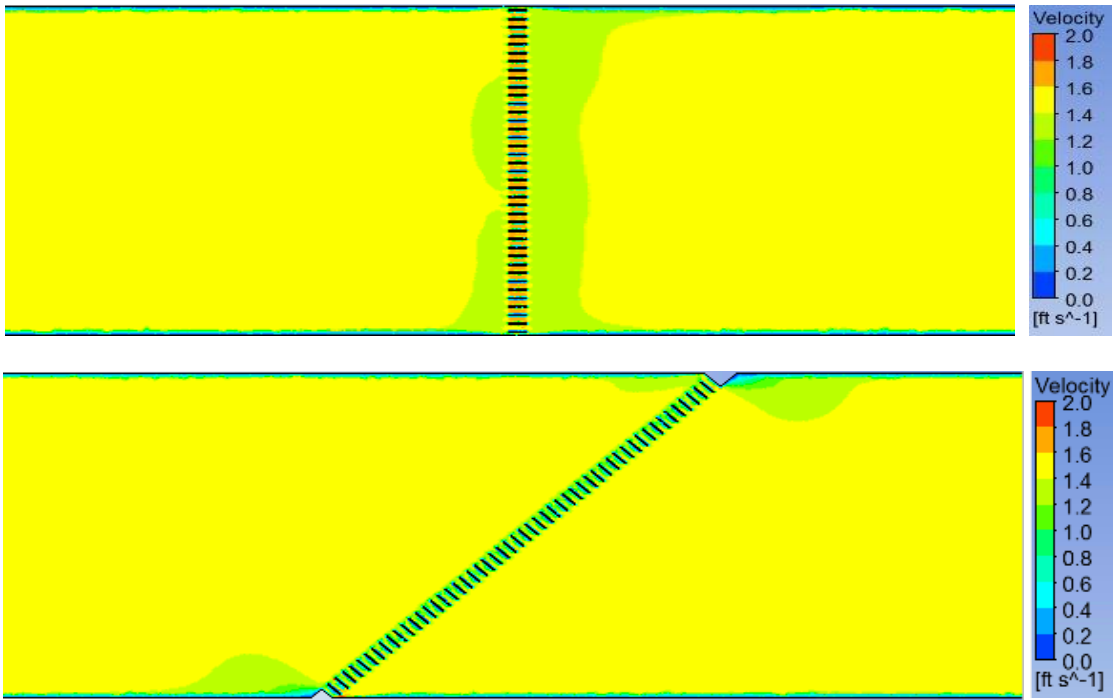
Figure B-7 - Simulated velocity contours of flow through the flume at 1.5 ft/s with a bar rack of 1.50 in. spacing at 90 and 45 degrees.
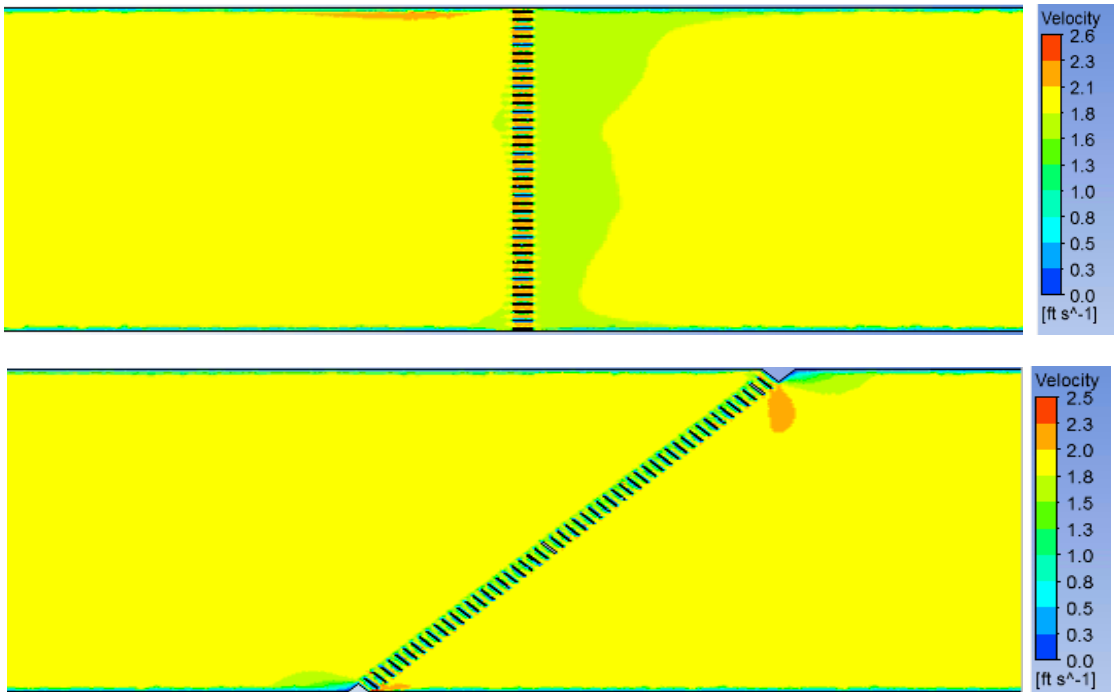
Figure B-8 - Simulated velocity contours of flow through the flume at 2.0 ft/s with a bar rack of 1.50 in. spacing at 90 and 45 degrees.
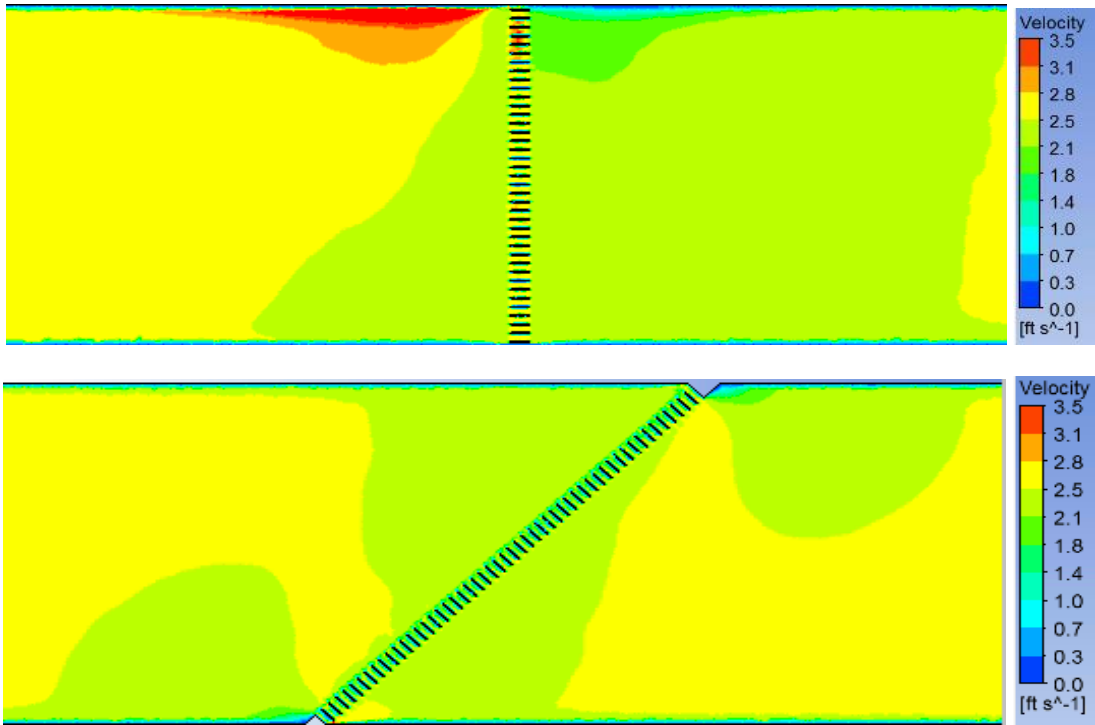
Figure B-9 - Simulated velocity contours of flow through the flume at 2.5 ft/s with a bar rack of 1.50 in. spacing at 90 and 45 degrees.

APPENDIX C: HYDRAULIC DATA

Table C-1 - Hydraulic Head Data

ANGLE (degrees)	SPACING (in)	AVG. APPROACH VELOCITY (ft/s)	HYDRAULIC HEAD (in)	HYDRAULIC HEAD (Volts)	PUMP RPM
45	0.75	1.34	1.00	2.33	291
		1.89	2.00	2.79	435
		2.27	2.38	2.78	491
90	0.75	1.50	0.50	2.13	330
		2.03	0.75	2.21	434
		2.47	1.00	2.29	525
45	1.00	1.54	1.00	2.38	339
		1.97	1.75	2.59	432
		2.50	2.75	2.92	540
90	1.00	1.51	0.25	2.12	334
		2.01	0.50	2.17	425
		2.49	0.75	2.24	525
45	1.50	1.51	1.00	2.43	354
		2.03	2.00	2.68	461
		2.52	2.88	2.97	568
90	1.50	1.51	0.25	2.13	347
		2.01	0.50	2.16	446
		2.50	0.75	2.21	535

Table C-2 - Upstream and Downstream Velocity Measurements

ANGLE (degrees)	SPACING (in)	UPSTREAM (2m)			AVG VELOCITY AT DEPTH	AVG. VELOCITY (U/S)
45	0.75	1.4312	1.4651	1.3169	1.4044	1.3381
		1.2307	1.4941	1.3624	1.3624	
		1.3297	1.2221	1.1906	1.2475	
		1.866	1.8544	1.8544	1.8583	1.8903
		1.9722	2.0012	1.998	1.9905	
		1.7936	1.9342	1.739	1.8223	
		2.4182	2.455	2.1708	2.3480	2.2740
		2.4213	2.5038	2.2398	2.3883	
		2.1153	2.0641	2.0777	2.0857	
90	0.75	1.5379	1.5025	1.3834	1.4746	1.5012
		1.5415	1.6260	1.4690	1.5455	
		1.5105	1.5210	1.4189	1.4835	
		2.2779	2.1321	1.7045	2.0382	2.0314
		2.1512	2.1453	1.9317	2.0761	
		2.0108	2.0647	1.8641	1.9799	
		2.6196	2.7145	2.135	2.4897	2.4698
		2.5874	2.6388	2.3842	2.5368	
		2.4626	2.3593	2.3271	2.3830	
45	1.00	1.6237	1.6337	1.3073	1.5216	1.5351
		1.5678	1.6089	1.5146	1.5638	
		1.5464	1.5460	1.4671	1.5198	
		2.1216	2.0390	1.6411	1.9339	1.9682
		2.0629	2.1067	1.9645	2.0447	
		1.9760	1.9558	1.8459	1.9259	
		2.6754	2.7426	2.2050	2.5410	2.5010
		2.5762	2.5845	2.3859	2.5155	
		2.4335	2.5026	2.4037	2.4466	
90	1.00	1.7152	1.5965	1.2964	1.5360	1.5144
		1.6186	1.6423	1.4887	1.5832	
		1.4744	1.4119	1.3856	1.4240	
		2.2745	2.0697	1.6749	2.0064	2.0088
		2.1083	2.1743	1.9762	2.0863	
		1.9152	2.0460	1.8402	1.9338	
		2.8504	2.8649	2.1852	2.6335	2.4913
		2.5432	2.6752	2.4119	2.5434	
		2.2531	2.4772	2.1605	2.2969	

Table C-2 - Upstream and Downstream Velocity Measurements (Continued)

		1.6338	1.5048	1.3317	1.4901	
		1.5260	1.5878	1.4615	1.5251	1.5066
		1.5216	1.5819	1.4106	1.5047	
45	1.50	2.2097	2.1713	1.6631	2.0147	
		2.1094	2.2377	1.9734	2.1068	2.0269
		1.9699	1.9793	1.9287	1.9593	
		2.6242	2.8292	2.2184	2.5573	
		2.7277	2.7049	2.4118	2.6148	2.5211
		2.2736	2.4682	2.4317	2.3912	
90	1.50	1.5886	1.4879	1.2321	1.4362	
		1.5775	1.6096	1.4993	1.5621	1.5113
		1.5705	1.6222	1.4136	1.5354	
		2.0683	2.0206	1.6364	1.9084	
		2.1833	2.1068	2.0208	2.1036	2.0071
		2.0469	2.0587	1.9220	2.0092	
		2.5809	2.6339	2.0422	2.4190	
		2.5658	2.7481	2.4451	2.5863	2.4957
		2.4567	2.5434	2.4449	2.4817	

Table C-2 - Upstream and Downstream Velocity Measurements (Continued)

ANGLE (degrees)	SPACING (in)	DOWNSTREAM (1.2m)			AVG VELOCITY AT DEPTH	AVG. VELOCITY (D/S)
45	0.75	2.1558	1.8538	1.3169	1.7755	
		2.1077	1.6888	0.5338	1.4434	1.5268
		2.0908	1.8747	0.1192	1.3616	
		3.0447	2.6166	0.2962	1.9858	
		3.3032	2.7098	0.7351	2.2494	2.1509
		3.4335	3.0835	0.1353	2.2174	
		3.4198	3.17	0.3742	2.3213	
		3.5326	3.1227	0.7117	2.4557	2.4310
		3.9266	3.3274	0.2944	2.5161	
90	0.75	1.4949	1.4727	1.2637	1.4104	
		1.4677	1.4565	1.3829	1.4357	1.4487
		1.4666	1.6093	1.4244	1.5001	
		2.1988	2.3632	1.7366	2.0995	
		2.1056	2.1167	1.8761	2.0328	2.0286
		1.9024	2.1035	1.8544	1.9534	
		2.6237	2.8722	2.1714	2.5558	
		2.4619	2.5046	2.2126	2.3930	2.4589
		2.437	2.4706	2.3759	2.4278	
45	1.00	2.3657	2.1567	0.2272	1.5832	
		2.4364	2.2080	0.5740	1.7395	1.6769
		2.3725	2.1791	0.5722	1.7079	
		3.1175	2.9516	0.2290	2.0994	
		3.0870	2.9174	0.5869	2.1971	2.1442
		2.9557	2.6658	0.7869	2.1361	
		3.8987	3.7872	0.4078	2.6979	
		4.1793	3.6771	0.8676	2.9080	2.7669
		3.7816	3.5281	0.7751	2.6949	
90	1.00	1.7156	1.6120	1.2628	1.5301	
		1.5291	1.5426	1.5087	1.5268	1.5293
		1.5027	1.5339	1.5559	1.5308	
		2.2184	2.2571	1.7355	2.0703	
		1.9205	2.0401	1.9655	1.9754	2.0224
		1.8939	2.0619	2.1089	2.0216	
		2.7845	2.8851	2.3514	2.6737	
		2.373	2.5384	2.4572	2.4562	2.5486
		2.3617	2.5937	2.5923	2.5159	

Table C-2 - Upstream and Downstream Velocity Measurements (Continued)

		2.5142	2.2980	0.2727	1.6950	
		2.4055	2.1068	0.6305	1.7143	1.7475
		2.7147	2.3594	0.4253	1.8331	
45	1.50	3.3269	3.1380	0.3851	2.2833	
		3.3403	2.9531	0.8638	2.3857	2.2933
		3.3333	2.9484	0.3510	2.2109	
		4.1330	4.0013	0.5685	2.9009	
		4.5548	3.9940	0.9982	3.1823	2.9812
		4.1462	3.9604	0.4741	2.8602	
90	1.50	1.7455	1.5736	1.2372	1.5188	
		1.5897	1.5656	1.4474	1.5342	1.5117
		1.5012	1.5668	1.3786	1.4822	
		2.1589	2.0795	1.6114	1.9499	
		1.9911	1.9703	1.8086	1.9233	1.9826
		2.0878	2.2759	1.8595	2.0744	
		2.6106	2.5569	1.7973	2.3216	
		2.3962	2.5661	2.3085	2.4236	2.4472
		2.5373	2.6986	2.5537	2.5965	

Table C-3 - Velocity Measurements at the Rack

ANGLE (degrees)	SPACING (in)	UPSTREAM (AT RACK - 0.2m)			AVG. VELOCITY (U/S - AT RACK)
45	0.75	1.3750	1.8809	1.9036	1.7107
		1.3796	1.7708	2.0092	
		1.3011	1.8019	1.9742	
		2.0088	2.6593	3.0146	2.6303
		2.1142	2.8833	3.1408	
		2.0685	2.679	3.104	
		2.4595	3.1654	3.5664	3.4542
		2.3952	3.4371	3.6732	
		2.2981	3.3874	3.4956	
90	0.75	1.6196	1.4685	1.2898	1.5016
		1.5412	1.5797	1.4362	
		1.6452	1.5355	1.3989	
		2.2544	2.0998	1.717	2.0515
		2.166	2.2427	1.9236	
		2.1643	2.0388	1.8571	
		2.6822	2.6871	2.1014	2.4981
		2.4601	2.6989	2.3496	
		2.61	2.5772	2.3162	
45	1.00	1.5311	1.9825	2.2468	1.9833
		1.5328	2.1191	2.4031	
		1.5045	2.0241	2.5058	
		1.9857	2.7549	2.9913	2.5792
		1.9588	2.6512	3.1953	
		1.7440	2.6655	3.2665	
		2.4460	3.5752	3.6478	3.2999
		2.3382	3.6199	3.9003	
		2.2509	3.5464	4.3742	

Table C-3 - Velocity Measurements at the Rack (Continued)

90	1.00	1.7081	1.5536	1.3202	1.5738
		1.6002	1.7175	1.5093	
		1.6205	1.6358	1.4994	
		2.1082	1.9228	1.6959	2.0428
		2.1460	2.2814	1.9659	
		2.0790	2.2074	1.9788	
		2.6612	2.8633	2.2015	2.5877
		2.6182	2.8713	2.4031	
		2.5545	2.6671	2.4487	
45	1.50	1.5357	2.1232	2.3733	2.0793
		1.5212	2.1671	2.6193	
		1.5300	2.1727	2.6715	
		2.1514	3.0153	3.3101	2.8057
		2.0972	2.9772	3.4242	
		1.8828	2.9675	3.4255	
		2.4807	3.6193	4.0947	3.4179
		2.5863	3.6089	4.2299	
		2.4251	3.5164	4.1995	
90	1.50	1.4951	1.4059	1.1688	1.5101
		1.6376	1.6105	1.4882	
		1.6287	1.7002	1.4555	
		2.1638	2.0744	1.4682	2.0634
		2.2603	2.2844	1.9096	
		2.1654	2.3207	1.9234	
		2.4934	2.7147	1.9625	2.5561
		2.6766	2.7396	2.4116	
		2.5992	2.8213	2.5859	

APPENDIX D: DEBRIS LOADING DATA

Table D-1 - Hydraulic Head Measurements

ANGLE (degrees)	SPACING (in)	APPROACH VELOCITY (ft/s)	BLOCKAGE	MID VEL	HYDRAULIC HEAD (in)	HYDRAULIC HEAD (Volts)
45	0.75	1.50	57%	1.5058	**2.38**	2.85
		2.00		2.0099	**4.00**	3.33
		2.50		2.5211	**6.25**	4.01
	0.75	1.50	37%	1.6335	**1.88**	2.64
		2.00		2.0278	**2.88**	3.00
		2.50		2.6155	**4.50**	3.51
	0.75	1.50	17%	1.6146	**1.50**	2.55
		2.00		2.2080	**2.38**	2.82
		2.50		2.7385	**3.75**	3.35
90	0.75	1.50	61%	1.4633	**3.38**	2.50
		2.00		1.9364	**5.63**	3.28
		2.50				
	0.75	1.50	43%	1.5099	**1.75**	2.10
		2.00		1.9671	**3.00**	2.55
		2.50		2.5643	**4.38**	2.95
	0.75	1.50	23%	1.5721	**1.00**	1.95
		2.00		2.1409	**1.50**	2.07
		2.50		2.5571	**2.38**	2.33
45	1.00	1.50	57%	1.5036	**2.25**	2.78
		2.00		2.0504	**3.75**	3.28
		2.50		2.6055	**6.00**	3.95
	1.00	1.50	37%	1.6539	**1.75**	2.58
		2.00		2.1036	**2.63**	2.92
		2.50		2.6412	**4.25**	3.37
	1.00	1.50	18%	1.6562	**1.38**	2.45
		2.00		2.1318	**2.13**	2.72
		2.50		2.6499	**3.38**	3.10

Table D-1 - Hydraulic Head Measurements (Continued)

90	1.00	1.50	61%	1.5192	**3.25**	2.09
		2.00		1.9407	**5.00**	3.67
		2.50				
	1.00	1.50	43%	1.6020	**1.75**	2.59
		2.00		2.0530	**2.75**	2.92
		2.50		2.4788	**4.00**	3.31
	1.00	1.50	23%	1.5936	**1.00**	2.33
		2.00		1.9855	**1.50**	2.48
		2.50		2.5531	**2.00**	2.69
45	1.50	1.50	57%	1.6606	**2.50**	2.85
		2.00		2.0508	**4.13**	3.38
		2.50		2.5618	**6.25**	4.01
	1.50	1.50	37%	1.6630	**1.50**	2.56
		2.00		1.9577	**2.75**	2.94
		2.50		2.6502	**4.00**	3.38
	1.50	1.50	17%	1.6465	**1.25**	2.49
		2.00		2.3151	**2.13**	2.80
		2.50		2.8409	**3.50**	3.17
90	1.50	1.50	61%	1.3967	**3.25**	3.12
		2.00		1.7978	**5.25**	3.71
		2.50				
	1.50	1.50	43%	1.4124	**1.63**	2.55
		2.00		1.8466	**2.50**	2.87
		2.50		2.2146	**3.38**	3.15
	1.50	1.50	23%	1.4483	**0.88**	2.32
		2.00		1.8907	**1.38**	2.47
		2.50		2.2996	**1.88**	2.66

Table D-2 - Water Depth Measurements

ANGLE	SPACING (in)	APPROACH VELOCITY (ft/s)	BLOCK-AGE	WATER DEPTH (in)						MEASURED DEPTH
				U/S (2.0 m)		AVG. U/S	D/S (1.6 m)		AVG. D/S	
45	0.75	1.50	57%	61.50	62.00	61.75	58.75	60.00	59.38	**2.38**
		2.00		62.50	63.00	62.75	58.00	59.00	58.50	**4.25**
		2.50		63.50	64.00	63.75	57.00	58.00	57.50	**6.25**
	0.75	1.50	37%	60.75	61.25	61.00	59.00	59.75	59.38	**1.63**
		2.00		61.63	62.00	61.81	58.50	59.25	58.88	**2.94**
		2.50		62.50	63.00	62.75	58.00	58.50	58.25	**4.50**
	0.75	1.50	17%	60.50	61.00	60.75	59.00	59.50	59.25	**1.50**
		2.00		61.00	61.25	61.13	58.50	59.38	58.94	**2.19**
		2.50		61.50	62.25	61.88	58.50	59.00	58.75	**3.13**
90	0.75	1.50	61%	62.00	62.00	62.00	59.00	59.00	59.00	**3.00**
		2.00		63.25	63.50	63.38	58.00	58.50	58.25	**5.13**
		2.50								
	0.75	1.50	43%	60.75	60.75	60.75	59.25	59.75	59.50	**1.25**
		2.00		61.50	61.50	61.50	59.00	59.00	59.00	**2.50**
		2.50		62.25	62.25	62.25	59.00	58.25	58.63	**3.63**
	0.75	1.50	23%	60.25	60.25	60.25	59.25	59.75	59.50	**0.75**
		2.00		60.50	60.50	60.50	59.25	60.00	59.63	**0.88**
		2.50		61.00	61.00	61.00	58.75	59.50	59.13	**1.88**
45	1.00	1.50	57%	61.38	61.00	61.19	59.00	58.25	58.63	**2.56**
		2.00		62.00	61.50	61.75	58.25	57.75	58.00	**3.75**
		2.50		63.50	63.00	63.25	57.25	56.75	57.00	**6.25**
	1.00	1.50	37%	60.75	60.50	60.63	58.50	59.38	58.94	**1.69**
		2.00		61.50	61.00	61.25	59.00	58.13	58.56	**2.69**
		2.50		62.25	61.75	62.00	58.00	57.50	57.75	**4.25**
	1.00	1.50	18%	60.75	60.50	60.63	59.88	59.00	59.44	**1.19**
		2.00		61.25	61.00	61.13	59.50	59.00	59.25	**1.88**
		2.50		62.00	61.50	61.75	58.25	59.00	58.63	**3.13**

Table D-2 - Water Depth Measurements (Continued)

	1.00	1.50		61.75	61.75	61.75	58.50	58.88	58.69	**3.06**
		2.00	61%	62.75	62.75	62.75	58.25	57.25	57.75	**5.00**
		2.50								
90	1.00	1.50		60.50	60.50	60.50	59.25	59.00	59.13	**1.38**
		2.00	43%	61.25	61.00	61.13	59.25	58.50	58.88	**2.25**
		2.50		62.00	61.50	61.75	59.00	58.25	58.63	**3.13**
	1.00	1.50		60.00	60.00	60.00	59.75	59.25	59.50	**0.50**
		2.00	23%	60.25	60.25	60.25	59.25	59.00	59.13	**1.13**
		2.50		61.00	60.50	60.75	59.25	58.75	59.00	**1.75**
	1.50	1.50		61.00	60.75	60.88	58.75	58.00	58.38	**2.50**
		2.00	57%	62.00	61.75	61.88	58.00	57.25	57.63	**4.25**
		2.50		63.25	63.00	63.13	57.25	56.75	57.00	**6.13**
45	1.50	1.50		60.75	60.25	60.50	59.00	58.13	58.56	**1.94**
		2.00	37%	61.25	61.00	61.13	58.50	57.75	58.13	**3.00**
		2.50		62.50	62.00	62.25	57.50	57.00	57.25	**5.00**
	1.50	1.50		60.25	60.00	60.13	59.00	58.50	58.75	**1.38**
		2.00	17%	61.00	60.50	60.75	58.38	58.00	58.19	**2.56**
		2.50		61.75	61.50	61.63	58.00	57.50	57.75	**3.88**
	1.50	1.50		61.75	61.75	61.75	59.00	58.50	58.75	**3.00**
		2.00	61%	63.00	63.00	63.00	58.50	57.75	58.13	**4.88**
		2.50								
90	1.50	1.50		60.50	60.50	60.50	59.63	59.13	59.38	**1.13**
		2.00	43%	61.00	61.00	61.00	59.25	58.88	59.06	**1.94**
		2.50		61.50	61.50	61.50	59.00	58.50	58.75	**2.75**
	1.50	1.50		60.00	60.00	60.00	59.75	59.13	59.44	**0.56**
		2.00	23%	60.00	60.00	60.00	59.63	59.13	59.38	**0.63**
		2.50		60.75	60.75	60.75	59.63	58.88	59.25	**1.50**

Table D-3 - Surface Velocity Measurements at the Rack

ANGLE (degrees)	SPACING (in)	APPROACH VELOCITY (ft/s)	BLOCKAGE	VELOCITY AT RACK		
45	0.75	1.50	57%	1.2684	1.7338	1.6083
		2.00		1.9448	2.1902	2.1076
		2.50		2.3576	2.8812	2.5893
	0.75	1.50	37%	1.6590	1.7140	1.6278
		2.00		2.2728	2.2711	2.2623
		2.50		2.5680	2.7808	2.5415
	0.75	1.50	17%	2.1216	2.0265	1.7844
		2.00		2.4887	2.4503	2.2877
		2.50		3.3774	3.2653	2.8466
90	0.75	1.50	61%	1.0192	1.1133	1.1426
		2.00		1.4446	1.5004	1.6311
		2.50				
	0.75	1.50	43%	1.4775	1.3866	1.5365
		2.00		2.0645	1.8761	2.1315
		2.50		2.0357	2.0356	2.1037
	0.75	1.50	23%	1.5245	1.3802	1.7529
		2.00		2.0587	1.9157	2.4110
		2.50		1.8643	2.1650	2.4181
45	1.00	1.50	57%	1.5626	1.7657	1.5866
		2.00		2.0431	2.2292	2.0531
		2.50		2.5287	2.8817	2.3779
	1.00	1.50	37%	1.6755	1.8476	1.9170
		2.00		2.1260	2.2781	2.2217
		2.50		2.6627	3.0793	3.0591
	1.00	1.50	18%	1.5661	1.8408	1.8269
		2.00		2.1513	2.4617	2.4517
		2.50		2.6374	3.2165	3.1186
90	1.00	1.50	61%	1.2654	1.1609	1.2924
		2.00		1.6108	1.4243	1.2986
		2.50				
	1.00	1.50	43%	1.5616	1.4998	1.3776
		2.00		1.9589	1.7871	1.6300
		2.50		2.5140	2.5793	2.2339
	1.00	1.50	23%	1.6740	1.4794	1.3366
		2.00		2.1719	1.9235	1.6591
		2.50		2.6113	2.5479	2.0699

Table D-3 - Surface Velocity Measurements at the Rack (Continued)

	1.50	1.50	57%	1.6171	1.6876	1.5151
		2.00		2.1000	2.2561	1.8599
		2.50		2.5876	2.9672	2.4021
45	1.50	1.50	37%	1.6130	1.9200	1.7344
		2.00		2.0212	2.4636	2.1907
		2.50		2.6177	3.3382	2.9030
	1.50	1.50	17%	1.5106	2.0053	2.0949
		2.00		2.0193	2.6248	2.7799
		2.50		2.4898	3.4283	3.5591
	1.50	1.50	61%	1.4619	1.3495	1.1963
		2.00		1.7194	1.5943	1.4149
		2.50				
90	1.50	1.50	43%	1.4771	1.3212	1.2437
		2.00		1.9868	1.8670	1.6914
		2.50		2.3236	2.2721	1.9589
	1.50	1.50	23%	1.6205	1.3409	1.1841
		2.00		2.1372	1.8509	1.5791
		2.50		2.5904	2.3333	1.9315

APPENDIX E: STATISTICAL ANALYSIS

Table E-1 - Descriptive Statistics

	Spacing	Velocity	Location	Mean	Std. Deviation	N
Length	.75	1.50	BYP	29.6338	2.96695	74
			ENT	27.7667	1.06927	3
			UPS	29.5000	3.90503	14
			Total	29.5516	3.07901	91
		2.00	BYP	29.1394	3.26081	66
			ENT	27.4875	2.12767	8
			UPS	29.0125	2.92303	8
			Total	28.9659	3.14687	82
		Total	BYP	29.4007	3.10751	140
			ENT	27.5636	1.84785	11
			UPS	29.3227	3.51364	22
			Total	29.2740	3.11612	173
	1.00	1.50	BYP	29.1837	2.14800	49
			ENT	27.7737	1.60341	19
			UPS	30.5182	2.99724	22
			Total	29.2122	2.44783	90
		2.00	BYP	30.0915	2.43184	47
			ENT	28.7600	2.46222	20
			UPS	31.0391	3.68520	23
			Total	30.0378	2.88711	90
		Total	BYP	29.6281	2.32441	96
			ENT	28.2795	2.12097	39
			UPS	30.7844	3.33875	45
			Total	29.6250	2.70092	180
	Total	1.50	BYP	29.4545	2.67049	123
			ENT	27.7727	1.52071	22
			UPS	30.1222	3.36266	36
			Total	29.3829	2.78060	181
		2.00	BYP	29.5354	2.97018	113
			ENT	28.3964	2.40470	28
			UPS	30.5161	3.57287	31
			Total	29.5267	3.05244	172
		Total	BYP	29.4932	2.81220	236
			ENT	28.1220	2.06766	50
			UPS	30.3045	3.44064	67
			Total	29.4530	2.91295	353

Table E-1 - Descriptive Statistics (Continued)

Width	.75	1.50	BYP	.8949	.14816	74
			ENT	.7733	.03215	3
			UPS	.9164	.21219	14
			Total	.8942	.15778	91
		2.00	BYP	.8582	.13389	66
			ENT	.7950	.09350	8
			UPS	.8663	.17096	8
			Total	.8528	.13430	82
		Total	BYP	.8776	.14230	140
			ENT	.7891	.08018	11
			UPS	.8982	.19551	22
			Total	.8746	.14816	173
	1.00	1.50	BYP	.9767	.16614	49
			ENT	.9205	.15483	19
			UPS	.9864	.18597	22
			Total	.9672	.16882	90
		2.00	BYP	.9432	.15433	47
			ENT	.9260	.13268	20
			UPS	.9474	.19278	23
			Total	.9404	.15912	90
		Total	BYP	.9603	.16051	96
			ENT	.9233	.14200	39
			UPS	.9664	.18836	45
			Total	.9538	.16413	180
	Total	1.50	BYP	.9275	.16004	123
			ENT	.9005	.15271	22
			UPS	.9592	.19665	36
			Total	.9305	.16698	181
		2.00	BYP	.8935	.14818	113
			ENT	.8886	.13523	28
			UPS	.9265	.18809	31
			Total	.8987	.15378	172
		Total	BYP	.9112	.15508	236
			ENT	.8938	.14179	50
			UPS	.9440	.19198	67
			Total	.9150	.16125	353

Table E-2 - Multivariate Tests

Effect		Value	F	Hypothesis df	Error df	Sig.
Intercept	Pillai's Trace	.981	8847.016[a]	2.000	340.000	.000
	Wilks' Lambda	.019	8847.016[a]	2.000	340.000	.000
	Hotelling's Trace	52.041	8847.016[a]	2.000	340.000	.000
	Roy's Largest Root	52.041	8847.016[a]	2.000	340.000	.000
Spacing	Pillai's Trace	.053	9.543[a]	2.000	340.000	.000
	Wilks' Lambda	.947	9.543[a]	2.000	340.000	.000
	Hotelling's Trace	.056	9.543[a]	2.000	340.000	.000
	Roy's Largest Root	.056	9.543[a]	2.000	340.000	.000
Velocity	Pillai's Trace	.010	1.717[a]	2.000	340.000	.181
	Wilks' Lambda	.990	1.717[a]	2.000	340.000	.181
	Hotelling's Trace	.010	1.717[a]	2.000	340.000	.181
	Roy's Largest Root	.010	1.717[a]	2.000	340.000	.181
Location	Pillai's Trace	.030	2.634	4.000	682.000	.033
	Wilks' Lambda	.970	2.645[a]	4.000	680.000	.033
	Hotelling's Trace	.031	2.655	4.000	678.000	.032
	Roy's Largest Root	.030	5.185[b]	2.000	341.000	.006
Spacing * Velocity	Pillai's Trace	.012	2.085[a]	2.000	340.000	.126
	Wilks' Lambda	.988	2.085[a]	2.000	340.000	.126
	Hotelling's Trace	.012	2.085[a]	2.000	340.000	.126
	Roy's Largest Root	.012	2.085[a]	2.000	340.000	.126
Spacing * Location	Pillai's Trace	.022	1.892	4.000	682.000	.110
	Wilks' Lambda	.978	1.894[a]	4.000	680.000	.110
	Hotelling's Trace	.022	1.895	4.000	678.000	.110
	Roy's Largest Root	.020	3.488[b]	2.000	341.000	.032
Velocity * Location	Pillai's Trace	.003	.297	4.000	682.000	.880
	Wilks' Lambda	.997	.296[a]	4.000	680.000	.880
	Hotelling's Trace	.003	.296	4.000	678.000	.881
	Roy's Largest Root	.003	.572[b]	2.000	341.000	.565
Spacing * Velocity * Location	Pillai's Trace	.001	.065	4.000	682.000	.992
	Wilks' Lambda	.999	.065[a]	4.000	680.000	.992
	Hotelling's Trace	.001	.064	4.000	678.000	.992
	Roy's Largest Root	.001	.121[b]	2.000	341.000	.886

a. Exact statistic
b. The statistic is an upper bound on F that yields a lower bound on the significance level.
c. Design: Intercept + Spacing + Velocity + Location + Spacing * Velocity + Spacing * Location + Velocity * Location + Spacing * Velocity * Location

Table E-3 - Levene's Test of Homogeneity of Variances

	F	df1	df2	Sig.
Length	2.509	11	341	.005
Width	1.161	11	341	.314

Tests the null hypothesis that the error variance of the dependent variable is equal across groups.
a. Design: Intercept + Spacing + Velocity + Location + Spacing * Velocity + Spacing * Location + Velocity * Location + Spacing * Velocity * Location

Table E-4 - MANOVA Analysis

Tests of Between-Subjects Effects

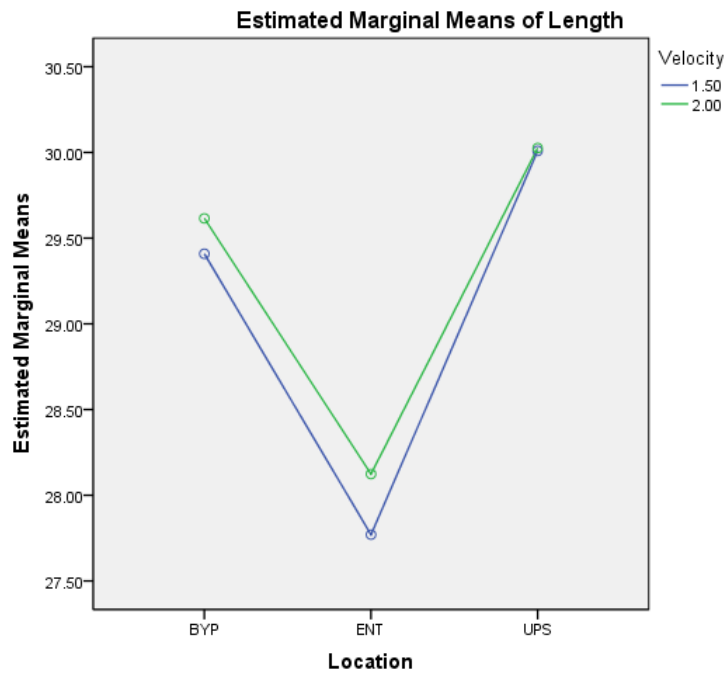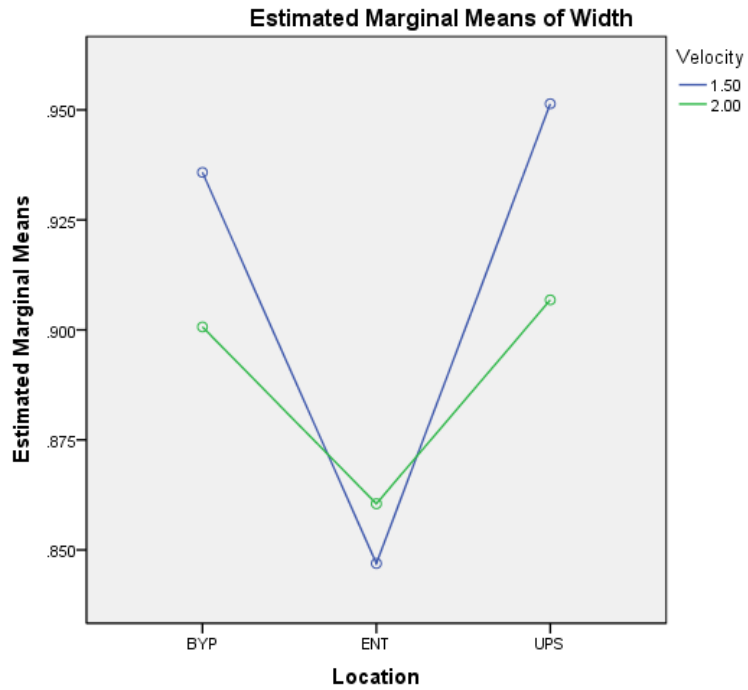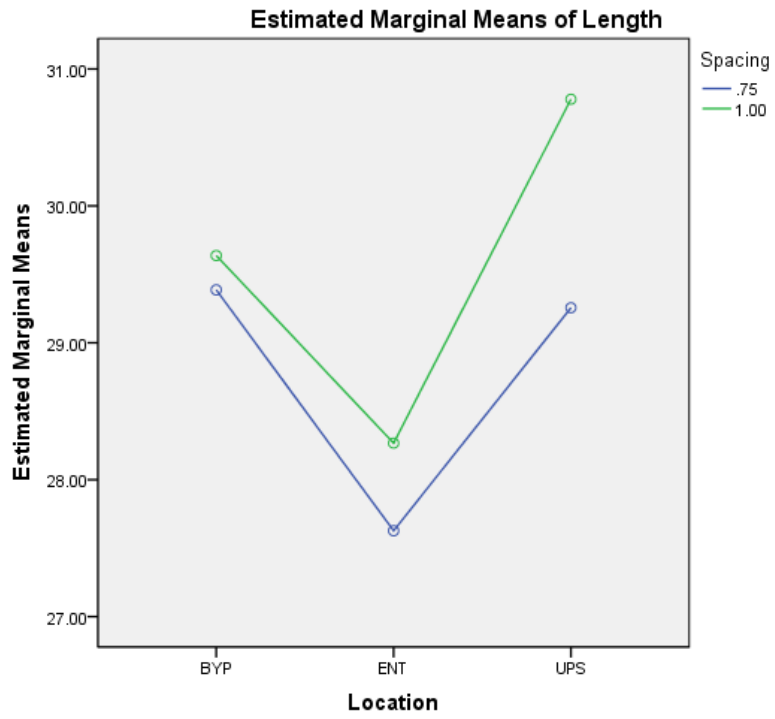| Source	Dependent Variable	Type III Sum of Squares	df	Mean Square	F	Sig.
Corrected Model	Length	218.656[a]	11	19.878	2.449	.006
	Width	.801[b]	11	.073	2.973	.001
Intercept	Length	133563.223	1	133563.223	16453.170	.000
	Width	127.343	1	127.343	5199.702	.000
Spacing	Length	25.411	1	25.411	3.130	.078
	Width	.388	1	.388	15.831	.000
Velocity	Length	1.453	1	1.453	.179	.673
	Width	.019	1	.019	.779	.378
Location	Length	83.336	2	41.668	5.133	.006
	Width	.121	2	.060	2.461	.087
Spacing * Velocity	Length	14.742	1	14.742	1.816	.179
	Width	3.721E-6	1	3.721E-6	.000	.990
Spacing * Location	Length	18.300	2	9.150	1.127	.325
	Width	.022	2	.011	.447	.640
Velocity * Location	Length	.626	2	.313	.039	.962
	Width	.018	2	.009	.359	.699
Spacing * Velocity * Location	Length	.441	2	.221	.027	.973
	Width	.001	2	.000	.018	.982
Error	Length	2768.163	341	8.118		
	Width	8.351	341	.024		
Total	Length	309206.450	353			
	Width	304.683	353			
Corrected Total	Length	2986.819	352			
	Width	9.152	352			

Table E-5 - Post-Hoc Tests

Multiple Comparisons

Dependent Variable	(I) Location	(J) Location	Mean Difference (I-J)	Std. Error	Sig.	95% Confidence Interval Lower Bound	95% Confidence Interval Upper Bound
Length Tukey HSD	BYP	ENT	1.3712*	.44357	.006	.3271	2.4154
		UPS	-.8113	.39441	.101	-1.7397	.1172
	ENT	BYP	-1.3712*	.44357	.006	-2.4154	-.3271
		UPS	-2.1825*	.53246	.000	-3.4359	-.9291
	UPS	BYP	.8113	.39441	.101	-.1172	1.7397
		ENT	2.1825*	.53246	.000	.9291	3.4359
Width Tukey HSD	BYP	ENT	.0174	.02436	.755	-.0399	.0748
		UPS	-.0328	.02166	.286	-.0838	.0182
	ENT	BYP	-.0174	.02436	.755	-.0748	.0399
		UPS	-.0502	.02925	.200	-.1191	.0186
	UPS	BYP	.0328	.02166	.286	-.0182	.0838
		ENT	.0502	.02925	.200	-.0186	.1191

Based on observed means.
 The error term is Mean Square(Error) = .024.

Table E-6 - Means Plots

Estimated Marginal Means of Length

Estimated Marginal Means of Length

Estimated Marginal Means of Width

Estimated Marginal Means of Width
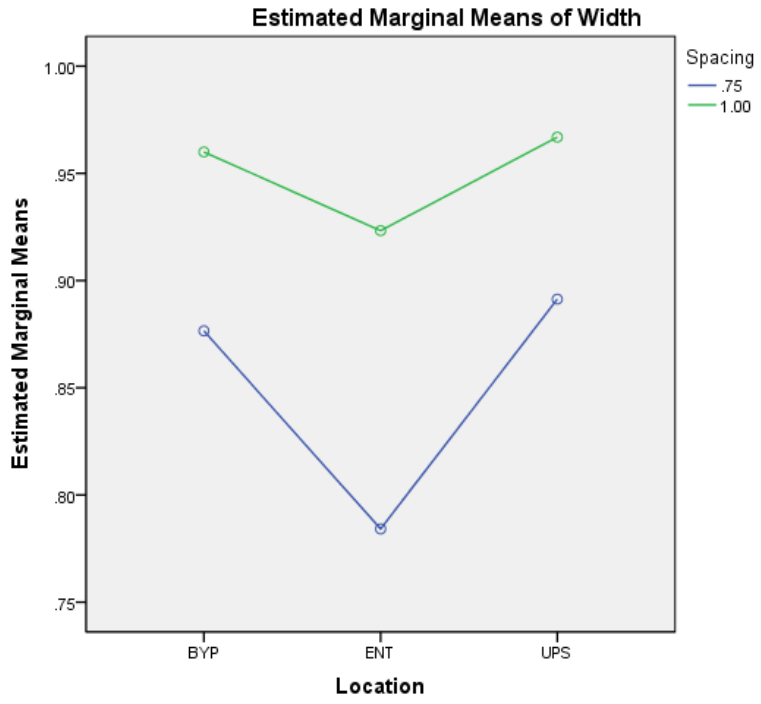
APPENDIX F: COMPARISON OF HEAD LOSS EQUATIONS

Angle (degrees)	Bar Spacing (inches)	$\dfrac{V^2}{2g}$	Kirschmer −Mosonyi (ft)	Meusburger (ft)	Clark (ft)	Zimmermann (ft)	Raynal (ft)	Idel'chik (ft)	Model (ft)	Physical Model Data (ft)
45	0.75	0.03	0.03	0.03	0.01	4.00	0.53	0.06	0.08	0.09
		0.06	0.06	0.06	0.02	4.03	1.06	0.11	0.16	0.18
		0.08	0.08	0.09	0.02	4.07	1.53	0.16	0.24	0.21
90	0.75	0.03	0.04	0.00	0.00	0.10	0.00	0.02	0.03	0.04
		0.06	0.06	0.00	0.00	0.12	0.00	0.03	0.05	0.06
		0.09	0.10	0.01	0.01	0.13	0.01	0.05	0.08	0.08
45	1.0	0.04	0.04	0.04	0.01	3.99	0.67	0.05	0.10	0.09
		0.06	0.06	0.07	0.02	4.01	1.10	0.09	0.17	0.16
		0.10	0.10	0.11	0.03	4.04	1.77	0.13	0.27	0.25
90	1.0	0.04	0.04	0.00	0.00	0.10	0.00	0.01	0.03	0.02
		0.06	0.06	0.00	0.00	0.11	0.00	0.02	0.05	0.04
		0.10	0.10	0.01	0.01	0.12	0.01	0.04	0.07	0.07
45	1.5	0.04	0.04	0.04	0.01	3.97	0.61	0.06	0.09	0.10
		0.06	0.06	0.07	0.02	3.98	1.10	0.10	0.16	0.18
		0.10	0.10	0.11	0.03	4.00	1.70	0.16	0.25	0.28
90	1.5	0.04	0.04	0.00	0.00	0.09	0.00	0.01	0.02	0.02
		0.06	0.06	0.00	0.00	0.10	0.00	0.01	0.04	0.04
		0.10	0.10	0.01	0.01	0.10	0.01	0.02	0.06	0.06